Development of a Computer Technique for the Prediction of Transport Aircraft Flight Profile Sonic Boom Signatures

Peter G. Coen
Bachelor of Aerospace Engineering
Polytechnic Institute of New York
1983

A Thesis submitted to
the Faculty of
The School of Engineering and Applied Science
of The George Washington University
in partial satisfaction of the requirements for the degree of
Master of Science
March 1991

Abstract

A new computer technique for the analysis of transport aircraft sonic boom signature characteristics has been developed. This new technique, based on linear theory methods, combines the previously separate equivalent area and F function development with a signature propagation method using a single geometry description. The new technique has been implemented in a stand-alone computer program and has been incorporated into an aircraft performance analysis program. Through these implementations, both configuration designers and performance analysts are given new capabilities to rapidly analyze an aircraft's sonic boom characteristics throughout the flight envelope.

The paper begins with a brief review of the elements of sonic boom theory embodied in the analysis methods to be employed. Several candidate computer programs for each analysis step were selected. These steps include: analysis of area due to volume, analysis of equivalent area due to wing and interference lift, F function development and signature propagation. Comparisons of the results of the selected analysis programs are presented. Included in this study are the results of an effort to reduce the computer time required for each analysis to a minimum without affecting accuracy. The process of linking the analysis routines to create the new sonic boom module is then described. The capabilities of the stand-alone analysis program, including the generation of boom data contours, are described. The paper concludes with a study of the application of the new technique to the analysis of two conceptual Mach 2.0 transport configurations. The boom signature shapes and overpressure levels are calculated for both configurations on a typical minimum fuel burn flight profile. New flight profiles are developed to reduce the climb overpressure levels. The results indicate that the climb overpressures can be reduced to cruise levels without significant performance penalties.

Acknowledgments

I would like to acknowledge all the individuals from the National Aeronautics and Space Administration and the George Washington University, particularly my branch head Mr. Sam Dollyhigh and my advisor Dr. John Whitesides, who have supported my work on this thesis. I would also like to acknowledge my wife Kathy for her support. A special acknowledgment is due to Mr. Dave Fetterman for his assistance during the early stages of my research.

Table of Contents

List of Tables

List of Figures

List of Symbols

A_e	equivalent area, ft.^{2}
A	axial force, lbs.
a	acceleration, ft./sec^2
C_A	axial force coefficient, A/qS
C_L	lift coefficient, L/qS
C_{L_α}	lift curve slope
C_N	normal force coefficient, N/qS
c	chord
$F(\tau)$	Whitham F function
g	acceleration due to gravity, ft./sec^2
h	altitude, ft.
k	Mach number parameter $((\gamma+1)M^4) / (\beta^{1.5}\sqrt{2})$
L	lift force, lbs
M	Mach number
N	normal force, lbs.
P	lifting surface element,
q	dynamic pressure, psf
r	perpendicular distance from reference axis aircraft to measurement point
S	wing reference area, ft.^{2}
s	distance measure along aircraft longitudinal axis, dummy variable of integration for τ
TOGW	aircraft takeoff gross weight, lbs
t	time, sec
x	distance along aircraft longitudinal axis
y	distance along aircraft lateral axis
z	distance along aircraft vertical axis
α	angle of attack, deg.

β	$\sqrt{M^2-1}$
γ	flight path angle, deg. or ratio of specific heats
$\dot{\gamma}$	rate of change of flight path angle, deg./sec.
Δp	incremental pressure measured from free stream pressure (over-pressure)
θ	Mach plane orientation angle, deg.
μ	Mach angle, $\sin^{-1}(1/M)$
τ	distance measured along aircraft longitudinal axis
τ_t	transposed position of τ

Subscripts

o	reference or centerline
1,2	incremental value (time) or airfoil notation
avg	average
camber	camber component
flatplate	flat plate component
int	interference component
l	lower
local	related to a specific airfoil
max	maximum
r	reference
t	trailing edge
u	upper
wing	wing component

I. Introduction

One of the important considerations in the design of a supersonic aircraft is the phenomenon of sonic boom. Problems with public acceptance of sonic booms were partially responsible for the cancellation of the United States SST program in the 1970's and the prohibition of civilian supersonic flight over land. Since the end of the U.S. SST program and the certification of the Anglo-French Concorde, most interest in sonic boom has focused on military aircraft. However, the recent identification of supersonic transport technology as a national research and development goal (ref 1) has prompted renewed interest in the design of commercial supersonic aircraft and the sonic boom problem. Preliminary studies by NASA, Boeing Commercial Airplanes and the Douglas Aircraft Company (ref 2) have indicated that there is a substantial market for a 250 -300 passenger supersonic transport if certain key environmental and technological obstacles can be overcome. One of the environmental obstacles is sonic boom. The aforementioned studies indicate that the capability of supersonic flight over land would greatly expand the size of the market for these transports. Currently, NASA is engaged in research to determine if there is sufficient technological justification to warrant a concentrated effort to develop a low sonic boom aircraft. As part of this research, several candidate configurations will be evaluated to determine the behavior of shaped sonic boom signatures and the impact of the required configuration shaping on the performance characteristics of such aircraft. In addition to the requirements of this research, there is a need to evaluate the sonic boom characteristics of any proposed supersonic aircraft configuration.

Research into methods to predict aircraft sonic boom has been going on for over 30

years. The proceedings of the First and Second Sonic Boom Symposia (ref 3 and 4) indicate that a great deal of progress was made during the U.S. SST program. Reference 5 indicates that a prediction method using computer programs based on supersonic linearized theory ("linear theory") was available in 1970. A more recent conference on the status of sonic boom methodology (ref. 6) indicated that linear theory methods are still considered acceptable for Mach numbers in the range from 1.2 to 3.0. When originally proposed, the linear theory methods were described as requiring prohibitively large amounts of computer time and were not considered practical for application to complete configuration analysis. Since that time, the speed of computers has increased by several orders of magnitude. These improvements have provided an opportunity to assemble the separate analyses required into a single tool that the aircraft designer and performance analyst can use to predict sonic boom overpressure at key points in the aircraft flight profile. These results can then be incorporated into the assessment of the overall vehicle performance.

The research presented in this thesis had two main objectives: the development of an integrated overpressure prediction tool and the incorporation of this tool as a module in an aircraft performance prediction program. Figure 1 (reproduced from reference 5) illustrates the basic steps necessary to compute a sonic boom overpressure. Since this method was proposed, many improvements have been made in the analysis methods used at various stages in the process, but the only real improvement in the overall process itself has been the replacement of computer card decks with disk-based files. The unification of the required analysis tools under a common geometry format would completely eliminate manual transfer of data-improving both the speed and accuracy of the sonic boom analysis process. Linking the new overpressure prediction tool with an aircraft performance prediction computer program would provide the capability of analyzing climb and cruise overpressures and facilitate the determination of flight path modifications to minimize overpressure on the ground.

The presentation of the results of this research project will begin with a brief review of the theory embodied in the prediction of an aircraft sonic boom. This section will focus on providing a background in the types of analysis required to compute a ground overpres-

sure given aircraft geometry and flight conditions. Particular attention will be devoted to the portions of these analyses which will be affected by efforts to combine them. The background section will be followed by the presentation of the results of the evaluation of several candidate computer programs for each required analysis step. Candidate computer programs were selected from those currently used in the disjointed processes of overpressure analysis. The evaluation of the programs concentrated on geometry and data transfer requirements. Also addressed were concerns of accuracy, sophistication, and reduction of required execution time.

Following the review of candidate analysis tools, a description of the process of assembling these tools into a sonic boom overpressure module will be provided. Comparisons of results from the new overpressure tool with previously published data will be presented. The process of integrating the boom module with an aircraft performance prediction program will then be described. This paper will conclude with an illustration of the application of the combined analysis technique to the computation of the climbout and cruise sonic booms for two Mach 2.0 transport configurations. This will include the effects of two dimensional maneuvers and modification of the flight path to reduce sonic boom overpressure.

II. Review of Sonic Boom Prediction Theory

The phenomenon of sonic boom is a result of the presence of shock waves in the pressure field surrounding an aircraft travelling at supersonic speeds. As shown in Figure 2 (ref. 5) the pressure disturbance from such an aircraft emanates in a conical region with a half cone angle equal to the Mach angle. The intersection of the cone and the ground plane defines a region where the effects of this pressure disturbance are felt. Figure 2 shows that although the pressure disturbance or signature near the airplane can be very complex, the effect on the ground generally takes the form of a pressure pulse with a distinctive N-like shape. The exact shape of this pressure disturbance is influenced by many factors including propagation distance, atmospheric turbulence and temperature gradients. The amplitude of this N wave is largest along the center of the flight track. The initial pressure rise, referred as Δp, is usually of the most interest. Off-flight track pressure signatures are also used in the assessment of the overall impact of the sonic boom.

Since the sonic boom is caused by an aircraft-induced pressure disturbance, the most accurate way of calculating the boom would be to accurately compute the pressure distribution around the aircraft. Such calculations are now possible using advanced computational techniques. Computer time requirements and loss of resolution at large distances are two problems that make these methods impractical for rapid application in an aircraft performance prediction problem. For this reason, this research utilized the linear theory models.

Linear theory models for the prediction of the pressure field around a body at supersonic speeds are based on the work of Hayes (ref. 7), Whitham (ref. 8), and Walkden (ref.

9). Hayes proposed that a complex aircraft could be represented through the use of an equivalent body of revolution. The source strength of the pressure distribution is proportional to the second derivative of the cross-sectional area distribution of the equivalent body. Whitham's work provided a method for correcting for the presence of shock waves around a body of revolution. Walkden extended Whitham's work to include lifting bodies. Reference 5 contains an excellent review of the application of this work to prediction of sonic booms. The elements of the theory germane to the computer techniques applied in this paper are now reviewed.

The linear theory methods are based on determining the effective cross-sectional area distribution of the equivalent body representing the aircraft configuration. This effective area consists principally of area due to the volume of the body and equivalent area due to lift. Other terms which may be included are the effects of boundary layer displacement and engine exhaust plume expansion. Sketch (a) illustrates the build-up of body and lift area. As shown in the sketch, the area due to volume is calculated as the forward projec-

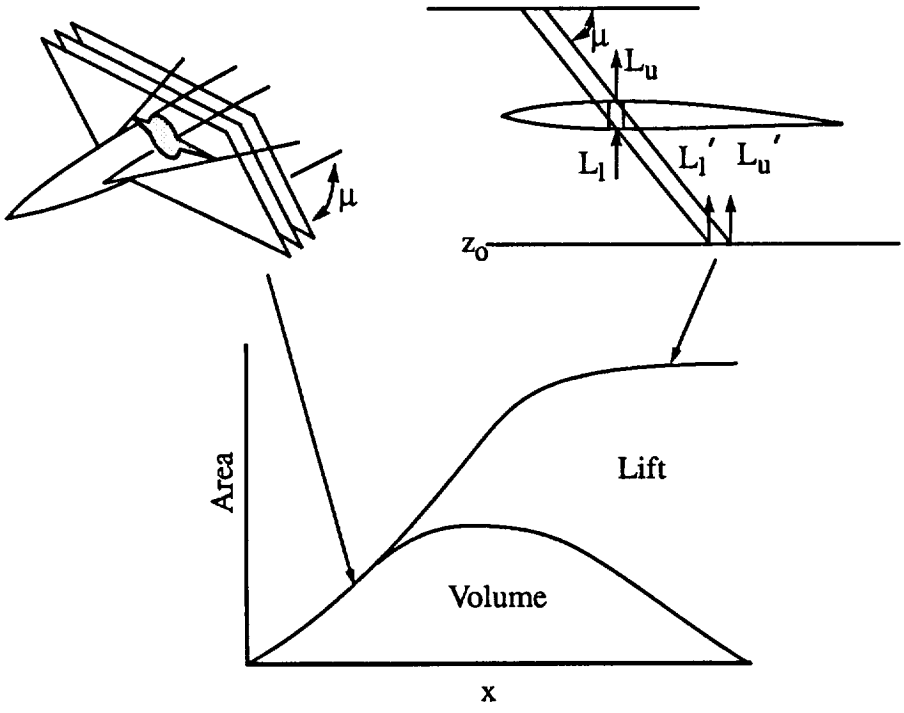

sketch (a)

tion of the area intercepted by a plane inclined at the Mach angle. The figure illustrates a Mach plane positioned properly to calculate the area required to determine the pressure directly below the aircraft. This Mach plane orientation angle is referred to as $\theta = -90°$. The total area due to volume is determined by calculating the area of a series of Mach plane intersections cutting the body from nose to tail. The equivalent area due to lift is determined by a summation of the lift forces on incremental elements of the lifting surfaces. The point of action of a unit of lift is determined by a Mach plane which intersects both the point where the lift is generated and the reference plane. This is shown in sketch (a) for a small section of an airfoil. This illustration indicates that displacements of a lifting surface due to camber, thickness and dihedral change the shape and length of the curve of equivalent area due to lift.The incremental lift forces are cumulative along the longitudinal axis. This means that the equivalent area for any point on the axis is proportional to the incremental lift at that point added to the total lift forward of that point. The constant of proportionality between the lift and the equivalent area is

$$\frac{\beta}{2q}\sin\theta$$

The lift forces include the lift generated by wings, tails and canards, and can include interference effects due to the presence of nacelles and other bodies.

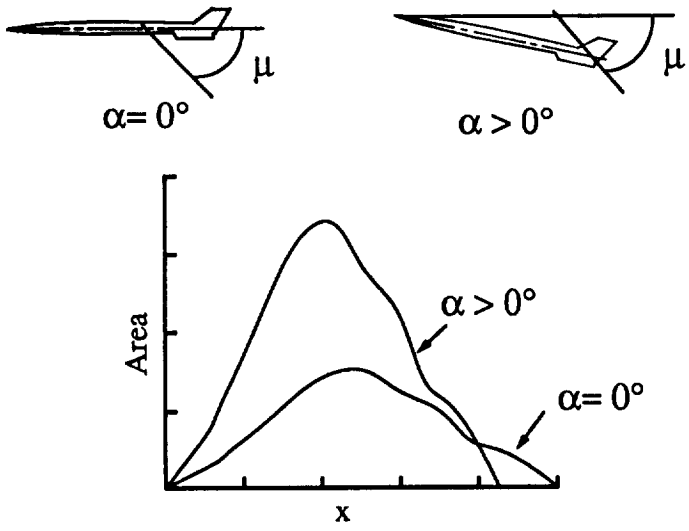

sketch (b)

The total equivalent area (volume and lift) is always calculated on a line which is parallel to the velocity vector of the airplane. Because of this, angle of attack affects the length and shape of the equivalent area distribution. Considering area due to volume, increasing angle of attack will increase the maximum cross sectional area while decreasing the effective length of the area distribution. This effect is illustrated in sketch (b) which shows the area curves for a configuration at zero and positive alphas. The difference in the area curves is exaggerated for the purpose of illustration. The effect of angle of attack in the equivalent area due to lift is illustrated in sketch (c). Note that this figure illustrates the

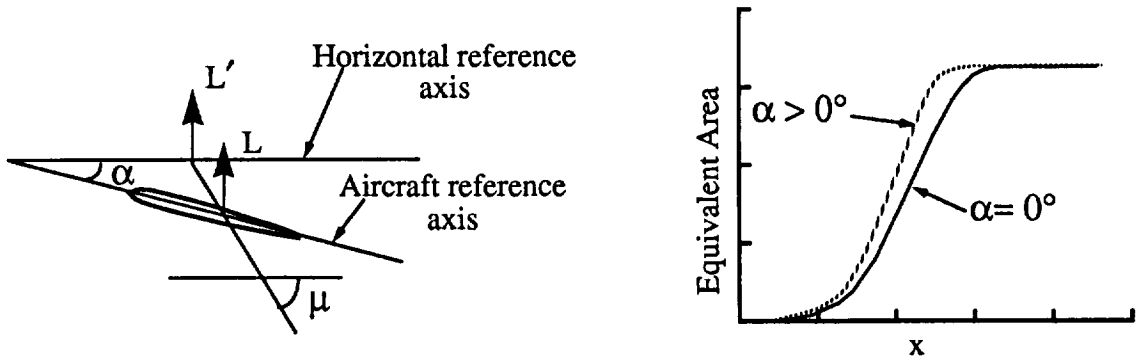

sketch (c)

difference between including angle of attack or not. This should not to be confused with the effect of increasing angle of attack, which of course results in increased lift. The figure shows that the aircraft angle of attack tends to rotate the aircraft reference axis away from the horizontal reference line, along which the equivalent area is measured. Since the lift is always perpendicular to the velocity vector, the magnitude of the lift is unchanged. However, the point where the lift acts, and therefore the length and shape of the equivalent lift area curve is affected.

Once the effective area curve has been calculated, this information is used to develop the Whitham F function

$$F(\tau) = \frac{1}{2\pi}\int_{o}^{\tau} \frac{A_e''}{(\tau - s)^{1/2}} ds$$

where τ is a point on the equivalent body axis. A technique for performing this integration

numerically is presented in reference 10. The F function can then be used to compute the pressure signature, including the location of shock waves. Reference 7 describes a graphical approach to solving for the pressure signature. A numerical procedure, suitable for application to complex aircraft configuration is described in reference 11. In simple terms, the method is described by sketch (d) (from ref. 11). The F function is converted to a "tilted" F function, $F(\tau_t)$ by the transformation

$$\tau_t = \tau - \frac{k}{\sqrt{r}} F(\tau)$$

In this transformation, the k term accounts for effects of Mach number, and the r term for distance from the aircraft to the signature.The location of shock waves is determined by applying an area balancing technique to the tilted F function. The area balancing tech-

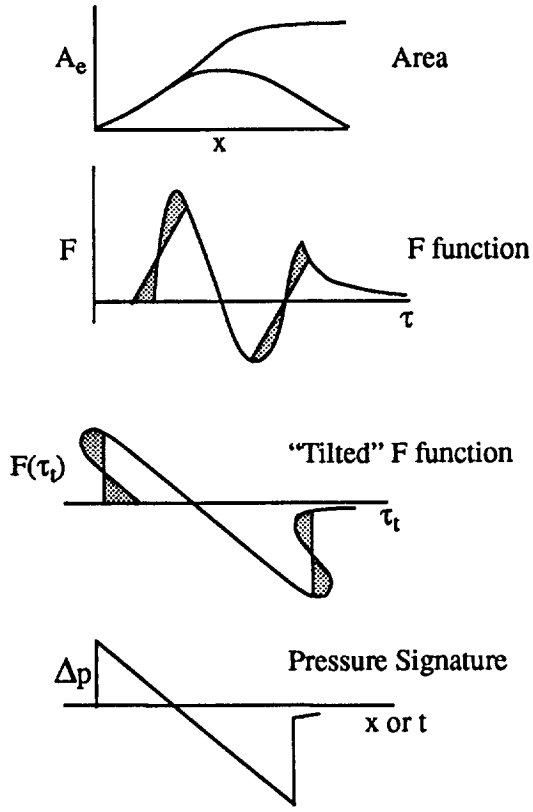

sketch (d)

nique is performed graphically by passing lines of slope $\frac{1}{k\sqrt{r}}$ through the $F(\tau)$ curve

such that lobes of equal area are created. In the numerical method, the area balance points are found by integrating the curve $F(\tau_t)$ and locating points where the resulting function crosses over itself.

The solution described above is valid only in a uniform atmosphere. In a real atmosphere, the pressure signature is distorted by temperature gradients, atmospheric winds and turbulence. When considering an aircraft in flight, any maneuvers made by the aircraft will also impact the propagation of the pressure signature.

Several methods have been developed to account for the effects of a real atmosphere and determine the resulting pressure signature at the ground. References 12 and 13 describe two of these methods. Both are based on the theory of geometrical acoustics. This theory, like its counterpart, geometrical optics, makes use of the concept of rays. In geometrical acoustics, the rays represent a trajectory of points moving in space, tracing the pressure signature propagation through the atmosphere. Sketch (e) (reference 13) illus-

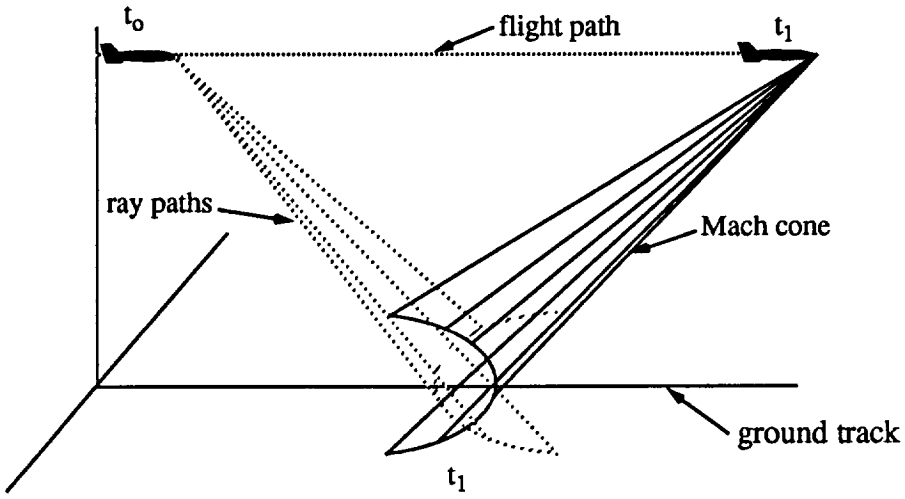

sketch(e)

trates that a sonic boom heard on the ground at time t_1 is actually generated by the aircraft at some earlier time t_0. The boom signature has propagated along rays which are affected by the characteristics of the atmosphere.

The changes in pressure and temperature in the atmosphere have an effect analogous

to refraction in geometrical optics. This refraction bends the rays so that they generally curve upwards. The fact that the rays curve has two important implications on the ground overpressure. These are the phenomena known as "cutoffs". The first cutoff phenomenon occurs at near-supersonic speeds. At these speeds there exists a range of flight conditions for which the rays will curve completely upward before reaching the ground. Thus an aircraft travelling at these speeds will produce no boom on the ground. The second cutoff phenomenon is that of the lateral cutoff. Rays that emanate perpendicular to the aircraft flight track are also curved upward. At a certain lateral distance, all of the rays will have curved completely upward and thus beyond that distance, no boom will be heard on the ground. The exception is the case of secondary booms. These booms, caused by refraction of rays propagating upward from the aircraft are not considered in this thesis. (See reference 6).

Another important concept in the application of geometrical acoustics is that of the ray tube. The ray tube can be visualized as a group of rays generated at times separated by a small increment. The area of the ray tube is used to determine how the acoustic energy of the signature varies during the propagation. As in geometrical optics, conditions exist that can cause focusing of the propagating rays. A surface in space where the ray tube area becomes zero is termed a "focus" or "caustic". The magnitude of the overpressure at a focus can be more than 2.5 times that of a normal boom. The theory of geometrical acoustics cannot be applied to predicting the overpressure at a focus. Aircraft maneuvers, including accelerations, pushovers and turns can cause the ray focusing and potential caustics.

Although by no means a complete treatise on the subject of sonic boom prediction methods, this review is intended to cover the principal theory behind the computer programs that will be combined to form the sonic boom module. The following chapter will focus on the details of these programs.

III. Selection of Analysis Methods

This chapter is devoted to a discussion of the study and selection of computer routines to perform the analysis required in the sonic boom overpressure module. Referring to figure 1, it can be seen that there are three types of analysis to be carried out with the help of computer programs. These are: calculation of area due to volume, calculation of equivalent area due to lift, and extrapolation of the pressure signature through the atmosphere. For the first and last of these analyses, there was a limited selection of candidate computer programs available. The process of computing the area due to volume is used only in wave drag and sonic boom analysis. For the extrapolation process, only two methods have been implemented in computer programs.

On the other hand, there are numerous programs available to calculate wing lift using linear or modified linear theory. However, there are only a very few that have been modified to convert the calculated pressure distribution to the lift equivalent area distribution necessary for determining sonic boom. For expediency, the decision was made to consider only those programs that were so modified and documented. In each case, the programs are shown to provide reasonable agreement with the lift and drag components measured in wind tunnel tests. Therefore, in the realm of linear methods, it was not deemed productive to initiate detailed comparison studies, particularly if a program required extensive modification to calculate the necessary sonic boom lift distributions. In addition, the methods selected have all been applied in studies such as those described in reference 14. In these studies, comparisons were made with wind tunnel measured near field pressure signatures, yielding good results for a number of different configurations.

Although the above conditions greatly reduced the number of candidate analysis tools,

several comparisons remained in the program selection process. For each step in the sonic boom analysis, the candidate programs were studied and compared to identify potential errors or weaknesses in the method and associated program. This involved making numerous test runs of the programs, exercising the options available in each, and testing several different types of geometries. While long and involved, this procedure did identify several programming errors in the candidate programs, and uncovered deficiencies in the methods of others that made them unsuitable for use in the overpressure module. Perhaps most important, the comparison process provided the author with a good working knowledge of each program. This proved valuable during the later process of integrating the selected programs into the overpressure module. A large part of the analysis of the candidate methods focussed on determining how to perform each analysis in the minimum computer execution time while introducing only small accuracy losses. Execution time will become important when applying the overpressure module in aircraft performance analysis. At this point, many analyses will be required. Minimizing the time expended on each analysis will keep the overall time requirements reasonable.

Analysis of Area due to Volume

The calculation of area due to volume involves determining the cross sectional area cut when a Mach plane is passed through the configuration. This process is part of the calculations made when computing supersonic wave drag and has been implemented in several computer programs. Three candidate programs were selected because of their widespread use in configuration analysis. The three programs are all derived from the technique outlined in reference 15 and are similar in most respects. There are several differences that distinguish the methods and these were studied before a selection was made. The first of these differences concerned geometry modelling. The geometry format described in reference 15 allows the fuselage to be modelled only as an uncambered body of circular cross section. This geometry format was later modified (ref. 16) to allow for cambered circular fuselages and for fuselages of arbitrary cross section. This is the geometry format used in the first two candidate programs. The third program (ref. 17) uses a completely arbitrary format. In this format, the x, y, and z coordinates of the points describing

the contours of all components are input. This allows for component contours with different orientations and provides the capability of modelling more unconventional configurations. This format is also easily adaptable to the LAWGS (ref. 18) geometry format. An investigation of the impact of these different geometry formats on the results for area due to volume was conducted. Figure 3 illustrates the Mach 3.0 configuration from reference 19 modelled with a cambered circular body and a blended body. The blended body configuration was prepared in both the arbitrary fuselage (methods one and two) and complete arbitrary geometry formats (method three). The circular body format (methods one and two) is popular in configuration analysis because of the ease with which the body radius can be varied to determine the area distribution required for the minimum wave drag. The blended body modelling is becoming more important because of the need for geometry compatibility with advanced aerodynamic methods. The primary goal in sonic boom analysis is to properly model the cross sectional area build up. Figure 4 shows that this is possible with all three geometry formats. The figure compares the calculated $\theta = -90°$ area distributions for the Mach 3.0 configuration modeled in all three geometry formats at Mach numbers of 1.4 and 3.0. The agreement is very good in all cases. The results for the blended fuselage geometry and completely arbitrary geometry models appear to overlay exactly. Figure 4 illustrates results for the combined areas of the fuselage, wing and fins. Figure 5 shows that an error was discovered when nacelles were added to the geometry. Although the overall agreement was still quite good, there seemed to be a fairly significant difference in the results for the nacelles. This was traced to an error in computing the inlet capture area in the program of reference 17. The capture area is the circular cross sectional area of the nacelles and can be computed exactly with little trouble. A brief review of the logic of the program did not yield the source of this error. A more detailed analysis is warranted but is beyond the scope of this work.

The second difference between the three candidate volume methods concerns the effects of angle of attack. As previously discussed, changing angle of attack affects the shape and length of the area due to volume distribution. Because of the limits of their geometry format, the first two candidate methods are forced to make an approximation to

this effect. The effective length and area are modified as follows:

$$x' = x \times \frac{\sin(\mu - \alpha)}{\sin\mu}$$

$$A'(x) = A(x) \times \frac{\sin\mu}{\sin(\mu - \alpha)}$$

Because the third method is dependent only on x,y,and z coordinates, an exact transformation of the geometry can be made. For a given reference of rotation, this transformation is

$$x' = (x - x_r)\cos\alpha - (z - z_r)\sin\alpha$$

$$z' = (x - x_r)\sin\alpha + (z - z_r)\cos\alpha$$

The effective length and area are computed based on the transformed coordinates. Concern had been expressed that the approximate method may not be sufficiently accurate when dealing with cambered fuselages. An investigation of these effects was performed using the fuselage of the Mach 3.0 configuration and the fuselage of the Mach 2.7 configuration of reference 20. The two fuselages are shown in side view in figure 6. Note that both are severely cambered with the Mach 2.7 configuration having a considerable z displacement at the aft end of the fuselage. The $\theta = -90°$ area distributions were computed for a Mach number of 1.4 at angles of attack of 2.0. 4.0 and 10.0 degrees. The results, summarized in figure 7 for the Mach 3.0 configuration and figure 8 for the Mach 2.7 configuration, indicate no major errors due to the difference in the angle of attack computations. It may be noted here that the cruise flight angle of attack for supersonic transport vehicles is usually low. When analyzing area distribution at severe off-design conditions, care must be taken to not let the angle of attack exceed the Mach angle.

Another area of concern for volume calculations involved a difference in the method of computing the area of lifting surfaces. In the program of method one, the area of lifting surfaces is divided into a set of three dimensional solid elements. In computing the Mach plane sliced area, each element is checked for intersection with the current Mach plane and if an intersection exists, the area is computed. The second method approximated the lifting surface as a two dimensional grid, with each element having a constant thickness.

This approximation was made to reduce the computational requirements from those of method one. Approximation can lead to an error in the computed area when a cambered lifting surface is considered. The magnitude of this error for a $\theta = -90°$ area distribution is shown in figure 9. When all θ values are considered, the errors due to camber are self-cancelling and have little effect on the computed wave drag. However, for sonic boom calculations, the results are unacceptable.

The final consideration given to the three candidate volume programs concerned the required execution time. The program of method one, originally very computational intense, had recently undergone a major logic restructuring, which greatly reduced its execution time. To compare execution times, the volumes for two different geometries were calculated. The geometries selected were the previously described Mach 3.0 and Mach 2.7 transport configuration. For each geometry, the volume calculations were performed for two different numbers of area cuts along the body axis. The programs used in this comparison were the original and new versions of method one and the programs of methods two and three. Table 1 presents a comparison of the required execution times. All times presented are typical results from an advanced workstation computer. The results show that the modified version of method 1 is approximately 50% faster than method 2. It is also as much as 10 times as fast as method 3.

As a result of all of the above comparisons, it was possible to select one program for the calculation of area due to volume. Method two had to be eliminated immediately due to the discrepancy in volumes of cambered lifting surfaces. Although method three had the small error in the nacelle volume calculation, it was still desired to use this program because of its connection to more detailed geometry formats. Unfortunately, the execution times for this program were much too long. It may be that a logic restructuring effort such as applied to method one would produce considerable reduction in the execution time. However, for the purpose of this research, it was decided to use the improved version of method one as the volume calculation tool.

Analysis of Equivalent Area Due to Lift

The determination of the equivalent area due to lift involves calculating the complete

distribution of lifting force over the surface of the wing. For the purpose of this work, only the lift components due to wings and nacelle interference were considered. The discussion of candidate methods for these two components will be presented separately.

Wing Lift Analysis

The analysis of the wing lift distribution can be carried out by any one of a number of methods for predicting the wing lift. There were two programs available that had been modified to perform the necessary summation and produce the lift equivalent area distribution. The first of these programs is a linear method for computing flat plate and camber lift of a wing with arbitrary planform. (ref. 21,22). The second is an extended linear method with an estimation of non-linear effects (ref. 23). This program calculates the flat plate, camber and thickness lift components. The principal advantages of the linear method were simplicity of input data requirements and short execution time. The modified linear method provides for estimation of certain non-linear effects such as wing root and three dimensional flow. This additional detail comes at the expense of slightly more complex input and increased execution time.

Both programs utilize the "Mach Box" method of representing the wing geometry and solving the linear theory equations. In this method, the wing platform is divided into a large number of rectangular elements. The surface slope of each element if then calculated and used to determine the local pressure coefficient. The calculation of the pressures takes into account the pressure results in the upstream region of influence. The second of the methods performs a considerably more detailed analysis. Rather than calculating the pressure coefficient directly, the program first calculates velocities and potential function values for each element. This includes both longitudinal and lateral velocities with flat plate, camber and thickness components. A non-linear correction term is applied to the velocity components, resulting in lift forces which are non-linear with angle of attack. The details of the procedures used in each method are available in the references.

The use of the "Mach box" approach as a basis for computing the required lift distribution and the non-linear character of the modified linear method results were two important

considerations in the evaluation of these methods.

The rectangular element grid representation of the wing planform used in the Mach box method is a fundamental part of developing the lift area distribution. When the lifting solution is complete, the pressure coefficient on each of these elements is known. These pressure coefficients can then be summed to determine the lift area distribution. The method and amount of detail used during this summation is a major difference between the two methods being considered. The difference manifests itself in the methods used to determine the effects of displacements due to camber, dihedral and angle of attack in the lift area distribution.

In its original form, the linear method calculated only flat plate lift components. Although extended to include camber lift effects, the method was not modified to include the effects of the displacements due to camber and angle of attack. An approximation for the camber and dihedral was developed using the displacements of the wing trailing edge relative to the reference origin to modify the length of the lift area curve. Referring to sketch (f) part a, the quantities z and c_{local} are computed for each defined airfoil. The weighted average is computed by summing over the number of airfoils

$$z_{avg} = \frac{\sum (c_{local}) \times z)}{\sum c_{local}}$$

z_{avg} is then used to displace the line of lift action. This displacement is included with the calculation of displacement due to angle of attack. As illustrated in sketch (f) part b, the relationship between a point x on the line of lift action and a point x' on the reference axis of equivalent area due to lift is given by

$$x' = \left(x - \frac{z}{\tan(\mu - \alpha)} \right) \times \frac{\sin(\mu - \alpha)}{\sin\alpha}$$

The modified linear method takes a considerably different approach to the calculation

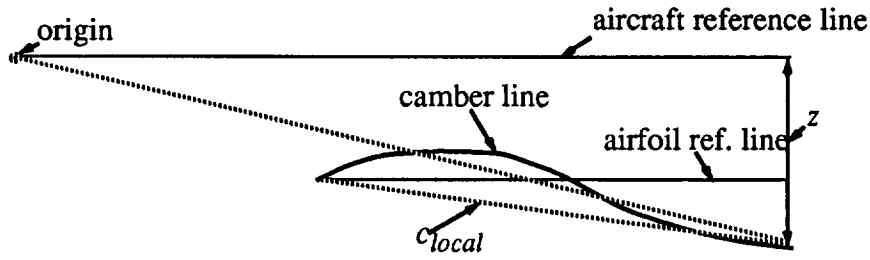

(a)

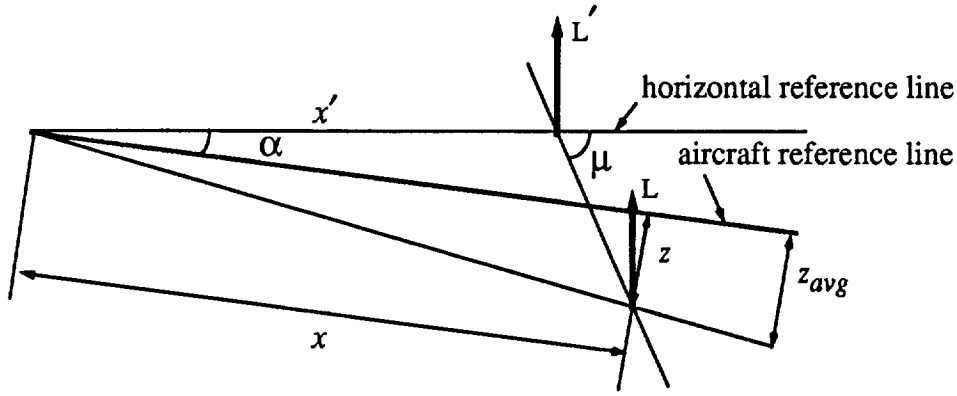

(b)

sketch (f)

of the above mentioned effects. The calculations are performed at the time of computation of the pressure on the individual Mach box elements. A somewhat simplified explanation of the procedure used is illustrated in sketch (g). Consider an element of lifting surface P which is displaced from the aircraft reference axis by the amount z. This displacement can include camber, thickness and dihedral. From the known pressure information, an incremental lift element L is calculated for P. The aircraft axis is rotated by the angle of attack α from the horizontal reference plane which is set up with a summation grid starting at the origin. The geometry is used to determine the position on the summation grid of the point of action of the incremental lift force L′. This procedure is repeated for each element making up the upper and lower surfaces. Each lift increment is added to the others with the same point of action. When the summation is complete, the equivalent area due to lift is

accurately known.

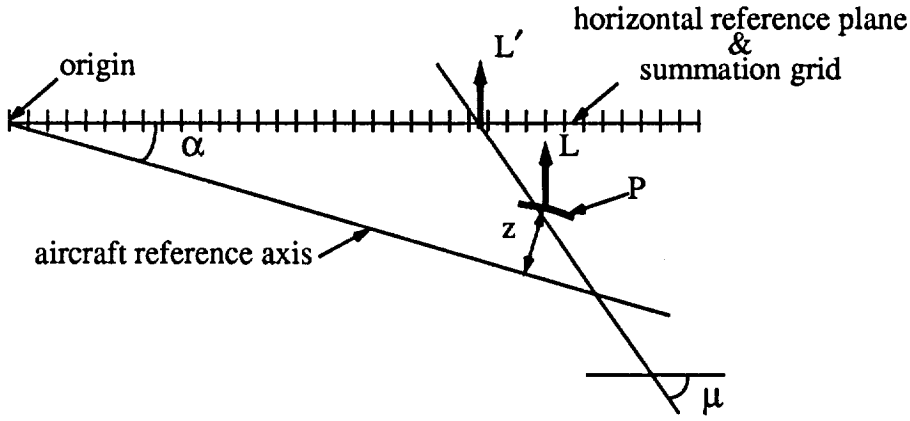

sketch (g)

Owing to the fact that the two methods for including displacement and angle of attack are intricately part of the individual programs, it is difficult to demonstrate clearly the difference in the two procedures. The purpose of the above was to illustrate one of the overall differences in the linear versus non-linear methods. The comparison of the overall results of the two methods will be shown in later discussions. It is, however, interesting to examine the results for including angle of attack individually in each of the methods. This was done for both the Mach 2.7 and Mach 3.0 configurations previously discussed. Figure 10 shows the results for the Mach 2.7 configuration at 60,000 foot altitude, $\alpha = 2.0$ deg. Figure 11 shows similar Mach 3.0 results at 65,000 foot altitude and $\alpha = 2.0$ deg. In both figures, part a shows the linear results and part b those from the modified linear method. Although 2 degrees is a relatively small angle of attack, it was chosen because it represents a typical cruise angle of attack for a supersonic transport. Despite the fact that the angle is small, the effect on the lift distributions is clear in all cases. As expected, including angle of attack shifts the lift distribution forward while the maximum equivalent area remains unchanged. The magnitude of the shift in the lift distribution appears to be similar for both the linear and modified linear methods.

Before proceeding to the comparison of the overall results of the two methods, an attempt was made to reduce to a minimum the execution time required by both methods. The parameter that seemed to have the greatest effect on execution time is one that con-

trols the number of chordwise strips into which the wing is divided and through this, the total number of Mach box elements used in the solution. The study of reducing execution time focused on determining how far this variable, named JBYMAX, could be reduced without affecting the resulting equivalent area distributions. Once again, the Mach 2.7 and 3.0 configurations were chosen as the test geometries. In this study, two Mach numbers were examined for each configuration. The total number of Mach box elements is a function of the Mach number, JBMAX and configuration geometry. Therefore, due to limits on program array sizes, the maximum value for JBYMAX varied with both Mach number and configuration. For each configuration, a series of calculations for varying JBYMAX was made at each of the two Mach numbers. Figures 12 and 13 show the results for the Mach 2.7 configuration while figures 14 and 15 show the Mach 3.0 results. The weights and altitudes were selected to match potential flight conditions. Table 2 contains the program execution times required to generate the data in the figures. The times shown indicate the large differences in execution requirements between the linear and non-linear methods. In all of the high Mach number cases, substantial savings of execution time could be realized with little impact on the resulting equivalent area distributions. At Mach 1.4, the results were different for the two methods. The results for the Mach 2.7 configuration, using the modified linear method, are much the same as the high Mach number data. For the other Mach 1.4 cases, it can be seen that a certain amount of waviness is present in all of the results. This waviness becomes very significant as JBYMAX is reduced from the maximum value for each method. The waviness is due to oscillations in the pressure coefficients resulting from sparsity of data for the smoothing routines. This is particularly true for the linear method, which has limited smoothing capabilities and considerably smaller array sizes.

The studies of the effects of angle of attack and JBYMAX sensitivity provided sufficient background information to support the overall comparisons of the linear and modified linear methods. The objective of these comparisons was to determine the trade off between the shorter execution time of the linear method and the improved accuracy of the modified linear method. To provide an accurate assessment of this trade off, it was neces-

sary to compute the lift distributions for different geometries over a range of Mach numbers and angles of attack. The first geometry tested was the reference arrow wing geometry from reference 14. This geometry, shown in figure 16, was selected because it represented a simple uncambered wing and would provide a baseline comparison of the two methods. The previously described Mach 2.7 and Mach 3.0 configuration geometries were also used in the comparison studies. The complete geometry for the Mach 2.7 configuration is shown in figure 17. Note that the wing geometry for this configuration is similar to the reference arrow wing except for the addition of camber. Using this geometry will provide an estimate of differences in the camber analyses of the two methods. Mach numbers for this study ranged from 1.2 (numerically the lower limit for linear methods) up to the design cruise Mach number for each configuration. Altitude and weight were held constant, which produced a sufficient variation of angle of attack over the Mach number range. The results of the comparisons are summarized in figures 18, 19 and 20. The corresponding angles of attack, JBYMAX and program execution times are shown in table 3. For the uncambered wing, the agreement was very good for all Mach numbers except 1.2. At Mach 1.2, the previously discussed oscillations and an under-prediction of lift area are noticeable in the linear method results. Table 3 shows that in all of the linear Mach 1.2 results, program array size restricted JBYMAX to 10. The results for the Mach 2.7 configuration at Mach 1.2 indicated an unacceptable amount of under-prediction and oscillation for the linear method. The results at other Mach numbers indicate good agreement of the overall shape of the equivalent area curves, with the linear method under-predicting the lift on the forward portions of the wing. The results for the Mach 3.0 configuration (Mach 1.2 excluded) in general show good agreement in both shape and magnitude of the equivalent area curves. It appears that the modified linear program predicts a slightly higher value of lift on the highly swept inboard portion of the wing. This results in the 'bump' in the modified method equivalent area curve.

The oscillation and severe under-prediction present at Mach 1.2 were found to almost completely vanish when the Mach number was increased above Mach 1.4. The execution time results indicate that if some inaccuracy can be tolerated, the linear method is substan-

tially faster than the modified method, particularly for Mach numbers between 1.4 and 2.0. Some of this time savings disappears at the higher Mach numbers.

Analysis of all of the comparisons made between the two method for computing the equivalent area due to wing lift indicates that the modified linear method is the better from the standpoint of accuracy. However, the rapid execution time of the linear method could be very important when computing the many flight points required for analyzing an aircraft climb profile. Because of these conflicting requirements, it was decided to include both methods in the sonic boom module. The decision of which method to use could then be based on the actual overpressure and signature shape results. Of course, the linear method would have to be restricted to Mach numbers greater than 1.4 unless the oscillation could be eliminated, perhaps through an increase in program array size.

Interference Lift

The second lift component to be considered was that of interference due to the presence of nacelles or pods under the wings. At supersonic speeds, the shock wave pressure field of the nacelles can have a significant impact on the pressure distribution of the lower surface of the wing.

Figure 21 presents examples of how much of the overall lift can be contributed by this shock induced lift component. The figure shows the wing and interference lift contributions to the equivalent area distribution for two configurations at different altitudes and total lift. In the case of the four nacelle Mach 2.7 configuration, the contribution of interference lift is small. The opposite is true for the six nacelle Mach 3.0 configuration. This figure is intended to convey that the impact of interference lift on the total equivalent area distribution is dependent on Mach number, altitude, total lift and configuration shape.

A method for calculating this interference pressure and the resulting effect on the sonic boom lift equivalent area distribution is described in reference 24. The method has numerous similarities to the methods for computing wing lift previously described, and was therefore a natural candidate for inclusion in the sonic boom module. The analysis of this program concentrated on exercising the program over a range of Mach numbers to deter-

mine if there were any points where the results become unreasonable. The effects of attempts to reduce the required execution time on the accuracy of the results was also studied. Finally, a series of comparisons of equivalent area distributions with and without interference were performed.

In the course of exercising the program over the range of Mach numbers, the discovery of anomalous results was traced to an error in a part of the program which sums interference pressures. The error was corrected and any affected results were recalculated.

The interference lift method is similar to the wing lift programs previously described. There is a program input similar to JBYMAX which controls the total number of spanwise elements on which the interference pressures are calculated. As before, the study of the effects of reducing execution time focused on varying this parameter. The results of this study are summarized in figures 22 and 23 and table 4. These figures show interference lift equivalent area distributions for the Mach 2.7 and Mach 3.0 study configurations. Results for two Mach numbers are presented with the corresponding execution time presented in the table. Varying JBYMAX from 50 to 20 resulted in some variations in the equivalent area distributions. There was no noticeable trend in the changes of results, nor did the reduced JBYMAX produce any instability or waviness in the results. The conclusion reached was that significant reduction in execution time could be achieved without sacrificing accuracy by reducing JBYMAX to approximately 30.

The final part of the study of lift analysis tools examined the differences in the total lift equivalent area distributions computed using wing lift alone and those computed using wing and interference lift. Figure 21 illustrates how the wing and interference lift components combine to produce the total lift. If the interference component is not computed, the total lift will be made up by having the wing fly at a slightly higher angle of attack. The result of this will be a differently shaped lift distribution. The magnitude of the difference will depend on how large the contribution of interference lift was. Lift equivalent area distributions were computed for the two study configurations over a range of Mach number, altitude and lift values. The results of this study are shown in figures 24 and 25. Table 5 contains the resulting angles of attack and sample execution times. For the Mach 2.7 con-

figuration, the effects of including the interference lift were generally small. The effects were somewhat larger for the Mach 3.0 configuration, especially at lower altitudes and lifts. In all cases, the required execution time was significantly reduced if the interference lift was not computed.

Summary

The study of methods for determining lift equivalent area distributions revealed both strong and weak points in each candidate method, and did not completely eliminate any one method. Obviously, the results for the linear method are unacceptable below Mach 1.4. However, when computing the overpressure for numerous points along a climb profile, it may still be desirable to use this method to reduce the required program execution time. At this point, it was not possible to make judgments as to how much the difference in equivalent area distributions would affect the final sonic boom overpressures and signatures. This can be determined once the lift computation routines have been integrated into the complete overpressure module. It was considered possible that there would always be a trade off between execution time and accuracy of results. Therefore, it was decided to include all three methods and provide a user option for which program to use. The verification of the performance of the complete module will further address the ramifications of using one method over another.

Pressure Signature Extrapolation

The final analysis tool required for the sonic boom module is used to extrapolate a previously computed pressure signature for the aircraft's position on the ground. There are two candidate methods for this process, both discussed previously. The computer programs that have been developed using these methods are commonly known as the ARAP (ref.12) and Thomas (ref. 13) methods. The principal difference in the methods is related to how they account for non-linear effects in extrapolating the signature. The ARAP method essentially performs the extrapolation using the method described in sketch (e) The difference is that the F function shape is modified to include the atmospheric effects. The Thomas or Waveform Parameter Method determines the extrapolation effects using a previously calculated near field pressure signature. This provides the additional capability of

using measured near-field characteristics to initiate a ground pressure signature calculation.

As originally written, neither program could directly use the total equivalent area distribution as input. The ARAP program has since been modified to include a version of the method described in reference 10. This technique is used to convert an input equivalent area distribution to an F function, which is then fed to the extrapolation logic. For the Thomas program, the required pressure signature input can be provided by an application of the method described in reference 11. This method essentially computes an F function based on total equivilant area distribution and then uses the uniform atmosphere extrapolation technique to find the pressure signature a short distance from the aircraft. This pressure signature can then be supplied to the Thomas program. The "short distance", usually expressed as a multiple of the length of the aircraft, is a variable which is not specified clearly in any of the references. The distance should be large enough for the assumptions of linear theory to be valid, but not so large as to exclude a significant amount of real atmosphere effects.

The similarities in the ARAP and Thomas methods seemed to indicate that there would be little difference between the results from the two methods. The comparisons of the two methods focused on proving this assumption true for a wide range of flight conditions. In addition, it was desired to determine if one program had significant execution time advantage over the other.

The Mach 3.0 configuration geometry was selected for this study. The volume analysis and modified linear lift analysis programs previously discussed were used to generate a series of total equivalent area distributions for a range of Mach numbers and altitudes. These were then used as input for both extrapolation programs to compute the resulting ground overpressures based on steady level flight conditions. The results of this study are summarized on figures 26, 27 and 28. Each figure shows the calculated ground overpressure signature for a series of altitudes at Mach 3.0, 2.0 and 1.2 respectively. The standard method for representing a sonic boom signature is to plot the change in pressure from existing conditions versus the length of the pressure wave or time of occurrence relative to a sta-

tionary observer. All of the figures in this report use distance as the independent variable. The pressure values shown in the figures are increased by a reflection factor to include the effect of the reflection of the pressure wave off the ground. The value used for this reflection factor typically ranges between 1.9 and 2.0. A value of 1.9 was used for all calculations in the report. Considering the results as a whole, the expected agreement between the two methods was found to be extremely good. At Mach 3.0 and 2.0, both signature shape and pressure level agree very well. At the higher altitudes,. the pressure signature has the standard N shape with two shocks. The lower altitude signatures have multiple peaks indicating that not all the aircraft component induced shocks have coalesced. At Mach 3.0 and 2.0 the Thomas method consistently predicts signatures that are slightly longer than those of the ARAP method. The Mach 1.2 results show larger differences between the two methods, at least in terms of the magnitude of the overpressure. The lower altitudes used at Mach 1.2 are probably the cause of those differences. The altitudes selected at each Mach number are designed to be representative of potential operating conditions for supersonic aircraft. It was found that the results from the Thomas program became more sensitive to the value selected for the distance from the flight altitude to the initial waveform as the aircraft altitude was reduced. This parameter could be varied to force better agreement between the two methods. This was determined to be a deficiency in overall application of the Thomas method. Fortunately, these errors seem to be limited to a narrow range of flight conditions. Turning to execution time considerations, it is seen in table 6 that the ARAP method required slightly less time in all cases.

In addition to steady flight overpressures, the extrapolation routines will be required to predict the overpressures for a maneuvering aircraft. For the purpose of this work, the maneuvers will be restricted to flight in two dimensions, i.e. acceleration, climb, and change in flight path angle. The two candidate methods were compared for their ability to predict the overpressure for different values of acceleration rate, flight path angle and rate of change in flight path angle. The results are summarized in figure 29 which shows calculated maneuvering ground overpressure results based on a Mach = 2.0, h = 55,000 ft. area distribution input.

Good agreement was obtained for all acceleration and $\dot{\gamma}$ values. For values at constant γ the magnitude of the overpressure agreed well but the length of the signatures did not. The ARAP results showed that the length of the signature increased slightly with increasing γ. The Thomas results showed a significant decrease in the signature length. Determining the correct method proved a difficult task. There were no data available in the literature describing measured signatures for aircraft in steady state climbs. On one hand, it could be argued that the signature length would shorten due to the change in aspect of the signature with respect to the ground. On the other hand, the longer propagation distance created by the positive flight path angle should cause the signature to grow in length. Since the overpressure magnitude agreed very well, it was decided to leave this question temporarily unresolved.

The evaluation of the two methods for calculating the ground overpressure did not leave a clear choice as to which method to employ in the complete overpressure module. The ARAP method was slightly faster and more consistent over a wider range of Mach numbers and altitudes. The Thomas method was more flexible and offered the possibility of expansion to include a method of estimating the overpressure in a focus condition (ref. 25) Based on these choices, it was decided to include both methods in the overpressure tool.

IV. Development of the Overpressure Module

This chapter will describe the process required to combine the selected analysis tools into the complete overpressure module. The integration steps were combined with the development of a stand-alone computer program. There were two reasons for creating this stand-alone program. The first was to satisfy the first goal of this research project. That goal was to create a unified tool for the analysis of sonic boom overpressure. In order for that tool to be useful to configuration developers, it must be available for use independently of the vehicle performance analysis process. Further enhancement of the tool's usefulness will be realized through the incorporation of features such as interactive input and graphical display of results. These features would not be used when computing overpressures during performance analysis. The second reason for developing a stand alone program is to provide a means of debugging and validating the new overpressure tool before it is linked to a performance analysis program. The technique adopted for integrating the analysis tools was to develop the necessary geometry and data transfer methods while limiting the changes to the individual analysis programs. This modular approach will allow easy replacement of the analysis tools should superior methods be found at a later date. For the most part, this technique was successful. At certain points, it was deemed easier to add a simple modification to analysis tool rather than develop a new subprogram in order to maintain modularity.

Each of the selected analysis programs were written in the FORTRAN programming language. Therefore, the natural choice for any programming was to use the FORTRAN language. In some cases, it was necessary to update the analysis tools to the FORTRAN 77 standard before integrating them. The program was compiled and run using the FORTRAN compiler on three different UNIX architecture computer systems.

The steps taken to develop the overpressure module will be illustrated with the help of a flow chart for the stand-alone program shown in figure 30. An executive routine had to be written to provide for reading input flight conditions as well as choices as to what lift calculation and signature extrapolation methods to use. The decision was made to provide for both interactive and "batch" mode operations in the program. In the interactive mode, the program will prompt for the required flight condition and analysis choice inputs and generate graphical output of area distributions, F functions, and ground pressure signatures. The batch mode is designed to be used when many flight conditions are to be run in succession and only the final signature data are required. In this mode, all additional input data are read from the geometry data file. The use of both of these modes will be illustrated later.

The calculations proceed in a manner similar to that illustrated in figure 1. Area due to volume and equivalent area due to lift are calculated in the appropriate modules. Each analysis program is linked to the main program through an interface routine. This routine handles any necessary geometry conversions and formats the analysis results as required by the main program. These results are combined into a total area distribution which is supplied to the selected propagation routine. The ground overpressure is then calculated. An option is provided to compute overpressures for a series of maneuvers using a fixed equivalent area distribution. The user then has the option to stop or to continue with a calculation based on new flight conditions.

The following sections will provide details of some of the geometry and data manipulations required at different steps in the analysis process.

Geometry Considerations

The most important step in creating the overpressure module was the development of a method to generate a consistent set of models for the lift and volume analysis from a single geometry format. The geometry format used in the volume analysis contained the most detail and was therefore considered the best candidate to serve as the geometry base. All other required geometry data were either derived from this base or generated as described in the following paragraphs.

The first analysis module to be called is the area due to volume calculator. This module, derived from the wave drag computer program described in reference 16, provides a convenient routine for reading the geometry data. The output from this module is an array of x values and a corresponding array of areas representing the area due to volume for α= 0. The appropriate angle of attack corrections are made later in the program. The geometry and area due to volume data are transferred into storage arrays for use in repeat cases.

The second analysis to be performed is the calculation of the equivalent area due to lift. At this point there is a selection to be made based on user input. Either the pure linear or the modified linear analysis can be performed. If the modified linear analysis is selected, there is a further option to include the interference lift. This arrangement of lift analysis options was designed to separate the "quick and dirty" analysis methods from the more detailed techniques. In all cases, a geometry conversion routine was required to extract the required module inputs from the previously read geometry data. Although the linear and non-linear methods use very similar inputs, there were sufficient differences to preclude the use of a single conversion routine. It was possible, however, to extract the data for the modified linear and interference programs using a single translator.

Regardless of the method to be used, the problem that had to be solved was that of creating a geometry model which adequately simulated the models normally used for lift analysis. In the simplest of lift analysis models, no attempt is made to account for the presence of the fuselage. Examining the illustrations of wave drag geometry (figures 3, 16, and 17) reveals that in general, the wing is defined from the side of the fuselage outward. For simple lift models, all that is required is to replace the fuselage with an appropriate centerline airfoil. The process of analyzing the lift characteristics of a configuration will often include an attempt to capture the influence of the fuselage by shaping the inboard wing airfoils to simulate the fuselage geometry. Figure 31 illustrates two such models. Part a of the figure shows a relatively simple model of the Mach 2.7 configuration in which only the centerline airfoil is shaped to simulate the fuselage geometry. A more detailed model for the Mach 3.0 configuration is shown in part b of the figure. In this model several airfoils have been inserted between the centerline and wing root airfoils to provide better fuselage

definition. Techniques were developed to create both simple and more complex lift analysis models from the wave drag geometry data. These will be illustrated with the help of sketch (h).

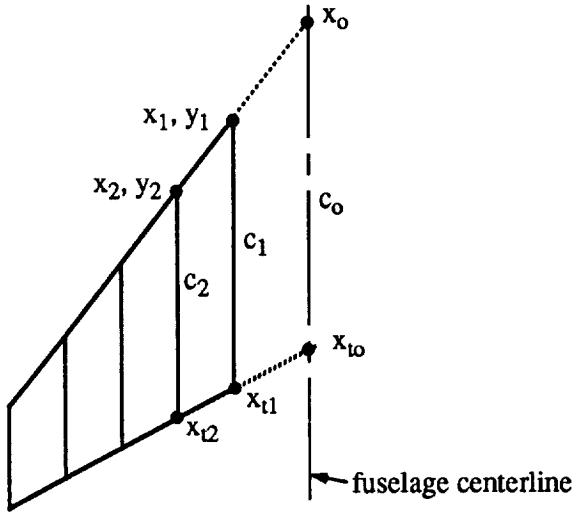

(a)

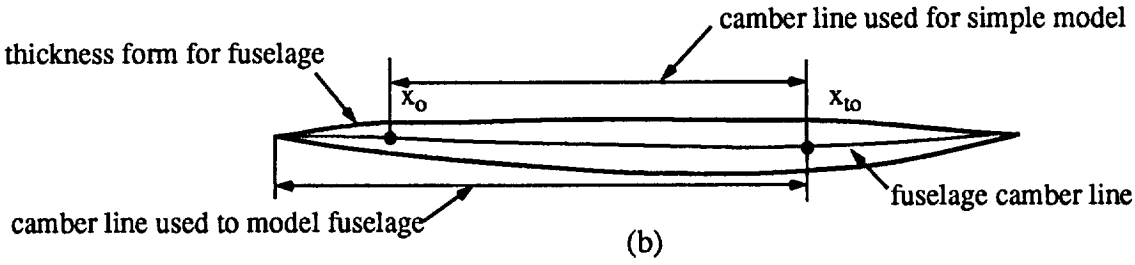

(b)

sketch (h)

In the wave drag geometry format, the wing is represented as a series of airfoils. Each airfoil is specified by the x,y,z coordinates of its leading edge, a chord length, z displacements for the camber line and thickness to chord ratios along that camber line. The latter two quantities are specified at fixed percent chord locations which are the same for each airfoil. Part a of the sketch shows a top view of the airfoils describing a wing. The new centerline airfoil coordinates for the simple wing model (x_0, c_0,x_{t0}) are created by extrapolating the values from the two innermost airfoils to y=0. The exception to this is if the extrapolation produces an x location which is beyond the nose of the aircraft. In such a case, the centerline airfoil leading edge is set at x_0=0. For both models, the camber line for the

centerline airfoil is determined from the camber of the fuselage.

Part b of sketch (h) illustrates the side view of a fuselage with its camber line. The points x_o and x_{to} locate the leading and trailing edges points projected from the root airfoil. In the case of the simple wing model, the camber for the centerline airfoil is taken as the portion of the fuselage camber line between these points. For the more detailed modelling, the camber line begins at the configuration nose. Either method will produce a smooth camber surface when applied to a configuration geometry with a well-integrated wing and fuselage. The thickness for the centerline airfoil is needed for the modified linear methods. For the simple model, the thickness ratios from the original side of the fuselage airfoil are used. As shown in the sketch, the upper and lower contours from the fuselage data are used to define the thickness for the more detailed model.The data needed to define the rest of the wing geometry were directly available from the wave drag geometry input. All that was necessary was to provide a means of extracting the data in new arrays which could be used by the lift analysis programs. Figures 32 and 33 show both simple and detailed models generated for the Mach 2.7 and 3.0 configurations. Note that for the Mach 3.0 configuration, the nose of the aircraft restricted the location of the leading edge of the centerline airfoil. The results in a slightly odd planform shape. The effect of such a planform change will be illustrated later.

The process of aircraft configuration development will generally yield models with wing and fuselage modelled separately. Thus in most cases, the above wing geometry modelling techniques must be applied. Occasionally, however, a detailed analysis model is created in using wing geometry alone. Such is the case of the Mach 3.0 configuration illustrated in of figure 31. This model accurately simulates both the volume and lift characteristics (The fuselage tailcone, fin and nacelles are not illustrated in the figure.) The capability to read configurations modelled in this format was included in the overpressure module. In this case, there was no need to generate a centerline airfoil. The geometry conversion modules were set up to recognize all wing geometry and bypass the above modelling steps. In general, it is not desired to include the tail of the fuselage in the lift calculations. A user-supplied input was selected as the method of identifying the x loca-

tion at which to terminate the wing model. Comparisons of the lift results for all wing versus wing-body models will be included in the analysis of the completed overpressure module.

The same geometry translator was used to extract wing geometry data for both the modified linear and interference lift programs. To avoid unnecessary confusion, the interference lift program was modified so that is used the same geometry variable naming convention as the modified linear program. The interference program also required the nacelle geometry as part of its input. In the wave drag geometry format, up to six nacelles or pods can be specified for each side of the fuselage. The pods are defined by an x,y,z location and array of cross sectional areas versus x station. Each pod must be of circular cross section but may be different from the other pods. However, since the pods are generally used to describe engine nacelles, they are usually identical except for their locations.

Exceptions to this include cases such as the Mach 3.0 configuration geometry (fig. 3) which, in addition to engine nacelles, uses small pods to represent boundary layer diverters. The interference lift program is restricted to using only identically shaped pods. This restriction forced a decision to use only pods representing engine nacelles in the interference lift analysis. A user input identified which pods to include in this analysis. An additional restriction of the interference lift program is that the pod cross sectional areas must be specified at equally spaced z increments. The geometry translator includes an interpolation scheme for this purpose.

Lift Analysis

Lift and Angle of Attack Calculations

One important operation that was required in the lift analysis routine involved the calculation of total lift and angle of attack. In the original separated process of computing boom, the lift is computed for a selected angle of attack. When aircraft performance analysis is being performed, lift is the known quantity and α must be computed. Both options were included in the sonic boom module.

In the case of the linear lift method, providing both options was a simple task handled

in the interface routine. The output of the linear program is separated into components due to camber and flat plate. Both the lift distribution and total lift data are so separated. The lift distribution is also non-dimensionalized by the total lift. The equation for the total lift coefficient is

$$C_L = C_{L_{camber}} + C_{L_{\alpha,flatplate}} \times \alpha$$

where $C_{L_{camber}}$ and $C_{L_{\alpha,flatplate}}$ are computed by the lift program. This equation can be solved for either C_L or α depending on which is required. Once C_L and α have been determined, the dimensional equivalent area curve can be computed and modified for angle of attack, as described earlier.

The situation is somewhat more complicated with the modified linear lift analysis. Because of the non-linear character of the pressure coefficient calculation, it is not possible to separate the camber, thickness and flat plate components of lift. Thus, a simple expression like the one above cannot be obtained. The program is designed to compute the C_L for any α but required modification to perform the opposite calculation by iteration. Close examination of the program logic revealed that it was possible to separate the calculation of the velocity components from the calculation of the pressure coefficients and incremental forces. The logic for calculating angle of attack for a specified lift is illustrated in the flow chart in figure 34. The separation of the two calculations results in a significant savings of execution time over using repeated passes through the entire program to solve for a single α. Once the angle of attack has been found, it and the related pressure coefficient data, along with the necessary geometry information, are used to compute the equivalent area distribution as described previously,

Interference Lift Increment

Another area in which it proved necessary to modify the lift analysis program was the incorporation of the lift increment due to interference. The total force generated by the shock induced interference is expressed in terms of a normal and axial force components

which are invariant with angle of attack. The shape of the lift equivalent area curves, however, are effected in the manner previously described. This suggested that the calculations could be separated as shown in the flow chart in figure 34. If interference is to be included, the interference forces are calculated before the wing lift. These calculations are performed without need of knowing the final α. The interference lift increment is then added to the wing lift in the lift program. In the case of finding the α required for a given lift, the interference increment is included in the iteration process. For any given estimate of α, the interference lift is calculated from

$$C_{L_{int}} = C_{N_{int}} \times \cos\alpha - C_{A_{int}} \times \sin\alpha$$

The total lift coefficient is then computed from

$$C_{L_{tot}} = C_{L_{wing}} + C_{L_{int}}$$

It is this value that is tested to determine if the proper α has been found. The angle of attack correction for the interference lift equivalent area distribution is made at the same time as the corrections to the volume area as described below.

Total Area Distribution

Once the individual components of the equivalent body area distribution have been calculated by the respective modules, they can be summed into a total distribution for use in the extrapolation routine. A subroutine was written in the overpressure module to handle this task. At this point in the process, regardless of the input selections, the angle of attack is known. Therefore, final angle of attack corrections are made to the volume area and interference lift distributions. The corrections to the volume area curve are made by using the approximate formulas described in an earlier section. The correction for the interference lift distribution effects the position where the lift acts through the equation

$$x' = x \times (1 - \beta\tan\alpha)\cos\alpha$$

After the corrections for angle of attack are complete, the overall length of the total equivalent area distribution can be determined. Because of corrections for angle of attack, and the displacement of lifting surfaces, each equivalent area distribution may have a different

length. The length of the total area distribution is determined by the difference between the minimum and maximum of each individual distribution. For those components with lengths less than the maximum length, the last area value is used to extend that distribution to the maximum length. The individual areas are then summed to develop the total area distribution. Both the F function calculation routine in the ARAP program and the near field signature routine in the Thomas program require that the input area distribution be at equally spaced x intervals. This is insured by an interpolation routine which is incorporated in the total equivalent area summation process.

Propagation Modules

Very little integration work was required to join either of the propagation programs to the overpressure prediction module. The total area distribution and the flight conditions had to be transferred to the programs via arrays. The original memory allocation scheme for the ARAP program made extensive use of the FORTRAN construct known as "blank common." The arrangement of this blank common proved difficult to manage in the integrated system. A new memory allocation structure utilizing named common blocks was created to solve these difficulties. For cases at high Mach numbers and altitudes, it was found that the original length of the input total area distribution did not always provide for an F function with length sufficient to determine the location of the tail shock in either propagation module. To solve this problem, the area distribution and resulting F functions were extended by adding a series of maximum equivalent area values at equal increments beyond the end of the computed total equivalent area distribution.

Both the ARAP and Thomas method contain logic to identify cut-off and focus conditions. For the purposes of this work, the identification of these calculations was all that was necessary. Both programs were modified to print out the location of such conditions and then return control to the main program, thus terminating the calculation for that particular case.

Additional Features

As stated previously, one of the purposes of developing the stand-alone version of the overpressure module was to provide a method of quickly evaluating the boom characteris-

tics of an evolving aircraft configuration. In order to provide a means of comparing results with those of other configurations a simple graphical output capability was added to the stand-alone program. This provides plots of the area distributions, F functions and ground overpressures which can be viewed on the computer screen or printed on a hard copy device.

Another important capability added to the stand-alone program involved saving the data necessary to rapidly repeat certain parts of the analysis. The total lift equivalent area distribution computed based on a Mach number, altitude and lift condition was stored to allow for the analysis of several different maneuver conditions or for the comparison of results from the two extrapolation methods. In addition, Mach number dependent data from the volume wing lift and interference lift analysis was stored to allow for computing a series of results at different altitude and lift conditions at a greatly increased execution speed.

The version of the program suitable for incorporation into a performance program was only slightly different from the stand-alone version. The executive program became an executive subroutine which would be called using the desired Mach, altitude lift or angle of attack and maneuver data as parameters. The interactive input mode was eliminated. All inputs such as choices for lift analysis and extrapolation method were passed to the program via a FORTRAN 'namelist" input which is read before the geometry data from a special input file. The plotting capability was deactivated, but the repeat case logic was retained. This was done to allow rapid evaluation of the boom characteristics at a series of cruise weight conditions. All of the required code was then stored as a library file which could be included in the load statement for the selected performance analysis program.

V. Validation of the Overpressure Module

The purpose of this chapter is to describe the process of validating the new overpressure module. This validation process consisted of two different steps. The first part of the process involved comparing the results of the new program with previously reported experimental and theoretical data. The second part of the validation process concentrated on finalizing answers to some of the questions regarding analysis and modeling methods that were raised in the earlier sections of this report.

A large body of data exists comparing the results of linear theory sonic boom signature calculations with flight and wind tunnel experiments. Some of these results are reported in references 3 and 4. Unfortunately, many of the geometry models used in these studies are no longer available and hence the resulting comparisons cannot be duplicated. However, this should not hinder the process of developing a validation of the new overpressure module. The body of published comparison data serves well in showing the validity of the linear theory methods applied. All that remains to be demonstrated is whether the combined methods can produce results similar to measurements and calculations made previously.

Comparison with Experimental Data

A good source of measured data is the low boom configurations tested in reference 14. The geometric data for the models used was still readily available. The Mach 2.7 reference arrow wing geometry described earlier is one of the configurations tested in this report. The report presents wind tunnel pressure measurements for two reference configurations and three configurations designed to produce shaped low boom ground pressure signatures. Theoretical comparisons are provided for the near field pressure measured on the low boom designs. Comparisons were made with the results for low boom arrow wing de-

sign. This model, shown in figure 35, is similar to the previously described reference arrow wing configuration. Differences include a longer lifting length and significant dihedral on the low boom configuration. The forebody of the low boom model is also shaped to control the nose shock. All of the models tested used uncambered wing geometry. The theoretical comparisons in the report used linear theory models. For the purposes of this report, the modified linear option was selected. The stand alone overpressure program was used to calculate the volume and lift equivalent area distribution for the low boom geometry at the reported test conditions of Mach 2.7, $\alpha = 2.033$ deg. The results of these calculations are compared with the data of reference 14 in figure 36, part a. The figure shows that excellent agreement was obtained, particularly in the region near the configuration nose. The format for these area distribution presentations is slightly different from earlier figures in that non-dimensional quantities were used. The equivalent length l_e was determined using the methods presented in reference 14. The pressure data presented in the reference were measured using a movable probe positioned approximately three body lengths away from the model in the uniform atmosphere of the wind tunnel. The new overpressure tool can calculate similar data using the near field wave form method associated with the Thomas signature extrapolation program. The results of these calculations are presented in part b of figure 36. The calculated pressure signatures are seen to agree reasonably well with the experimental results and very well with the theoretical results presented in reference 14. In reference 14, better agreement with the experiment was obtained by adding a boundary layer thickness correction to the calculated area distribution.

Comparison with Theoretical Data

A comparison with some more recent results was performed using data available from the authors of reference 26. This paper presented a study of overpressure trends with weight, altitude, and Mach number for two Mach 2.0 transport configuration models. One of these configurations represented a vehicle designed to optimize aerodynamic performance with little regard to sonic boom considerations. The configuration, shown in figure 37, has certain characteristics in common with the Mach 3.0 vehicle used in other sections of this report. Reference 26 designates this as Configuration I and this designation will be

applied in this report. The second (designated Configuration II and illustrated in figure 38) was designed to produce a shaped pressure signature at the ground. This overpressure shape, known as a "flat top" signature, has been shown to be more acceptable to the human ear that the N wave. In addition to beneficial effects of shape, this signature makes it possible to achieve a lower nose shock Δp for a given value of lift. A Δp of 1.0 psf has long been considered a guideline value for acceptable overland supersonic flight. The flat top signature shape is obtained through careful tailoring of both the volume and lift distribution of the low boom model. Demonstrating the capability to calculate such signatures was an important part of validating the new overpressure module.

In reference 26, the overpressure trend curves were generated by first calculating detailed volume, wing and interference lift distributions at fixed altitude, lift and Mach number. Overpressure trends with altitude were then computed using a feature of the ARAP program that approximates the variation of the lift distribution with changing C_L.The comparisons presented in this report will focus on duplicating selected baseline total area distributions and ground pressure signatures. It is believed, however, that the new overpressure program is capable of generating more accurate trend data because it includes the effect of angle of attack on both volume and lift as lift coefficient varies.

Comparisons of the total area distributions and ground pressure signatures for data generated in the new overpressure program and reference 26 are shown in figures 39 through 42. The first two results are for Configuration I at Mach 2.0 and 1.2 respectively. The equivalent area distributions were calculated using the modified linear method and included interference lift effects. A value of JBYMAX of 30 was used in the lift analysis. The figures show that excellent agreement was obtained for both the equivalent area distribution and the corresponding ground overpressure and signature shape.

Figures 41 and 42 show similar results calculated for configuration II. In the design of a low boom configuration, a certain Mach/altitude/weight combination must be selected as a design point. These parameters are then used in the boom minimization theory to develop a target equivalent area distribution curve. The actual configuration volume and lift distribution is then developed to closely match this theoretical shape. For configuration II, the

design point selected was Mach = 2.0, h = 55,000 ft, L = 50,000 lbs. The results for this design point are shown in figure 41. In addition to the results from reference 26, and the present method, curves showing the required theoretical shape and corresponding boom signature are included. It can be seem the term flat top signature derives from the fact that the signature is characterized by an initial shock followed by a constant pressure section. The volume distributions show that although the overall agreement was good, neither reference 26 results nor the present method results agree exactly with the theoretical minimum shape. The corresponding ground signatures reveal that both calculated results do not predict an ideal flat top wave form. In the area of theoretical constant pressure both signatures contain many small shock related pressure jumps. There are three explanations for this behavior. The first, at least for a portion of the disagreement, derives from the fact that the calculated area distributions do not exactly match the theoretical curve. Since the design of such a tailored volume and lift distribution involved a complicated interaction of both configuration shaping and wing design, it is not possible to get an exact agreement. In addition, the integration scheme from reference 10 uses an integration method of linked parabolas to determine the F- function. This method introduces discontinuities in the F function which can affect the resulting pressure signature. The third factor may be that there are components of the configuration producing small shock waves which do not coalesce before the pressure disturbance reaches the ground. The important fact to realize is that the new overpressure module is able to calculate the low boom configuration overpressure shape to the same degree of accuracy as the original separate analysis processes. This fact resolved a major concern in the validation of the new tool.

To complete the comparisons with the results of reference 26, an off design flight condition was analyzed for configuration II. The results of this comparison, shown in figure 42, again showed that good agreement was obtained with the new program. The ground overpressure signature indicates that the low boom configurations can produce undesirable off design wave forms. The effects of these signatures will be addressed further when the overall flight performance of this configuration is discussed.

Lift Analysis Method Selection

The discussion above addressed the overall accuracy of the results obtained using the new overpressure program. The following sections are devoted to finalizing the answers to some of the questions raised in evaluating the different analysis tools. This will be done by using the new program to compute ground overpressure signatures based on complete configurations. Signatures will be generated using each analysis method or model in question. Comparison of these results will be used to make the final judgements.

The first area to be addressed is that of the choice of appropriate lift analysis methods. Recall that in the section that evaluated the linear and modified linear methods, it was found that in some cases, it was difficult to determine a clear choice of method based on the equivalent area distribution results alone. The selection was clarified by computing ground overpressures for the same flight conditions as used in the lift method study. The results of the new study are presented in figures 43, 44 and 45 for the reference arrow wing, the Mach 2.7 and the Mach 3.0 configurations respectively. The pressure signatures shown were computed using the same Mach, altitude and lift combinations used in the previous analysis. However, the signatures are based on total equivalent area, not just the lift area. The comments on the results apply to all these configurations equally. With the exception of Mach 1.2, the pressure signatures computed with the linear and modified linear programs seem to agree very well. Both the magnitude of the initial overpressure (Δp) and the overall length of the signatures are predicted very closely. There are differences in magnitude and position of intermediate shock-induced pressure changes. For the purposes of this work, these errors are not deemed important. This is not true, however, for the results at Mach 1.2. As could be expected, the rapid changes in the slope of the linear area curve produced substantial differences in the two computed ground signatures. Based on these results, it can be stated the use of the linear method is perfectly valid above Mach 1.4. Below that Mach number, the modified linear method must be used to insure accurate results.

A comparison of ground overpressure for results of the study of interference lift effects was also performed. Again in this study, ground overpressures based on complete configu-

rations were calculated using the same Mach, altitude and lift values as the previous studies. The resulting signatures for the Mach 2.7 and 3.0 configurations are shown in figures 46 and 47. The figures reveal that in all cases, the addition of the interference lift component does little to change the initial overpressure or the lengths of the signatures. In general, the only differences are in the location of the intermediate shocks.

The overall conclusion of these two studies is that for the purposes of computing sonic boom during performance analysis, it is possible to generate accurate pressure signature data using linear lift analysis alone. This is not true, of course, at Mach numbers below 1.4.

Lift Analysis Modeling

Another area of the new overpressure module which required further validation was the difference in the type of model used for the analysis of the lift equivalent area distributions. In the previous chapter a simple wing alone modeling and a more detailed model including a representation of the fuselage were discussed. In addition, an all -wing geometry representation was introduced. It is the purpose of this section to compare the results of these different types of models. The comparisons were performed by calculating total equivalent area distributions and ground pressure signatures using all three types of modelling. The results of these comparisons for the Mach 2.7 and Mach 3.0 configurations are shown in figures 48 and 49. Two Mach numbers were analyzed for each model. The upper portion of each figure illustrates the lift equivalent area distributions while the lower shows the ground pressure signature corresponding to the total area distribution. The lift equivalent area distributions are shown to more clearly illustrate the difference in the modeling methods. The ground pressure signature results show the effects of the differences on the overall answer. Because of differences in available all-wing geometries, different conclusions were drawn from the analyses of the Mach 2.7 and 3.0 configurations. These conclusions will be presented separately.

Considering figures 31a and 32, which illustrate the different models of the Mach 2.7 configuration, it can be seen that the all-wing model uses only a modified centerline airfoil to include the fuselage geometry. Because of the close relationship between this model

and the wing-fuselage modelling method, it was expected that the results from these two models would agree closely. Figure 48 confirms that expectation. The wing alone results do not predict any lift off the forward fuselage and this can be seen in the lift equivalent area distributions. However, the resulting curves are similar in their other characteristics, particularly the slopes of the curves. These similarities result in ground pressure signatures which agree remarkably well. The conclusion drawn from this analysis is that in linear analysis, fuselage lift modeling does not have a major impact on the sonic boom overpressure.The fuselage model is important in configuration moment analysis, however.

Figure 49 illustrates similar lift area and ground overpressure data for the Mach 3.0 configuration models. In this case however, the best agreement is between the wing alone and the wing/fuselage model. The small difference these two results stems from the fact that this is a highly blended configuration, with the wing extending forward to the nose of the fuselage. Neither of these two models agree very well with the results from the all-wing model. The differences do not show very much in the Mach 1.2 lift distributions, but at Mach 3.0 significant slope differences are noticeable. The ground pressure signature reveals that most of the differences are absorbed in the extrapolation of the waveform based on the total area distribution. Nose shock overpressure and signature shape changes are apparent, however. The difference in the lift analysis results were at first thought to result from the blunted nose and additional fuselage thickness present in the all-wing model. (Compare figures 31b and 33.) This raised concern over the validity of the method used for lift analysis modeling in the new overpressure module. A closer examination of the all-wing model revealed a significant difference in the centerline camber when compared to the fuselage camber of the wing body model. Correcting this difference resulted in a virtually complete agreement between the three types of modeling. The conclusion reached from this comparison study was that the shape of the camber surface is perhaps the main driver of the shape of the lift area distribution and care must be taken to model this part of the configuration geometry accurately.

Pressure Signature Extrapolation

The final area for which a question of best method was left unresolved concerned the

ARAP and Thomas signature extrapolation methods. In generating all of the ground signatures illustrated above and in the following chapters, the two methods continually exhibited good agreement in nose shock overpressure levels. Signature shape agreement was also good, with the exception of cases involving non-zero flight path angles. The near field wave form program used with the Thomas method proved an important tool for validating wind tunnel measurements. It was found, however, that the ARAP program was a considerably more robust computer code. While the Thomas program would occasionally "crash" for unknown reasons, the ARAP method completed every calculation. For this reason, the ARAP option became the option of choice in the application of the new boom module in aircraft performance prediction.

VI. Application to Aircraft Performance Analysis

Upon completion of the validation of the new overpressure module using the stand-alone program version, it was possible to integrate the new program with an existing aircraft performance program and study the sonic boom characteristics of an aircraft throughout its flight envelope. It is the purpose of this chapter to provide the details of this process. The chapter begins with a description of the performance prediction program and the integration process. The two Mach 2.0 configurations described in reference 26 are then used to illustrate the application to performance analysis study. This will include a study of boom signatures along typical supersonic transport flight profiles and at other points in the aircraft flight envelope. The effects of two dimensional maneuvers typical in supersonic flight will be illustrated. Finally, the results of a study of climb flight path modification for reduced ground overpressure will be presented.

Aircraft mission performance analysis involves using a computer program to predict the flight characteristics and fuel usage of an aircraft for a particular flight or mission. The program uses a numerical representation of the aerodynamic and propulsion characteristics of the aircraft to solve the two dimensional equations of motion in various flight segments. These segments include climb, cruise descent and hold segments for the primary and reserve missions. The vehicle weight at the end of a given segment is used as the starting weight for the next segment. Typically, the parameters of interest are the total distance that can be flown for a given fuel load (range), the fuel burn or time required for a particular mission segment, or the fuel required to fly a specified range. The Mach number (or speed) -altitude schedule that the airplane follows during a flight is termed the flight profile. This profile may be varied to determine the minimum fuel burn or time required to perform a single or combination of segments. The complete range of Mach number -alti-

tude combinations for which the airplane can maintain equilibrium (non-accelerated) flight without violating structural or other constraints is known as the flight envelope.

There are many different computer programs available for the calculation of aircraft performance. The program selected for this study is described in reference 27. The principal reasons for using this program was the ready availability of the FORTRAN source code and this author's familiarity with the program. Integration of the sonic boom module proved a relatively easy task. It was first necessary to find the points in the program where any iteration to solve the equation of motion for a single step along a segment of the flight profile was complete. At that point the lift, Mach number, altitude, flight path angle, pitch and acceleration rates are known and can be passed to the boom module. Note that the lift value is passed to the boom module rather than the weight. In equilibrium or cruise flight, lift and weight are approximately equal. A slight difference in the two values results from the effects of flight path angle and any angle between the thrust force and velocity vectors. In non-equilibrium (climbing or descending) flight, lift is not equal to weight. It is the required lift that is important to the boom analysis. Weight, however, is generally used in the measure of aircraft performance. The mission segments considered in this study consisted of the supersonic ($M > 1.16$) portions of the main mission climb, cruise and descent segments. Inputs were added to the performance program to control whether or not the boom calculations would be performed and whether or not the maneuver data would be used in the extrapolation of the pressure signatures. The boom module was modified so that the required geometry data were read on the initial call to the module. The previously described batch mode input is used to read data for selection of analysis methods.

Flight Profile Analysis

The next section of the chapter will address the calculation of overpressure along typical flight profiles for the two Mach 2.0 configurations studied in reference 26. As mentioned previously, the low boom configuration described in the report was designed to achieve a flat top pressure signature at $M = 2.0$, $h = 55{,}000$ ft, and $L = 550{,}000$ lbs. For the purpose of comparing the two configurations, a decision was made to try a match the lift and Mach number at the start of the cruise segment. The cruise altitude would be deter-

mined by the cruise optimization logic in the performance program. This was achieved by varying the takeoff gross weight of the two configurations. For configuration I, the TOGW that resulted in the closest match at the start of cruise was 585,000 lbs. Configuration II required a TOGW of 590.000 lbs.

After determining the gross weight required to match the selected start of cruise conditions, the boom module was activated and the boom overpressure levels and signature shapes were calculated to baseline flight profiles. For configuration I, the results of these calculations are illustrated in figure 50 and table 7. The flight profile represented in the figure is typical of the type of profiles used for minimum fuel burn to a specified range. In these flight profiles, the aircraft will accelerate at low altitude until a constraint such as dynamic pressure limit is reached. On this profile, q_{max} of 1000 psf is reached at M = 1.25. The configuration then climbs and accelerates at the dynamic pressure limit until the cruise Mach number is reached. A climb at constant Mach number is then performed until the optimum cruise altitude is reached. The cruise is flown at constant C_L which forces a very gradual climb during the cruise leg. The descent is flown at the maximum available lift-drag ratio. For clarity, only the supersonic portions of the flight profile are shown on the figure.

In addition to illustrating the flight profile, figure 50 also illustrates ground overpressures generated at ten specific points along the flight profile. Each of the signature shapes is plotted to the same scale to provide an image of how the signature varies during the flight. Table 7 presents the nose shock overpressures (Δp) corresponding to the signatures. The signatures were calculated using the modified linear theory with JBYMAX = 30. Interference lift was not included. The low altitude of the initial climb results in very large values of Δp for this segment. Also, the signatures exhibit a large amount of near-field behavior. More specifically, the short propagation distance does not allow the shock waves produced by various aircraft components to coalesce into the familiar N-wave shape. The result is a signature with a series of small pressure jumps and one large pressure increase. This behavior continues until the cruise Mach number is reached. As the aircraft climbs to the start of the cruise point, the signature becomes more far-field and develops the charac-

teristic N wave shape. Note also the increasing signature length as the aircraft climbs and accelerates. Table 7 indicates that the nose shock overpressure varies from 1.6 to 1.1 psf as the altitude increases and required lift decreases during cruise. The figure also indicates that there is a substantial decrease in the magnitude of a secondary pressure jump in the signature. The descent segment shows that the signature transitions from an N-wave to a near-field type signature as the aircraft decelerates and descends. The overpressure magnitude is considerably less than that developed during the climb. This is, of course, due to the higher altitudes and lower weights during this portion of the flight.

The signatures shown in figure 50 were computed based on a steady state fight analysis. The effect of acceleration and changing flight path angle were not included in this first analysis. The calculations were then repeated with the maneuver option selected. The results of including the maneuver effects are summarized in table 8. This table contains the flight path angle, and the acceleration and pitch rates computed by the performance program and passed to the sonic boom analysis module for each point illustrated in figure 50. It can be seen from the table that at least for supersonic transport-type aircraft, the rate of change of both velocity and pitch angle are very low. The majority of the climb and descent segments take place at small flight path angles. Because of this, the effect on both the nose shock overpressure and the signature shapes are found to be very small. Table 8 contains a comparison of the overpressure results. An exception to these small effects may be the result of the focus condition that occurs as an aircraft accelerates through Mach 1.0. Such conditions were not evaluated as part of this research project. One reason for this is the desire to keep the present analysis well within the accepted region of validity for linear methods. This restricted the Mach numbers to values above M = 1.2. In addition, acceleration rates typical of supersonic transports resulted in cut-off conditions for Mach numbers less than 1.15 and altitudes above 35,000 feet. Because of this no focus conditions were found at ground level in the present analysis. This does not mean that the sonic boom focusing is not a problem for supersonic transport aircraft. The focus phenomenon certainly requires further study.

The flight profile analysis was also performed for the low boom configuration of refer-

ence 26. The flight profile flown was identical to that of the analysis for configuration I. The results for configuration II are shown in figure 51 and table 9. Overall, the results show that configuration II achieves significantly lower boom levels than configuration I. Figure 51 does show that during the minimum fuel climb, a rather strong nose shock is present. During climb to cruise Mach number, this shock damps out and the flat top signature shape is achieved. The flat top signature is maintained throughout the cruise flight despite large lift and altitude variations from the design point. During the descent, a nose and secondary shock phenomenon appears in the signature. The magnitude of the overpressure is again greatly reduced from the climb value due to the low weight and higher altitude of this mission segment.

The above description serves to demonstrate that the new boom module, combined with an aircraft performance analysis program, can be used to reveal a great deal about the characteristics of the boom signature during an aircraft's flight. Perhaps most importantly, it has been revealed that an aircraft with otherwise acceptable cruise boom characteristics may exhibit excess overpressure levels during certain mission segments. The following sections of this chapter will describe a method through which the new boom module may be used to alleviate these problems.

Boom Contours

In order to develop methods to reduce the ground overpressure resulting from a particular flight profile, it is necessary to study how the boom characteristics vary throughout the complete flight envelope of a configuration. A unique new capability for performing such studies was created through the development of the new overpressure module. The repeat case logic in the stand alone program can be used to rapidly compute ground overpressure data for a large number of Mach-altitude flight conditions. These calculations can be performed at either constant lift or lift varying with Mach number. The results of these calculations can then be used with a contour generation program to develop contours that show the variation of overpressure parameters through an aircraft's flight envelope. Such contours, illustrating the nose shock overpressure levels for the two Mach 2.0 configurations, are shown in figures 52 and 53. For each configuration, contour data are shown for

constant lift values of 550,000 and 350,000 lbs. These lift values were chosen because they correspond approximately to the required lift at the start and end of cruise for the flight profiles previously illustrated. Additional contours were generated with the lift varying with Mach number to simulate the effect of weight changes during the climb. The climb fuel requirements for these aircraft varied between 30,000 and 50,000 lbs. Incorporating such a variation of lift did not result in contours significantly different from the contours shown for the constant 550,000 lb. lift case. Because of this, it was deemed unnecessary to include the varying lift results. Valid observations about the overpressure characteristics during both climb and cruise segments can be drawn from the constant lift contours.

Before analyzing the specific characteristics of each configuration, some general conclusion can be drawn from the study of the nose shock Δp contours. The first of these conclusions relates to the Δp levels at low altitudes. In all cases studies, the Δp levels begin to increase rapidly below an altitude of approximately 30,000 ft. In addition, the overpressure at these altitude become less dependent on Mach number and lift and are more a function of altitude alone. These high overpressures at low altitude are generally not a problem for supersonic transport aircraft. An exception to this occurs during minimum fuel climb segments. This will be further discussed in the next section. A second phenomenon common to all of the contours shown is a rapid increase of overpressure that occurs in an altitude band which varies depending on configuration and lift. This increase is due principally to the transition from near-field type signatures to far-field N-wave signatures. This transition is caused by the coalescing of the numerous small shocks in a near-field signature into a large nose and tail shock. After transition occurs, the Δp values again begin to decrease with altitude due to the attenuation of the atmosphere.

A third interesting phenomenon common to all of the contours has to do with the Mach number at which a minimum Δp can be achieved. Considering altitudes above 30,000 ft., the minimum Δp seems to occur in the Mach number range of approximately 1.25 to 1.5. This fact has important implication in the study of dual Mach number configurations. These vehicles would be designed to cruise at a low Mach overland for reduced

boom levels. They would fly at higher Mach numbers over water where the overpressure level is not a problem. Such mixed Mach number flights were not considered as part of this research.

Some more specific comments can be made about the contours for each configurations. For configuration I, it can be seen that at 550,000 lbs. lift, the target overpressure of 1.0 psf can only be achieved in a very small region of the flight envelope. The relatively low Mach number and high altitude for this point makes efficient flight at this condition very difficult. The region of 1.0 psf Δp expands somewhat when the lift is decreased to 350,000 lbs. It is also important to note that at 550,000 lbs., minimum Δp values of only slightly less than 2.0 are possible at the cruise Mach number of 2.0. Values as low as 1.4 are possible at 350,000 lbs. Compared to the results for the low boom configuration, the contours of figure 52 appear somewhat irregular. The reason for this is the fact that there are numerous relatively strong shock waves in the configuration I pressure signature. Depending on Mach number, these shocks coalesce at different altitudes causing small increases in the nose shock, Δp. This results in the irregular contour shapes and small islands of depressed or elevated Δp levels.

The secondary shocks in the signature for configuration II are much smaller. Therefore, the contours in figure 53 show a steady rate of change with Mach and altitude. Overall, the Δp levels of this configuration are much lower than for configuration I. This fact applies at altitudes above 30,000 ft. It is interesting to note that below this altitude, the trends for the two vehicles are much the same. At 550,000 lbs, the low boom configuration can achieve a Δp of 1.0 psf at all Mach numbers. The altitudes required to achieve this are reasonable from a performance standpoint above Mach 1.2. One of the important facts gained from figure 53 is that the Δp contours for the low boom configuration are relatively independent of weight. At 350,000 lbs., there is a larger region where Δp of less than 0.7 psf can be achieved. Also, at this lower weight, the transition altitude has moved beyond the limits of the flight envelope. However, when considering overpressures greater than 0.9 psf, the two contour plots are quite similar. This is important because it relieves any need to tailor the cruise flight to meet any boom restrictions.

It is important to note that the transition for low to high Δp for this configuration takes place over a very small altitude range. Above this transition point, the Δp levels are clearly unacceptable for overland flight. The transition behavior is consistent with results from reference 26. For this configuration, however, the transition altitude is at the high limit of altitude for efficient cruise flight.

Reduced Boom Climb Profiles

The information contained in the contour plots described above can be used to develop flight profiles with reduced ground overpressure levels. The flight profile studies previously presented indicated that the largest overpressure problem concerned the climb segment of the flight. This section will present the results of an effort to reduce the climb overpressure levels by modifying the Mach-altitude climb schedule. Consider again the Δp contours for lift equal 550,000 lbs. The contours are shown again in figures 54 and 55. In these figures, several lines have been added to illustrate potential climb schedules. To more correctly simulate the overpressure contours for climb flight, these contours should be calculated at varying lift. However, as mentioned previously, the effect of the weight change on contour shape has been found to be small. The development of a low boom climb path for configuration I will be illustrated first. Figure 54 shows two climb schedules. The minimum fuel climb path is the one described in the previous flight profile analysis section. It is clear from the figure that the low altitude used to minimize fuel burn forces the climb into the boom contour region below 30,000 ft. where excessively high ground overpressures are developed. To avoid this area, the supersonic portion of the climb must be flown at higher altitude. How high can be determined from a combination of the boom contour data and consideration of some practical operational constraints. The high drag associated with transonic flight generally requires that an aircraft accelerate through this region at constant or near constant altitude. Given only this constraint, the boom contour data suggest that the ideal minimum boom climb schedule would force the configuration to climb subsonically to approximately 48,000 ft. and the accelerate to Mach 1.25 while climbing only slightly. From that point, a slight descent would be required while accelerating to Mach 1.82. A level acceleration to Mach 2.0 would complete the

climb. This profile, however, is not practical for several reasons. Climbing to a very high altitude before accelerating through Mach 1.0 puts the aircraft in a position where the ratio of thrust to drag (thrust margin) is small. This small thrust margin results in very low acceleration rates and high fuel consumption. The requirement for a descent during a climb segment is not practical from the point of view of either passenger comfort or air traffic control system integration. A much more practical low boom climb path is illustrated in figure 54. Although this path does not reach the lowest Δp value possible, it produce a relatively constant ground overpressure value. The altitude for transonic acceleration is much more reasonable and a constant climb is maintained. Figure 56 and table 10 present the ground overpressure levels and signatures calculated for this new climb profile. The signature schematics in this figure are plotted on the same scale as those in figure 50. While the signature shapes and lengths do not change a great deal, the magnitude of the overpressure is dramatically reduced. The effect on the cruise and descent portion of the flight was negligible in this case. Allowing the performance program to determine a minium fuel path for the subsonic portion of the flight resulted in a small overall performance penalty for the low boom climb path. Table 11 shows the climb fuel and time and the overall range for the two flight profiles. A 1.5 percent range decrease is a small price to pay for an average 25 percent reduction in Δp during climb.

The development of low boom climb paths for configuration II offered some more choices than the effort for configuration I. Examining figure 55 once again indicates that the minimum fuel climb path is incompatible with maintaining a low boom during this segment. However, the shape of the boom contours above 30,000 ft. makes the selection of a practical low boom climb path a fairly easy task. The slope of the lines of constant Δp correspond closely to climb paths for Mach numbers above 1.3. It is even possible to set a target maximum boom level for this portion of the climb. Two such climb schedules are shown in figure 55. The first represents a 1.2 psf. climb and the second a 1.0 psf. maximum overpressure limit. It can be seen from the figure that the maximum overpressure limits can not be applied below M = 1.3 if a practical climb profile is to be maintained. However, the overpressure levels will still be significantly reduced from those of the min-

imum fuel path. The ground overpressure values and signatures calculated for these two paths are presented in figures 57 and 58 and table 12. The figures indicate that the overpressure reduction is due partly to the increased altitude and partly to a change in the signature shape. In both cases, the relative strength of the nose shock is greatly reduced in comparison to the results of figure 51. For the 1.2 psf. climb, the signature shape approaches the ideal flat top shape. In the 1.0 psf. case, a relatively strong secondary shock appears in the signature. Also in this case, the climb altitude is such that the cruise Mach number is reached at an altitude greater than the altitude for most efficient cruise. The cruise is therefore flown at constant altitude until the best cruise profile is intercepted. An analysis of the effects of these low boom paths on the overall mission performance can be conducted with the help of the climb fuel, time and range data in table 13. Again in these cases, the subsonic portion of the climb is optimized to reduce the overall impact on performance. The penalties in terms of fuel and range are seen to be slightly greater than those assessed to configuration I. The altitudes selected for both of these low boom paths are higher than the altitudes for the corresponding path for configuration I. The penalties associated with this extra altitude are compounded by the relative aerodynamic inefficiency of the low boom configuration with respect to configuration I. A 2.0 percent range penalty (for the 1.2 psf path) is acceptable when considering that the undesirable climb overpressure signatures are eliminated. The acceptability of an additional 3.1 percent range loss to get to a 1.0 psf limit would have to be more carefully weighed against the additional disturbance caused by the increased overpressure.

VII. Concluding Remarks

A new computer technique for the analysis of transport aircraft sonic boom characteristics has been developed. This new method combines the previously separate analysis steps into a single analysis using a single geometry description. The new technique has been implemented in a stand-alone computer program and has been incorporated as a module in an aircraft performance analysis program. The process of developing this new technique has revealed several interesting facts about sonic boom analysis using linear theory techniques. The application of the new method to aircraft configuration analysis has provided some important new capabilities and revealed new information about sonic boom ground signature characteristics during the climb and cruise flight segments of two conceptual Mach 2.0 transport configurations. The conclusions drawn from the development and application of this new tool are summarized below.

Geometry modeling. The geometry format selected for the new overpressure tool was derived from a wave drag analysis method. It was found that for the analysis of area due to volume, either a simple circular body or a detailed blended fuselage model could be used. Sufficiently accurate results can be obtained with the simple model provided the actual configuration volume distribution is simulated. More detailed models, usually developed later in the design cycle, provide a link to advanced computational techniques. For the purpose of the analysis of equivalent area due to lift, an accurate simulation of the fuselage camber was found to be the most important addition to the data describing the wing geometry.

Lift analysis methods. Three lift analysis methods: linear and modified linear wing lift and nacelle interference lift, were studied as part of this research. From the point of view

of the calculating ground pressure signature, it was found that the linear wing lift analysis method alone provided consistent results at Mach numbers above 1.4. The ground pressure results were found to agree very well with both experimental and other theoretical data. The linear results were found to break down at Mach numbers less than Mach 1.4. This problem was thought to lie more with the particular implementation studied than with linear theory in general. The modified linear wing analysis and interference lift methods did not produce significantly different ground pressure signatures for most flight conditions. At some extremes of the flight evelope, these methods may be required. Due to the above problem with the linear method, the modified linear technique was applied in the performance analysis studies.

Signature propagation methods. Two methods for propagating the pressure signature to the ground were studied. The methods were found to be very similar with the exception of cases of non-zero flight path angle. The Thomas method offered features of a uniform atmosphere propagation method and possible extension to calculating focus overpressures. The ARAP computer code proved to be the more robust of the two methods.

Boom contour generation. The development of a stand-alone program based on the new overpressure prediction tool will provide aircraft configuration developers with a method of rapidly analyzing the boom characteristics of a current design and comparing those characteristics with the results from other vehicles. Interactive input, graphical output, and rapid repeat case logic are features of the new program that make this possible. One other important feature of the stand-alone program is the ability to generate contours of sonic boom signature data for the aircraft flight evelope. Nose shock overpressure contours were generated as part of this report, but this capability could be extended to other important parameters. This contour information provides a new capability to examine the variation of boom parameters throughout the aircraft's flight evelope rather than at just a few selected points. Contour plots for the two Mach 2.0 configurations revealed that for a given weight, the minimum ground overpressure occurred between Mach 1.25 and 1.5.

Application to aircraft performance analysis. The new overpressure prediction tool was integrated into an aircraft performance program to provide a capability of analyzing

the variation of overpressure signature characteristics on an aircraft's flight profile. Climb, cruise and descent signatures were studied for two Mach 2.0 configurations. Typical minimum fuel climb profiles for these configurations were found to produce excessive Δp values at the ground. Including two dimensional maneuver parameters in the analysis did not significantly alter the overpressure level or the signature shape for the two configurations studied. The capability of generating boom contours, coupled with subsonic fuel burn optimization, was used to develop new climb profiles for the two configurations. Using these new profiles reduced the calculated climb Δp values to levels near the cruise results. These levels could be obtained with acceptable penalties on the climb fuel and overall range.

References

1. *National Aeronautical R&D Goals-Agenda for Achievement.* Executive Off. of the President, Off. of Science & Technology Policy, Feb. 1987.

2. Anon.: *High-Speed Civil Transport Study.* NASA Contractor Report 4233, September 1989

3. *Proceedings of the Sonic Boom Symposium.* Journal of the Acoustical Society of America, vol. 39 Number 5, 1966.

4. Ribner, H.S.; and Hubbard, Harvey H.: *Proceedings of the Second Sonic Boom Symposium.* Journal of the Acoustical Society of America, vol. 51 and 52, 1972

5. Carlson, Harry W.; and Maglieri Domenic J.: *Review of Sonic Boom Generation Theory and Prediction Methods.* Journal of the Acoustical Society of America, Vol. 51, 1972, pp.675-682.

6. Darden, Christine M.; Powell, Clemans A.; Hayes, Wallace D.; George, Albert R.; and Pierce, Allan D., *Status of Sonic Boom Methodology and Understanding.* NASA CP-3027, June 1989.

7. Hayes, Wallace D.: *Linearized Supersonic Flow.* Thesis, Calif. Inst. Of Technology, Pasadena Calif. 1947.

8. Whitham, G. B.: *The Flow Pattern of a Supersonic Projectile.* Communication on Pure and Applied Mathematics, vol. V, no. 3, August 1952.

9. Walkden, F.: *The Shock Pattern of a Wing-Body Combination, Far From the Flight Path.* Aeronautical Quarterly, vol. IX, part 2, May 1958.

10. Carlson, Harry W.: *Correlation of Sonic Boom Theory with Wind Tunnel and Flight Measurements.* NASA TR R-213, Dec. 1964.

11. Middleton, Wilbur D.; and Carlson, Harry W.: *A Numerical Method for Calculating Near Field Sonic Boom Pressure Signatures.* NASA TN D-3082, July 1965,

12. Hayes, Wallace D.; Haefeli, Rudolph C.; and Kulsrud, H.E.: *Sonic Boom Propagation in a Stratified Atmosphere with Computer Program.* NASA CR-1299, 1969.

13. Thomas, Charles L.: *Extrapolation of Sonic Boom Pressure Signatures by the Waveform Parameter Method.* NASA TN D-6832, June 1972.

14. Mack, Robert J.; and Darden, Christine M.: *Wind-Tunnel Investigation of the Validity of a Sonic-Boom-Minimization Concept.* NASA TP-1421, 1979.

15. Harris, Roy V., Jr.: *An Analysis and Correlation of Aircraft Wave Drag.* NASA TM

X-947, 1964.

16. Middelton, W. D.; Lundry, J. L.; and Coleman, R. G.: *A System for Aerodynamic Design and Analysis of Supersonic Aircraft. Part 2 - User's Manual.* NASA CR-3352, 1980.

17. Craidon, Charlotte B.: *User's Guide for a Computer Program for Calculating the Zero Lift Wave Drag of Complex Configurations.* NASA TM-85670, Nov. 1983.

18. Craidon, Charlotte B.: *LaWGS: A Description of the Langley Wireframe Geometry Standard Format.* NASA TM-85767, Feb. 1985.

19. Robins, A. Warner; et. al.: *Concept Development of a Mach 3.0 High Speed Civil Transport.* NASA TM-4058, Sept. 1988.

20. Martin, Glenn L.; and Walkley, Kenneth B.: *Aerodynamic Design and Analysis of the AST-204, -205, and -206 Blended Wing-Fuselage Supersonic Transport Configuration Concepts.* NASA CR-159223, March 1980.

21. Middleton, Wilbur D.; and Carlson, Harry W.: *A Numerical Method for Calculating the Flat Plate Pressure Distributions on Supersonic Wings of Arbitrary Planform.* NASA TN D-2570, Jan. 1965.

22. Middleton, Wilbur D.; and Carlson, Harry W.: *Numerical Method of Estimation and Optimizing Supersonic Aerodynamic Characteristics of Arbitrary Planform Wings.* Journal of Aircraft, vol. 2, no. 4, July-Aug. 1965, pp. 261-265.

23. Carlson, Harry W.; and Mack, Robert J.: *Estimation of Wing Nonlinear Aerodynamic Characteristics at Supersonic Speeds.* NASA TP-1718, Nov. 1980.

24. Mack, Robert J.: *A Numerical Method for Evaluation and Utilization of Supersonic Nacelle-Wing Interference.* NASA TN D-5057, Nov. 1968.

25. Plotkin, Kenneth J.: *Evaluation of a Sonic Boom Focal Zone Prediction Model.* WR 84-43, Wyle Labs, Feb. 1985.

26. Needleman, Kathy E. and Mack, Robert J.: *A Study of Sonic Boom Overpressure Trends With Respect to Weight, Altitude, Mach Number and Vehicle Shape.* AIAA 90-0367, Jan. 1990.

27. Fetterman, David E., Jr.: *Preliminary Sizing and Performance of Aircraft.* NASA TM-86357, July 1985.

Table 1 - Comparison of execution times required by volume analysis methods.

Method	**Time required for analysis (sec)**	
	nx=60	nx=100
Mach 3.0 configuration		
1 - original	9.1	14.5
1 - modified	1.8	2.3
2	2.6	3.4
3	13.1	19.8
Mach 2.7 configuration		
1 - original	11.6	18.7
1 - modified	1.5	1.9
2	2.2	2.8
3	12.9	19.7

Table 2 - Comparison of execution times required by lift analysis methods for varying values of JBYMAX.

Mach 2.7 Configuration

Method	Mach	JBYMAX	Time (sec.)
Linear	1.4	20	14.0
"	"	15	4.9
"	"	10	1.2
Mod. Linear	"	40	517.6
"	"	30	172.1
"	"	20	38.7
Linear	2.7	40	20.0
"	"	30	6.9
"	"	20	1.8
Mod. Linear	"	64	331.4
"	"	50	132.5
"	"	40	58.7
"	"	30	23.1
"	"	20	7.0

Mach 3.0 Configuration

Method	Mach	JBYMAX	Time (sec.)
Linear	1.4	20	13.3
"	"	15	4.6
"	"	10	1.2
Mod. Linear	"	40	493.7
"	"	30	164.7
"	"	20	38.1
Linear	3.0	40	15.5
"	"	30	5.3
"	"	20	1.3
Mod. Linear	"	70	349.0
"	"	50	100.7
"	"	40	45.9
"	"	30	18.3
"	"	20	6.9

Table 3. - Angle of attack, JBYMAX, and execution time data for the comparison of the linear and modified linear lift analysis methods.

		Linear		Modified Linear		
Mach	**Alpha**	**Time**	**JBYMAX**	**Alpha**	**Time**	**JBYMAX**
Reference Arrow Wing						
1.2	2.58	2.9	10	2.70	458.7	30
1.7	1.54	35.7	30	1.65	95.2	30
2.2	1.04	14.7	30	1.09	44.7	30
2.7	.78	8.2	30	.83	25.7	30
Mach 2.7 Cambered Arrow Wing						
1.2	3.62	2.6	10	2.66	409.5	30
1.7	.81	29.6	30	.94	86.3	30
2.2	-.60	12.7	30	-.52	39.9	30
2.7	-1.28	6.9	30	-1.17	23.9	30
Mach 3.0 Configuration Wing						
1.2	3.07	2.5	10	2.44	378.1	30
1.8	1.05	24.3	30	1.11	69.7	30
2.4	.14	10.3	30	.10	31.2	30
3.0	-.38	5.4	30	-.37	18.0	30

Table 4 - Comparison of execution times required by the inteference analysis method for varying values of JBYMAX.

Mach 2.7 Configuration

Mach	JBYMAX	Time (sec.)
1.4	24	30.1
"	20	22.6
"	10	10.7
2.7	50	38.3
"	40	26.7
"	30	19.1
"	20	13.4

Mach 3.0 Configuration

Mach	JBYMAX	Time (sec.)
1.4	29	64.7
"	20	31.1
"	10	13.4
3.0	50	43.4
"	40	29.0
"	30	20.5
"	20	14.5

Table 5. - Angle of attack, JBYMAX, and execution time data for the comparison of the wing lift alone and wing + interference lift results.

			Wing alone		Wing + interference	
Mach	**Lift** (lbs.)	**Altitude** (ft.)	**Alpha** (deg.)	**Time** (sec.)	**Alpha** (deg.)	**Time** (sec.)
			Mach 2.7 configuration			
1.4	400,000	40,000	.08	143.9	-.80	180.8
1.4	400,000	60,000	2.82		2.68	
1.4	600,000	40,000	.40		.27	
1.4	600,000	60,000	5.72		5.58	
2.7	400,000	50,000	-1.84	23.4	-1.91	41.5
2.7	400,000	70,000	.33		.25	
2.7	600,000	50,000	-1.17		-1.24	
2.7	600,000	70,000	2.14		2.07	
			Mach 3.0 configuration			
1.4	350,000	40,000	0.05	134.9	.00	214.1
1.4	350,000	60,000	2.77		2.43	
1.4	550,000	40,000	1.21		.87	
1.4	550,000	60,000	5.01		4.67	
3.0	350,000	50,000	-.73	17.8	-.87	38.8
3.0	350,000	70,000	.62		.48	
3.0	550,000	50,000	-.25		-.39	
3.0	550,000	70,000	1.89		1.75	

Table 6. - Comparison of required execution times for the ARAP and Thomas signature extrapolation methods. Mach 3.0 Configuration, L= 550,000 lbs.

		time (sec.)	
Mach	**Altitude**	**ARAP**	**Thomas**
3.0	65,000.	13.5	16.0
"	55,000.	12.9	15.8
"	45,000.	13.2	15.2
"	35,000.	13.1	14.3
2.0	65,000.	4.0	4.5
"	55,000.	3.8	4.5
"	45,000.	3.7	4.5
"	35,000.	2.8	4.1
1.2	55,000.	3.9	5.6
"	45,000.	3.9	5.4
"	35,000.	3.8	4.1
"	25,000.	3.8	4.5
Maneuvering results: Mach = 2.0, h = 55,000 ft.			
	a/g=.5	3.8	4.5
	γ= 10. deg.	3.8	4.6
	$\dot{\gamma}$= 5. deg/sec	3.7	4.4
	a/g=.5, γ= 10., $\dot{\gamma}$= 5.	3.7	4.7

Table 7. - Mach, altitude, lift and nose shock overpressure results for Configuration I on the baseline flight profile. TOGW = 585,000 lbs.

Mach	Altitude(ft)	Lift (lbs)	Δp
1.2	21,300.	566,500	3.48
1.4	26,500.	562,900	3.00
1.6	32,500.	559,500	2.53
1.8	37,500.	556,500	2.44
2.0	42,000.	553,100	2.23
2.0	57,600.	549,700	1.60
2.0	68,800.	308,000	1.10
1.8	68,800.	307,000	1.07
1.5	63,500.	307,000	.98
1.2	56,500.	307,000	1.31

Table 8. - Data for the comparsion of Δp results with and without the effects of two dimensional maneuvers. Mach 2.0 Configuration I, TOGW= 585,000 lbs., baseline flight profile.

Mach	Altitude	a/g	γ	$\dot{\gamma}$	Δp w/ man.	Δp w/o man.
1.2	21,300.	.085	0.39	-0.001	3.43	3.48
1.4	26,500.	.087	2.46	-0.001	2.85	3.00
1.6	32,500.	.100	2.44	0.003	2.43	2.53
1.8	37,500.	.102	2.04	-0.004	2.41	2.44
2.0	42,000.	.033	5.52	0.312	1.98	2.23
2.0	57,630.	.000	0.00	0.000	1.60	1.60
2.0	68,800.	.000	0.01	0.000	1.10	1.10
1.8	68,800.	-.097	0.00	0.000	1.07	1.07
1.5	63,500.	-.088	-1.36	-0.002	0.99	0.98
1.2	56,500.	-.079	-1.88	-0.004	1.29	1.31

Table 9. - Mach, altitude, lift and nose shock overpressure results for Configuration II on the baseline flight profile. TOGW = 590,000 lbs.

Mach	Altitude(ft)	Lift (lbs)	Δp
1.2	21,300.	569,100	2.70
1.4	26,500.	564,900	2.34
1.6	32,500.	561,100	1.92
1.8	37,500.	557,700	1.68
2.0	42,000.	554,300	1.49
2.0	53,800.	551,600	1.03
2.0	63,200.	340,000	.74
1.7	61,100.	339,800	.74
1.5	56,700.	339,700	.76
1.2	51,300.	339,500	.90

Table 10. - Mach, altitude, lift and nose shock overpressure results for Configuration I on the reduced boom flight profile. TOGW = 585,000 lbs.

Mach	Altitude(ft)	Lift (lbs)	Δp
1.2	40,000.	560,400	2.12
1.4	41,900.	556,900	1.67
1.6	42,500.	554,100	1.92
1.8	43,400.	551,500	2.00
2.0	44,200.	548,900	2.08
2.0	57,700.	545,900	1.60
2.0	68,800.	308,000	1.10
1.8	68,800.	308,000	1.06
1.5	64,100.	307,700	.96
1.2	57,100.	307,600	1.29

Table 11. - Comparison of climb fuel and time and overall range for minimum fuel and reduced boom climb profiles. Configuration I, TOGW= 585,000 lbs.

	Minimum fuel	Reduced boom
Climb fuel (lbs.)	30,900	34,800
Climb time (min.)	15.30	14.58
Overall range (n.mi.)	7,134	7,027

Table 12. - Mach, altitude, lift and nose shock overpressure results for Configuration II on the reduced boom flight profiles. TOGW = 590,000 lbs.

		Δp_{max} = 1.2 psf	
Mach	**Altitude(ft)**	**Lift (lbs)**	**Δp**
1.2	41,900.	559,400	1.23
1.4	44,200.	554,700	1.17
1.6	45,900.	551,000	1.17
1.8	47,800.	547,700	1.18
2.0	49,300.	544,600	1.17
2.0	54,100.	543,500	1.01
2.0	63,200.	340,400	.75
1.7	61,800.	340,200	.73
1.5	57,200.	340,100	.76
1.2	52,000.	339,900	.88

		Δp_{max} = 1.0 psf	
Mach	**Altitude(ft)**	**Lift (lbs)**	**Δp**
1.2	46,800.	553,500	1.08
1.4	49,900.	547,000	.97
1.6	51,800.	542,500	.97
1.8	53,500.	538,700	.99
2.0	55,000.	535,200	.99
2.0	63,200.	340,500	.75
1.7	62,100.	340,300	.72
1.5	57,500.	340,200	.74
1.2	52,800.	340,000	.87

Table 13. - Comparison of climb fuel and time and overall range for minimum fuel and reduced boom climb profiles. Configuration II, TOGW= 590,000 lbs.

	Minimum fuel	**Reduced boom**	
		Δp_{max}= 1.2	**Δp_{max}= 1.0**
Climb fuel (lbs.)	33,400	40,965	47,400
Climb time (min.)	13.7	15.0	16.3
Overall range (n.mi.)	5,027	4,926	4,766

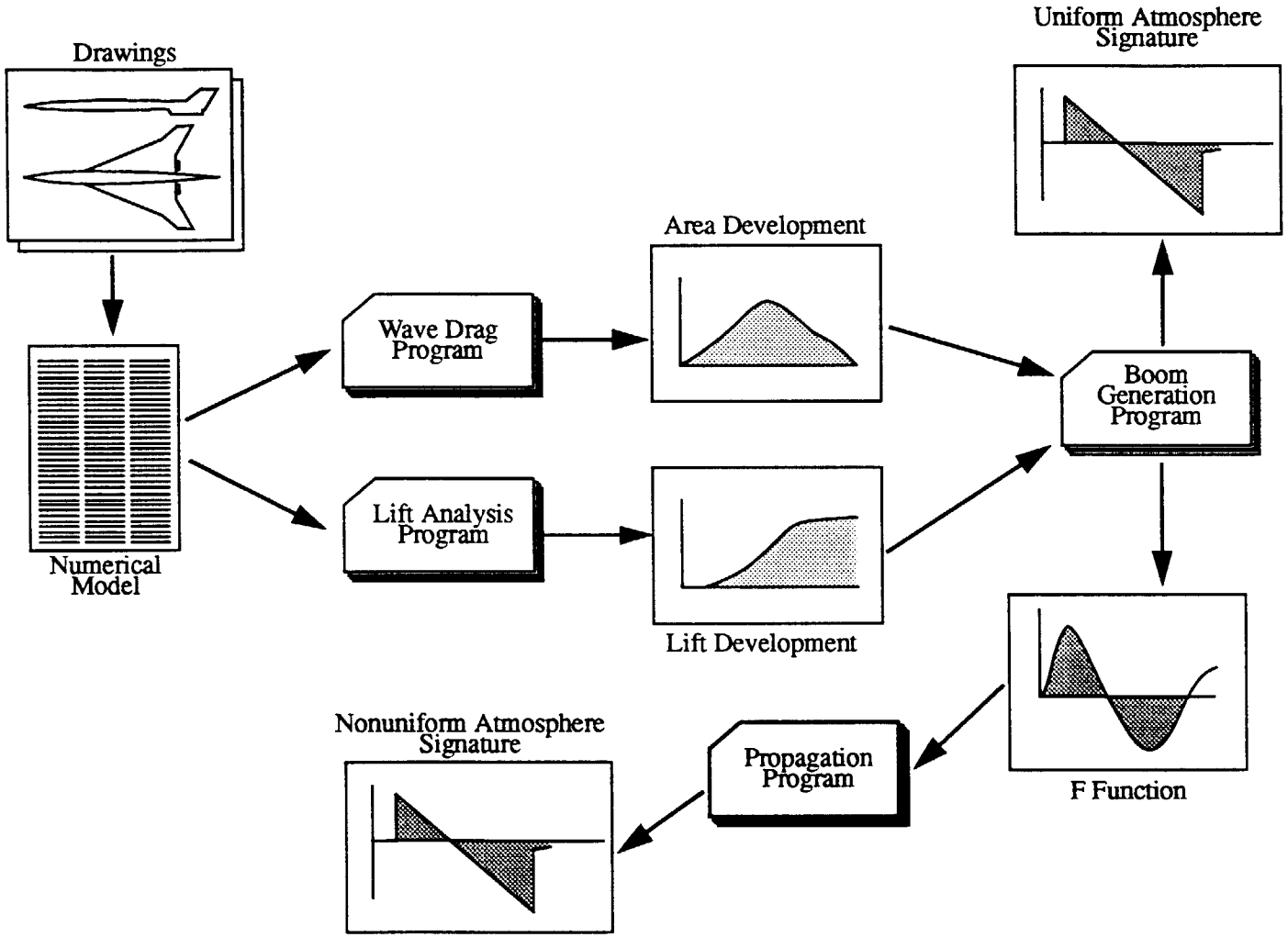

Figure 1. - Steps required for the use of computer programs in the analysis on aircraft sonic boom (ref.5).

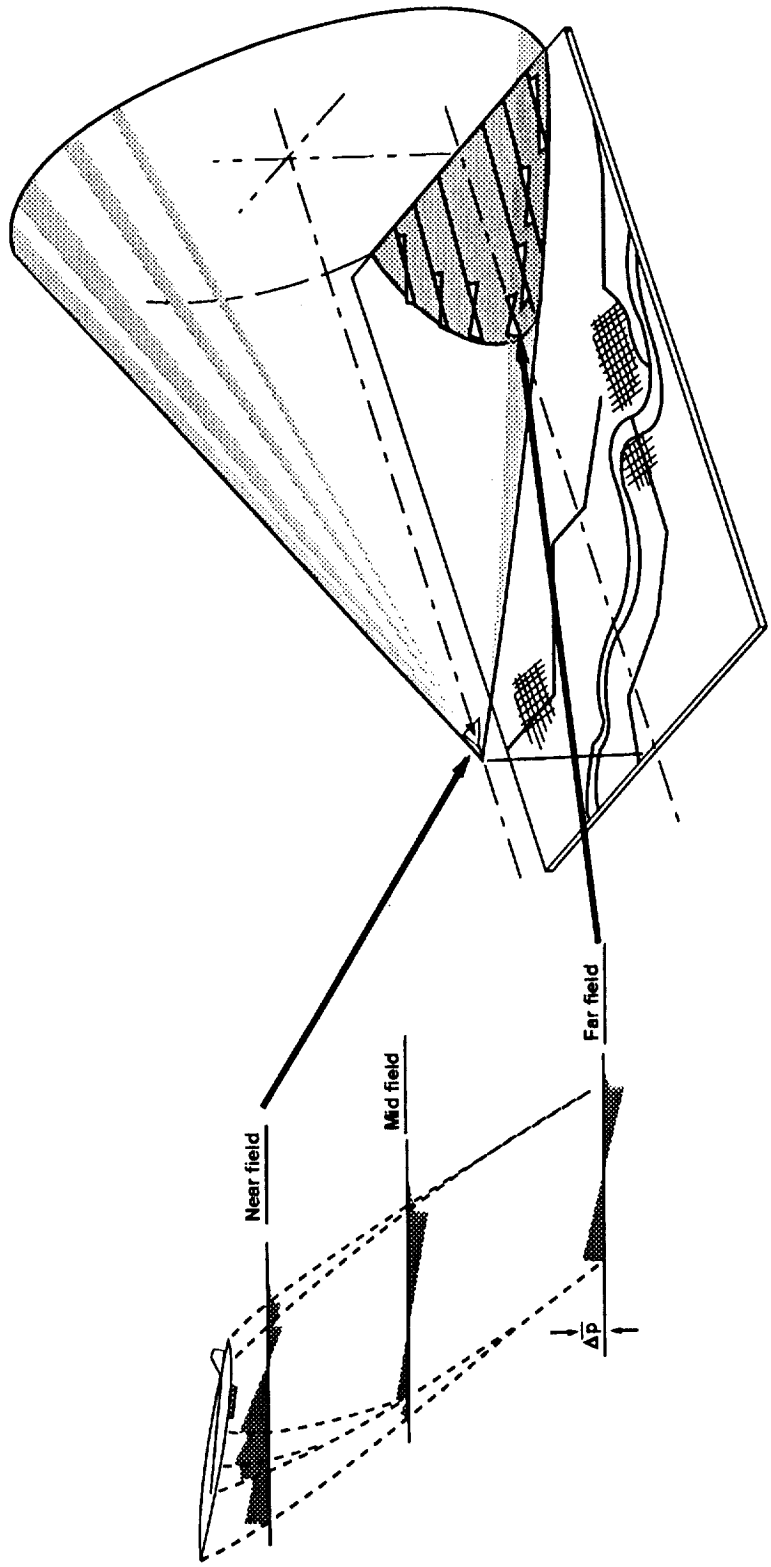

Figure 2. - Sonic boom pressure field.

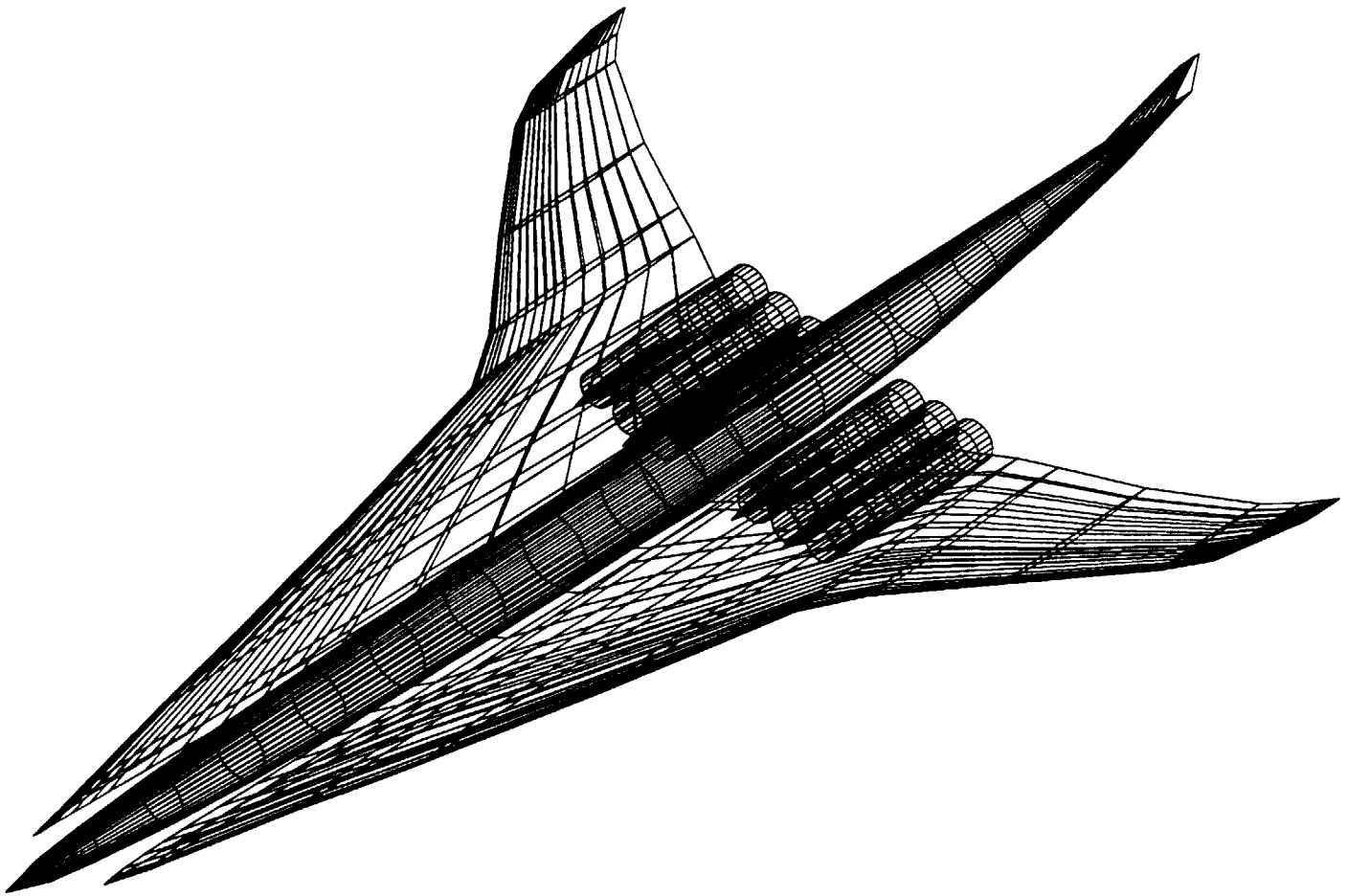

(a) Circular body representaion.

Figure 3. - Numerical model of a Mach 3.0 transport configuration.

(b) Blended body representaion.

Figure 3. - concluded.

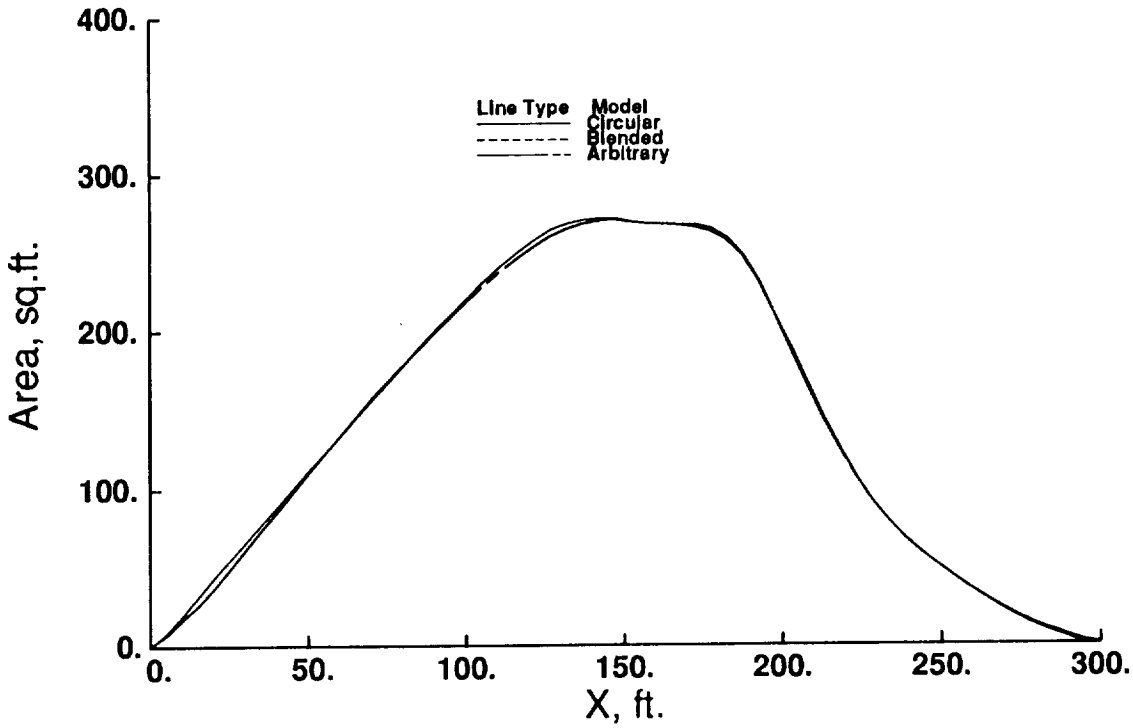

(a) Mach 1.4

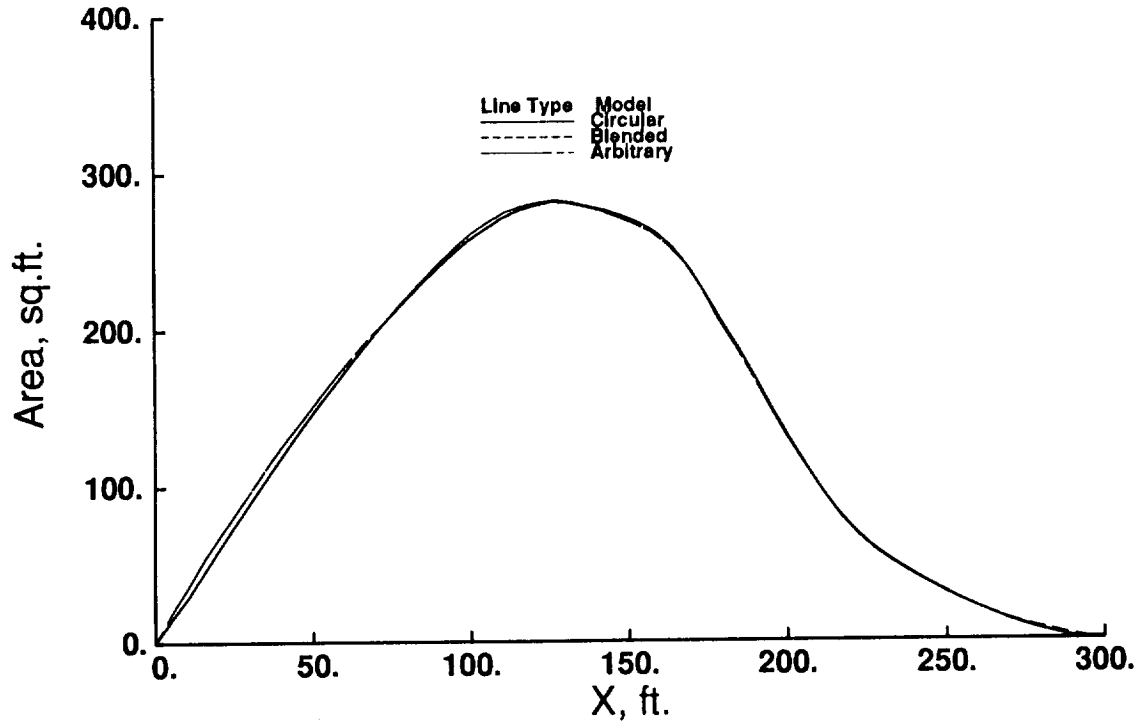

(b) Mach 3.0

Figure 4.- Comparison of area due to volume results for the Mach 3.0 configuration geometry including fuselage, wing and fin.

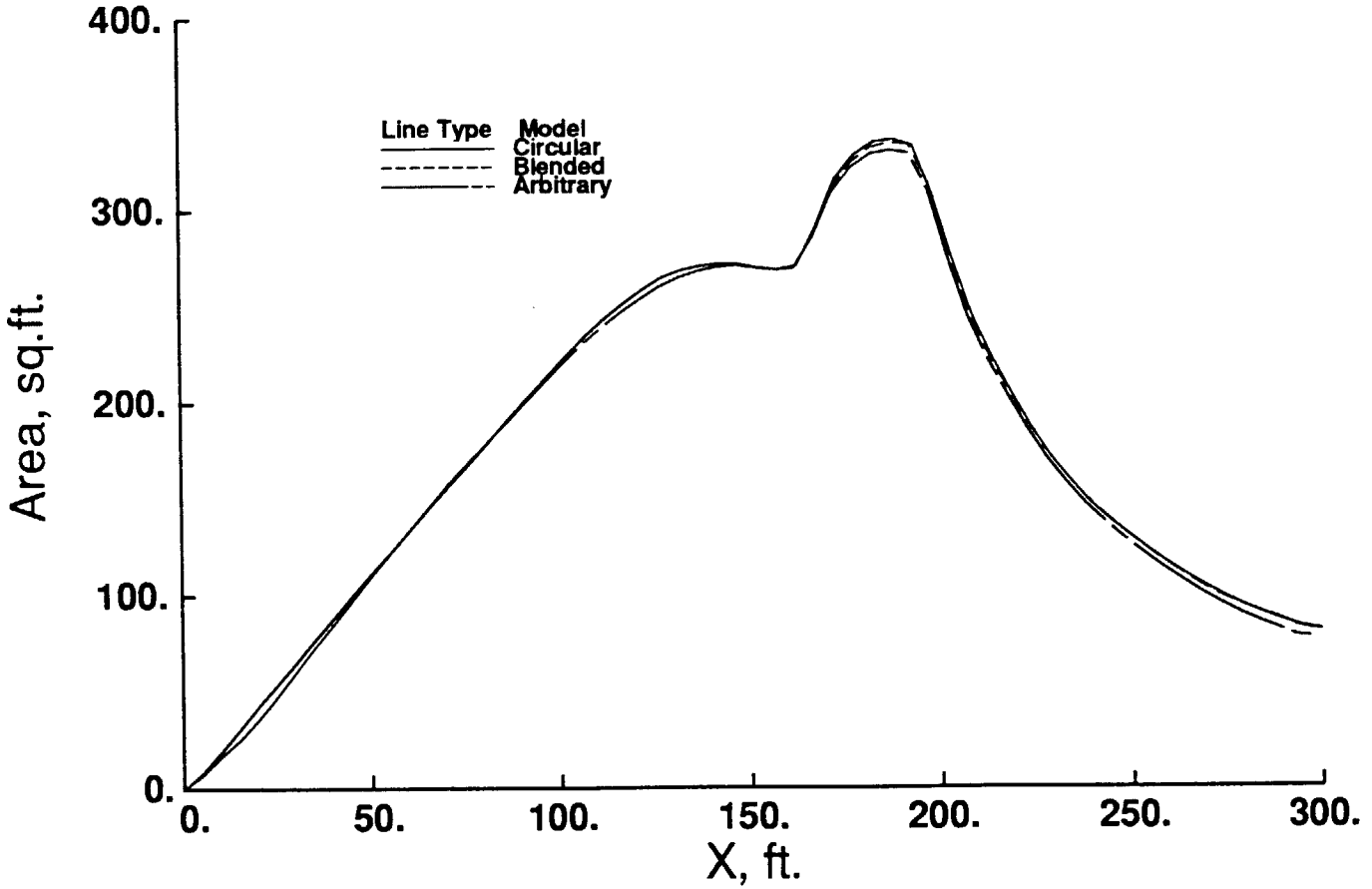

Figure 5.- Comparison of area due to volume results for the Mach 3.0 configuration geometry at Mach 1.4. Includes fuselage, wing, fin and nacelles.

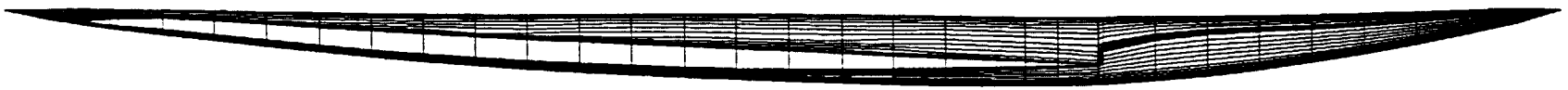

(a) Mach 3.0

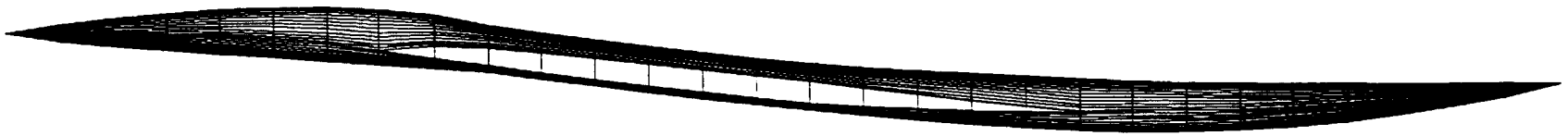

(b) Mach 2.7

Figure 6. - Cambered fuselage geometry models used to compare angle of attack correction methods.

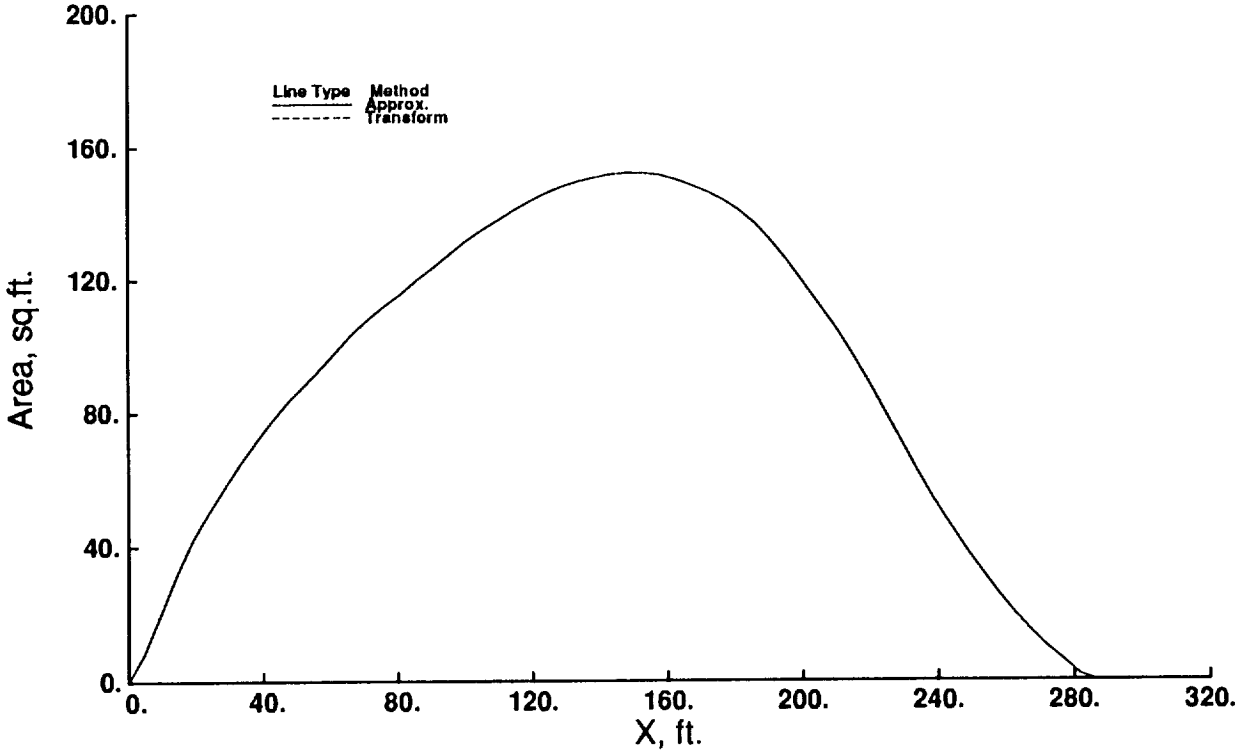

(a) $\alpha = 2.0$ deg.

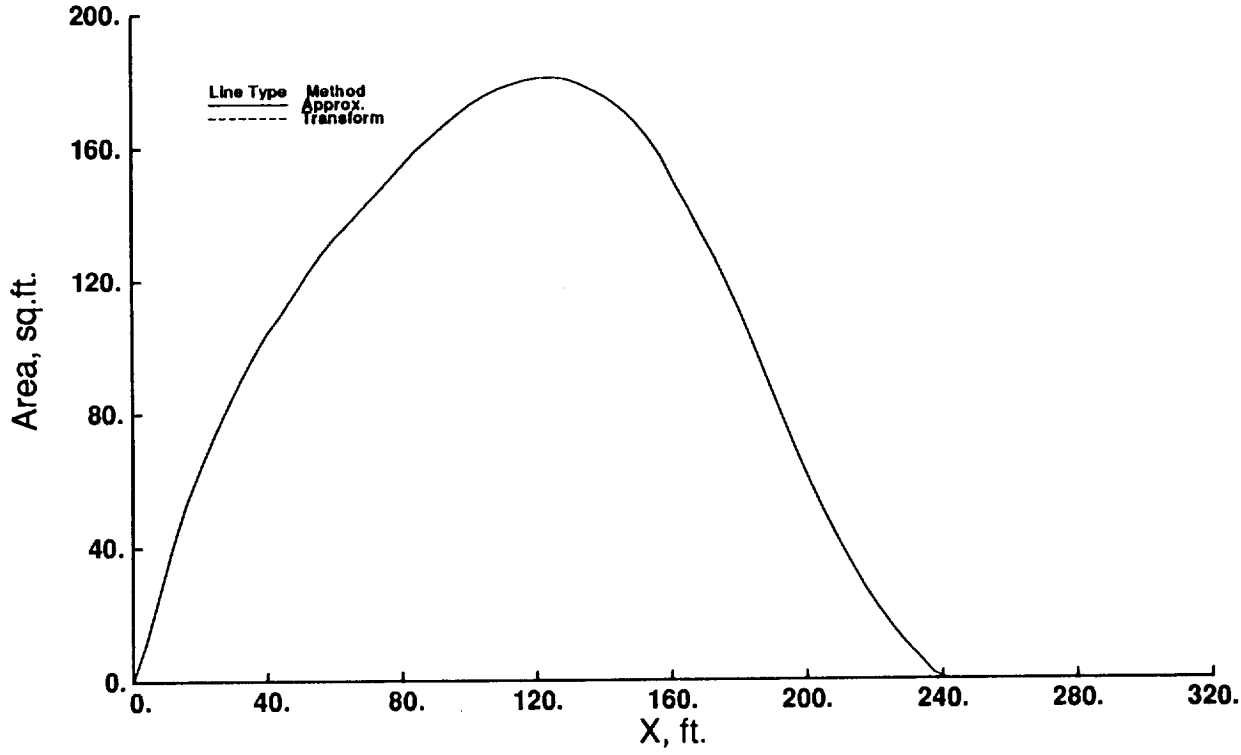

(b) $\alpha = 10.0$ deg.

Figure 7. - Comparison of fuselage area distribution results.
Mach 3.0 configuration geometry.

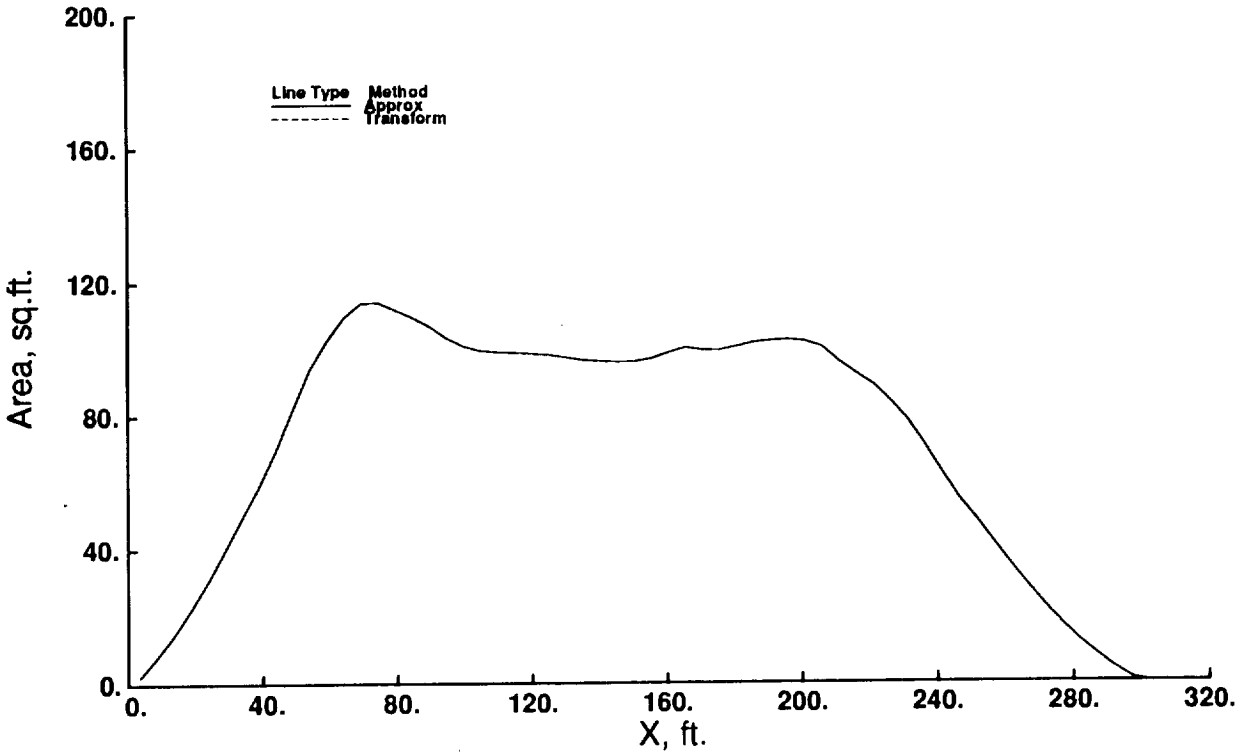

(a) $\alpha = 2.0$ deg.

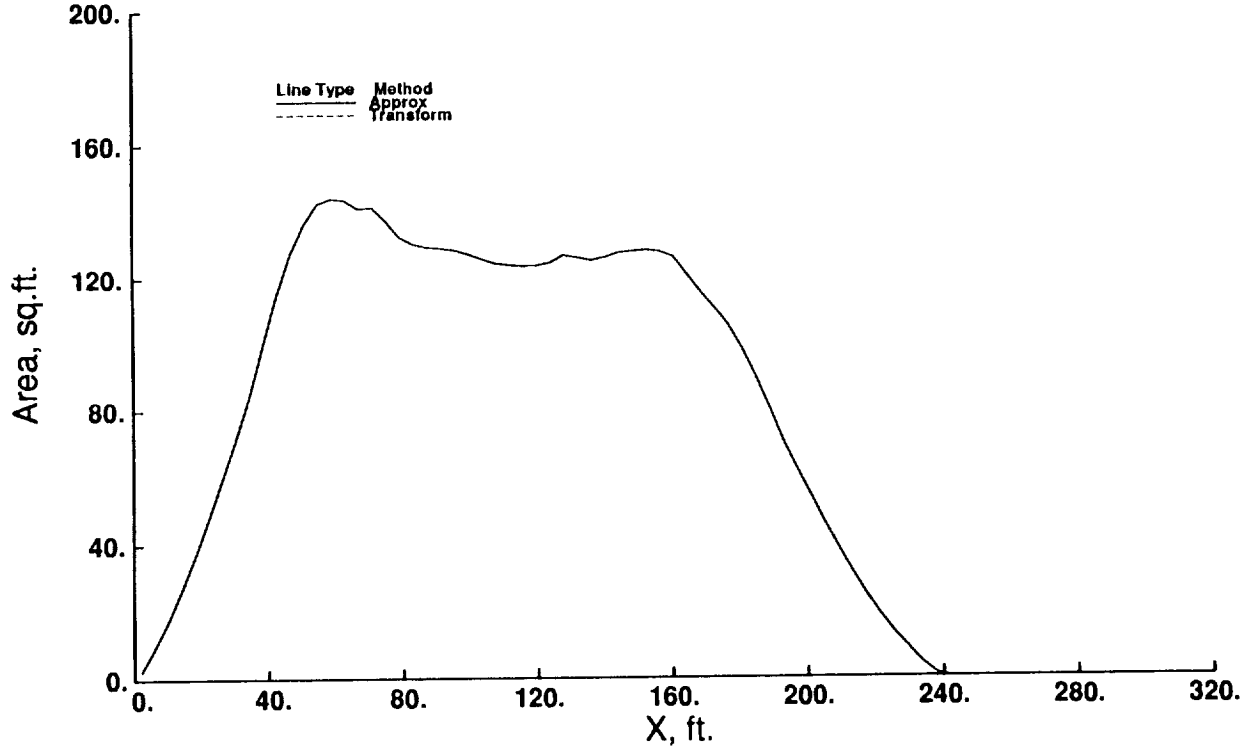

(b) $\alpha = 10.0$ deg.

Figure 8. - Comparison of fuselage area distribution results.
Mach 2.7 configuration geometry.

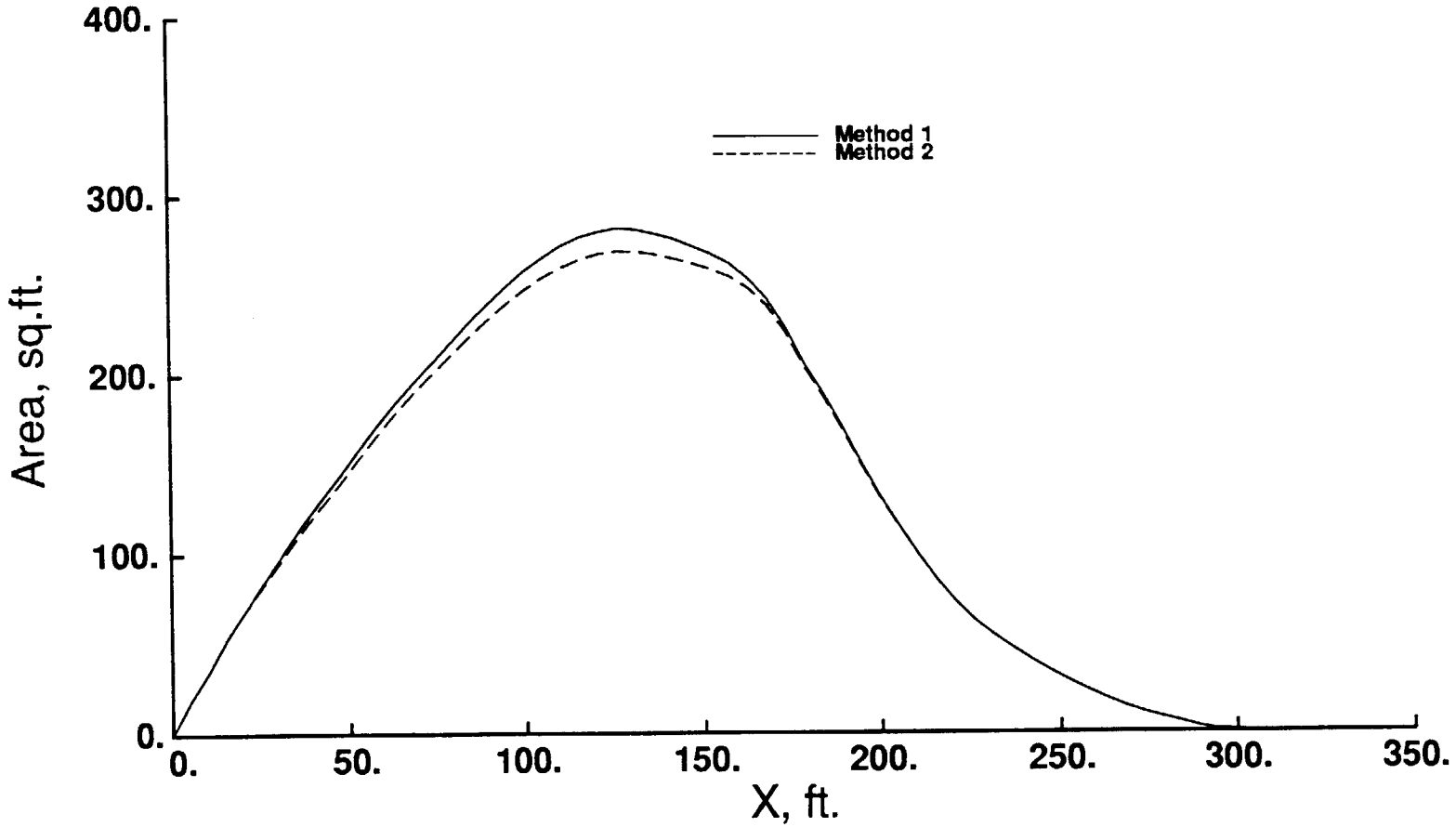

Figure 9. - Comparison of wing volume results for the exact and approximate cambered lifting surface representations.
Mach 3.0 configuration geometry, Mach = 3.0, α = 0.0 deg.

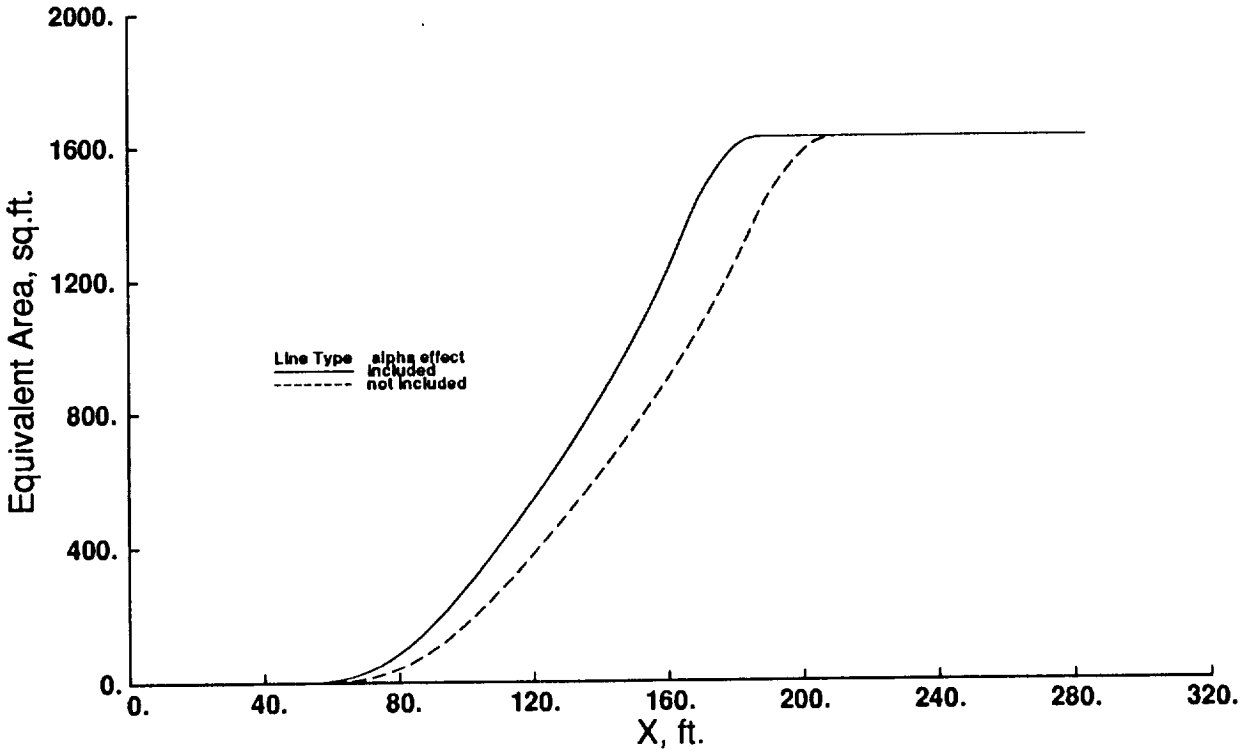

(a) Linear method

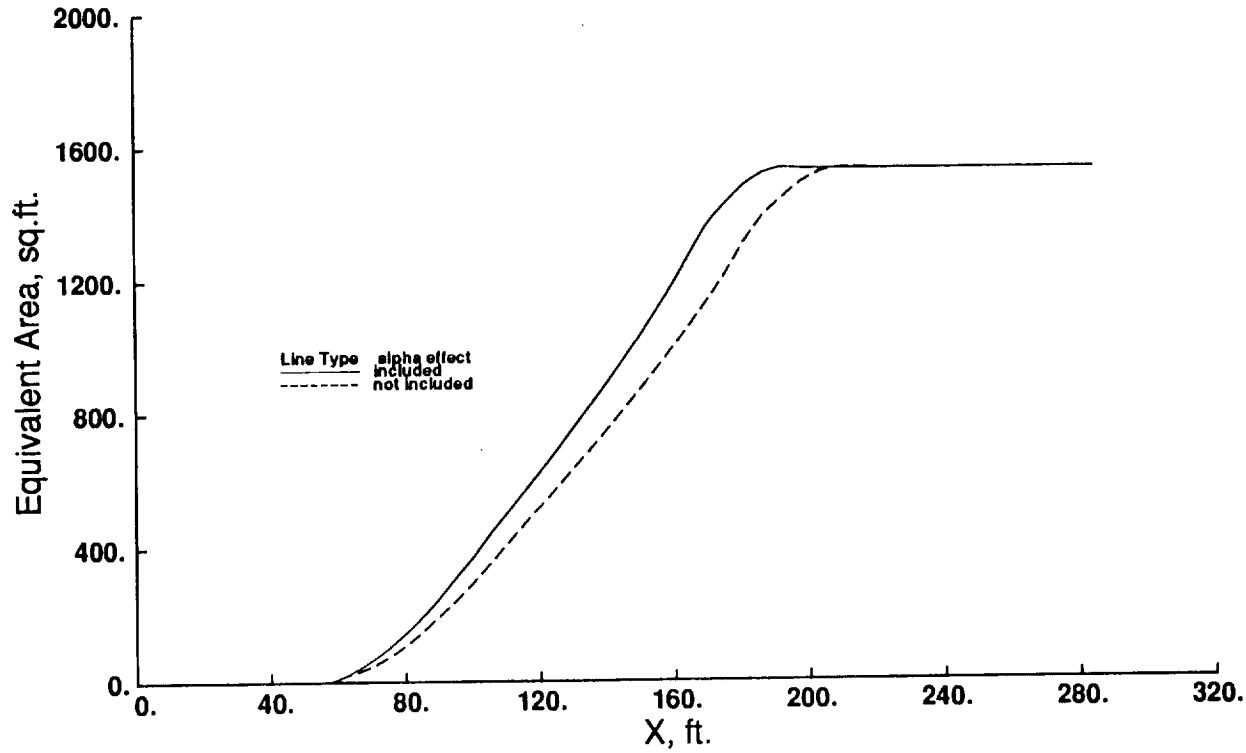

(b) Modified linear method

Figure 10.- Comparison of equivalent area due to lift results for the Mach 2.7 configuration geometry illustrating the effect of angle of attack corrections.
Mach = 2.7, h = 60000. ft., alpha = 2.0 deg.

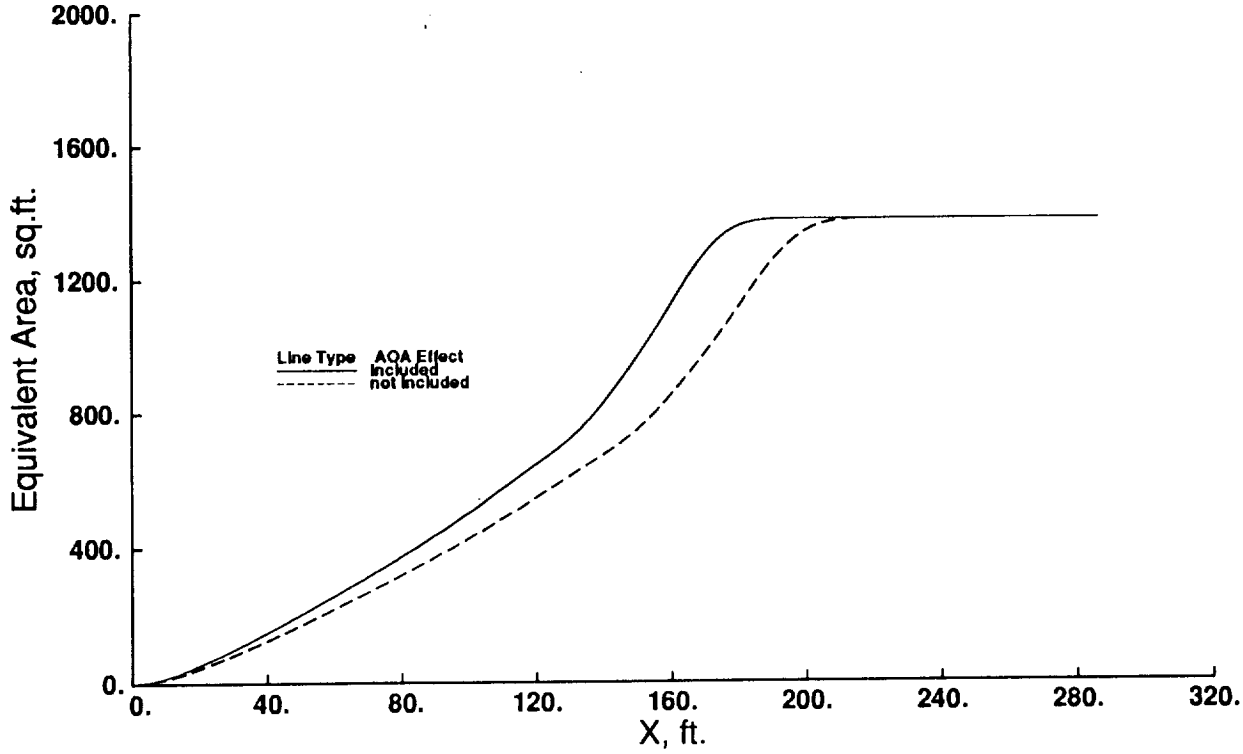

(a) Linear method

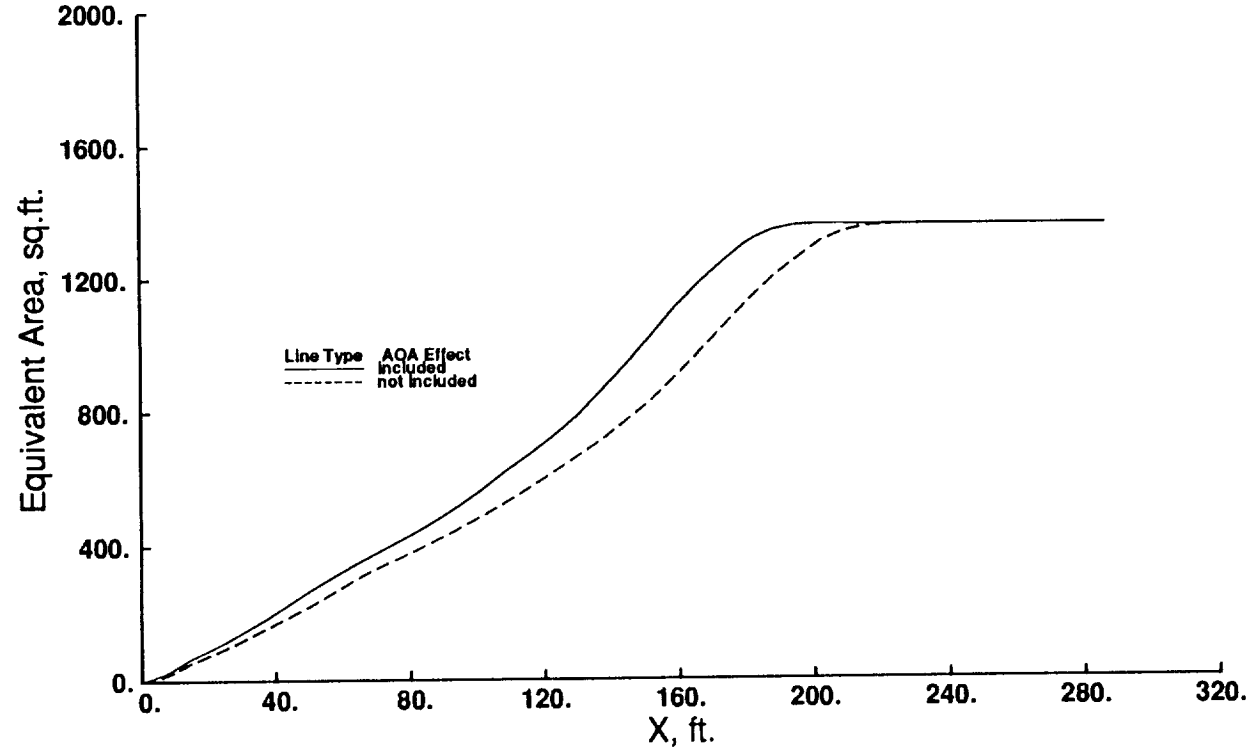

(b) Modified linear method

Figure 11.- Comparison of equivalent area due to lift results for the Mach 3.0 configuration geometry illustrating the effect of angle of attack corrections.
Mach = 3.0, h = 65000. ft., alpha = 2.0 deg.

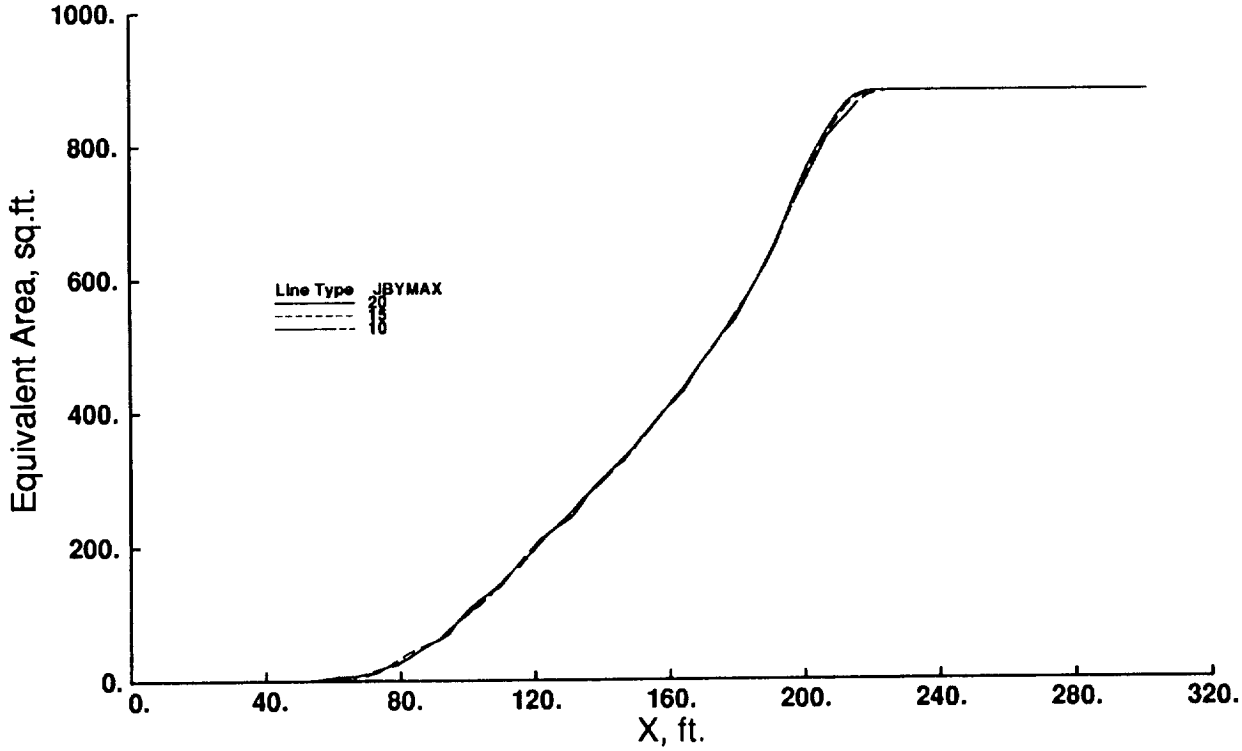

(a) Linear Method

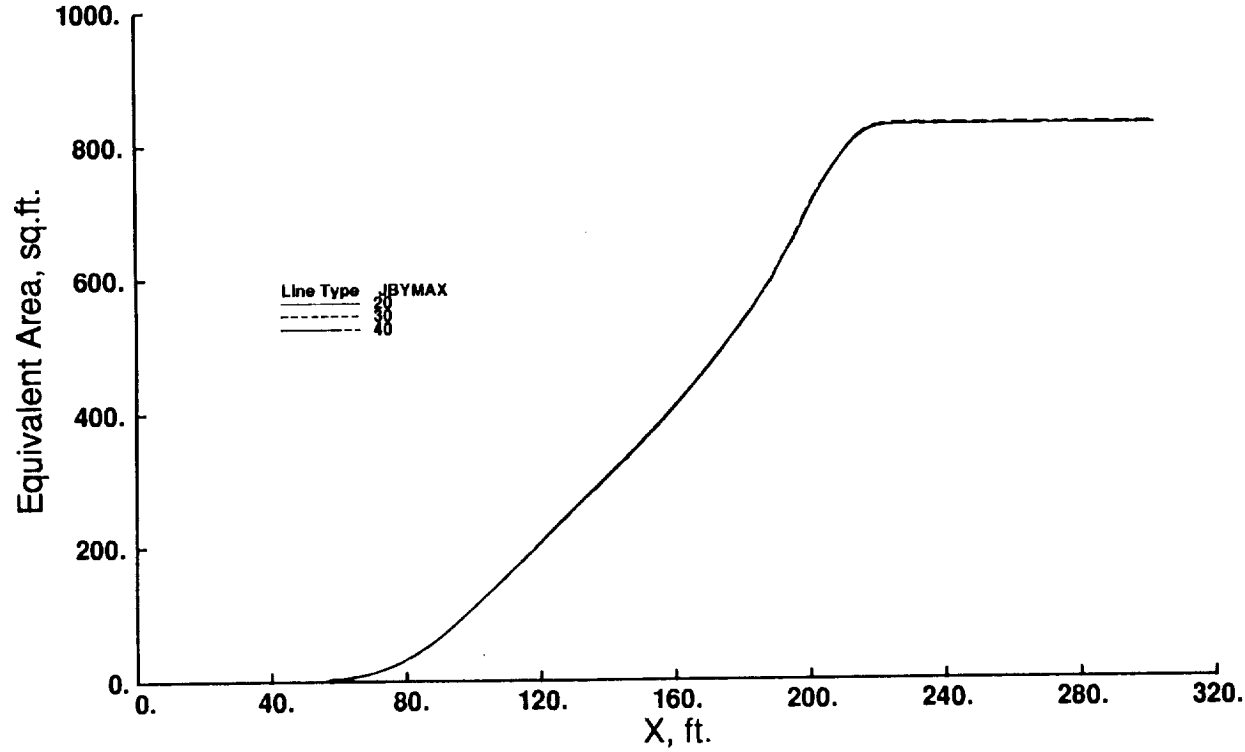

(b) Modified Linear Method

Figure 12. - Sensitivity to JBYMAX for the Mach 2.7 configuration geometry. Mach = 1.4, h = 50,000 ft., L = 600,000 lbs.

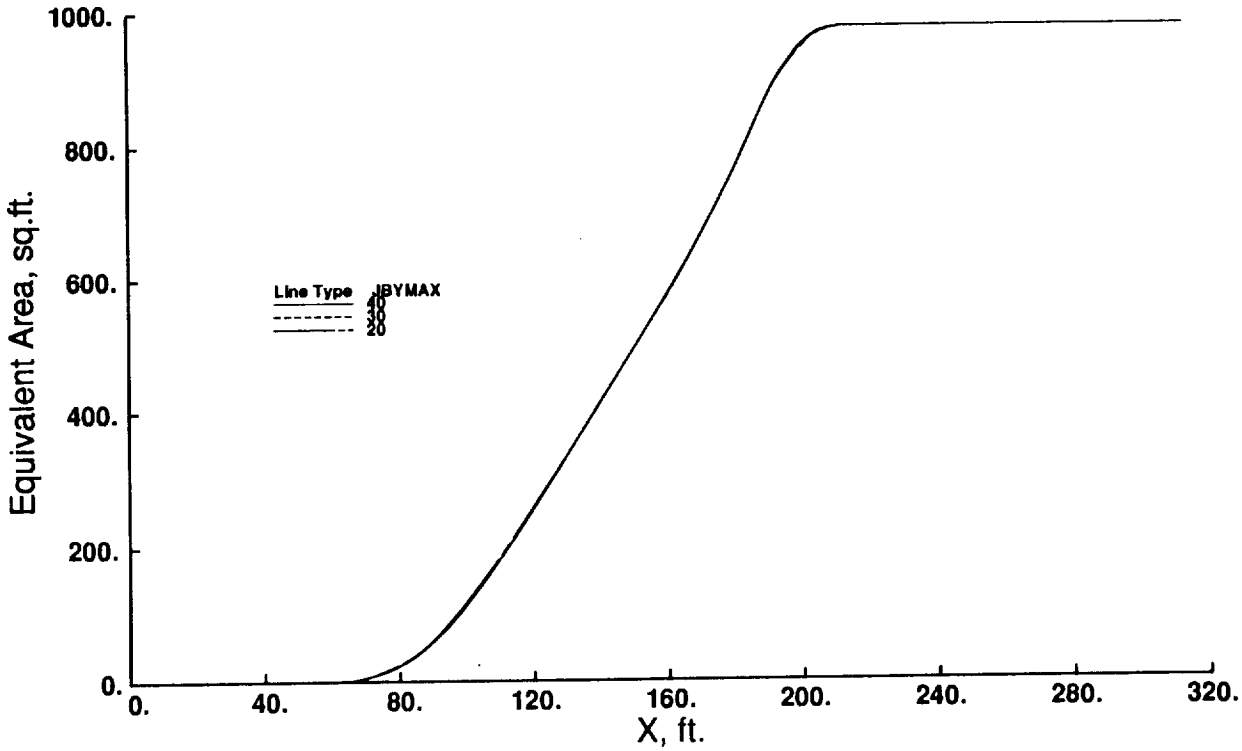

(a) Linear Method

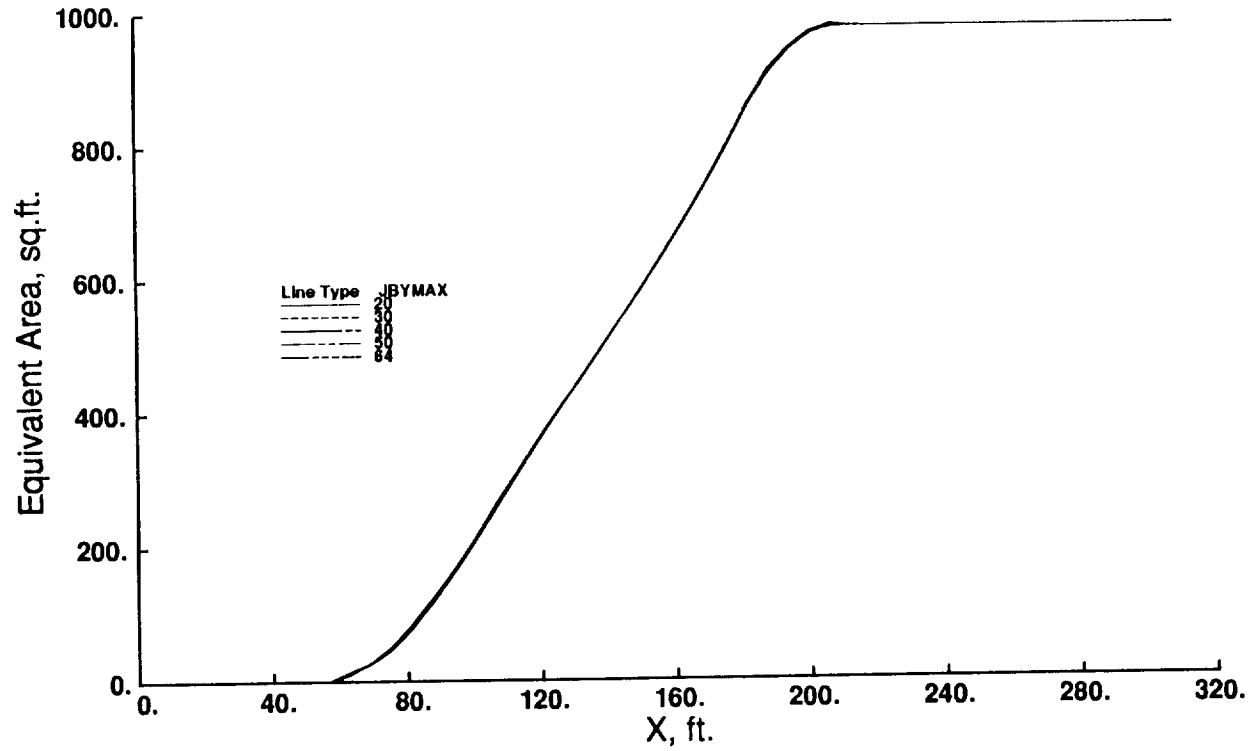

(b) Modified Linear Method

Figure 13. - Sensitivity to JBYMAX for the Mach 2.7 configuration geometry.
Mach = 2.7, h = 60,000 ft., L = 600,000 lbs.

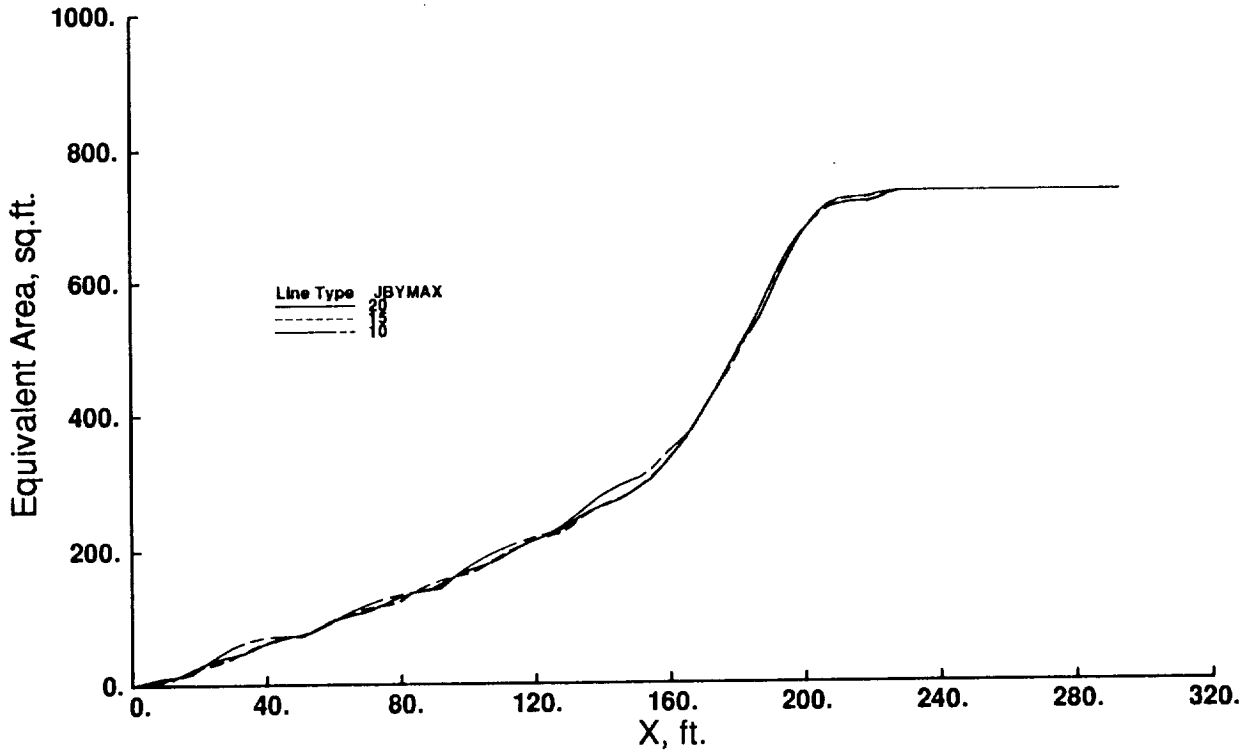

(a) Linear Method

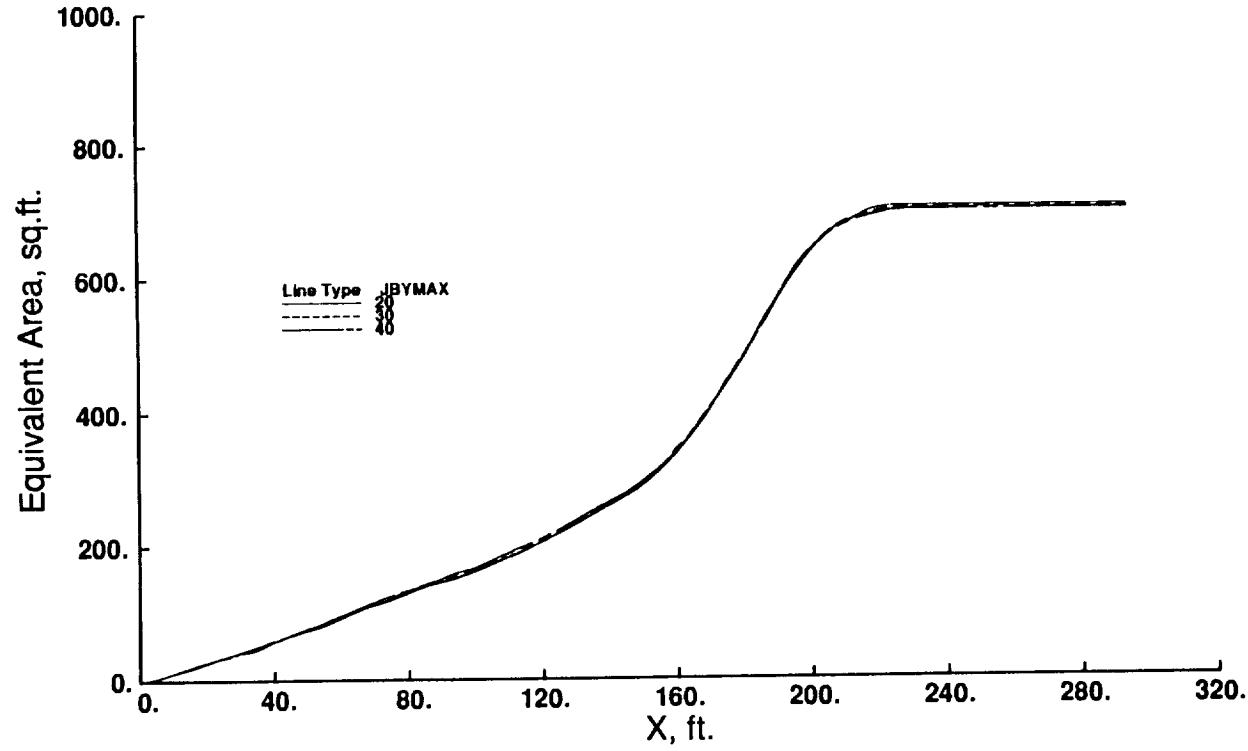

(b) Modified Linear Method

Figure 14. - Sensitivity to JBYMAX for the Mach 3.0 configuration geometry.
Mach = 1.4, h = 50,000 ft., L = 500,000 lbs.

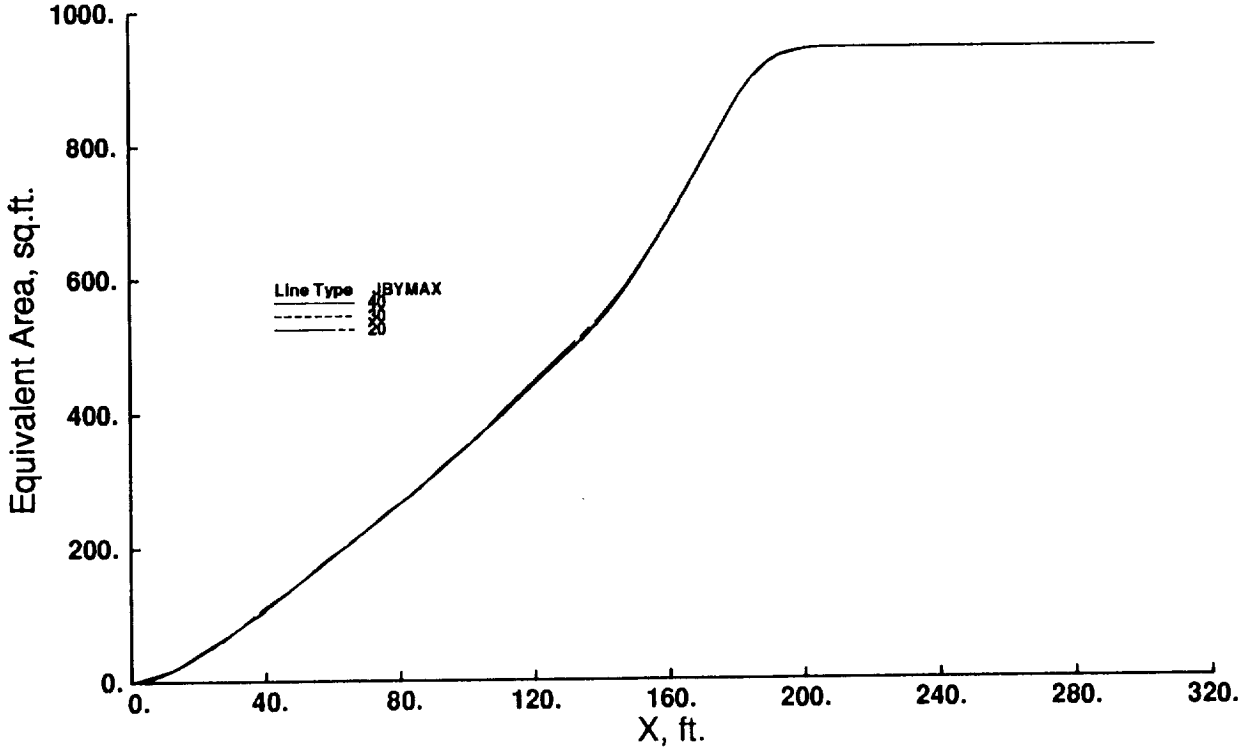

(a) Linear Method

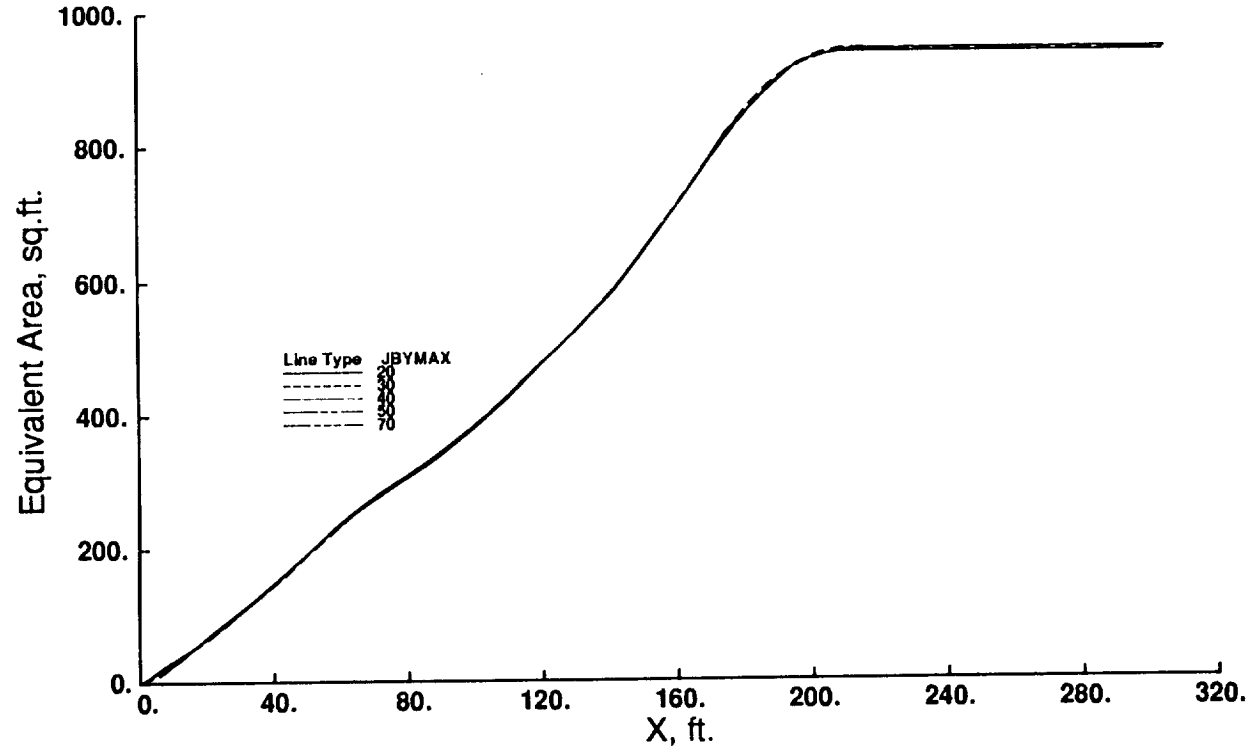

(b) Modified Linear Method

Figure 15.- Sensitivity to JBYMAX for the Mach 3.0 configuration geometry.
Mach = 3.0, h = 65,000 ft. L = 500,000 lbs.

Figure 16. - Numerical Model for the reference arrow wing geometry.

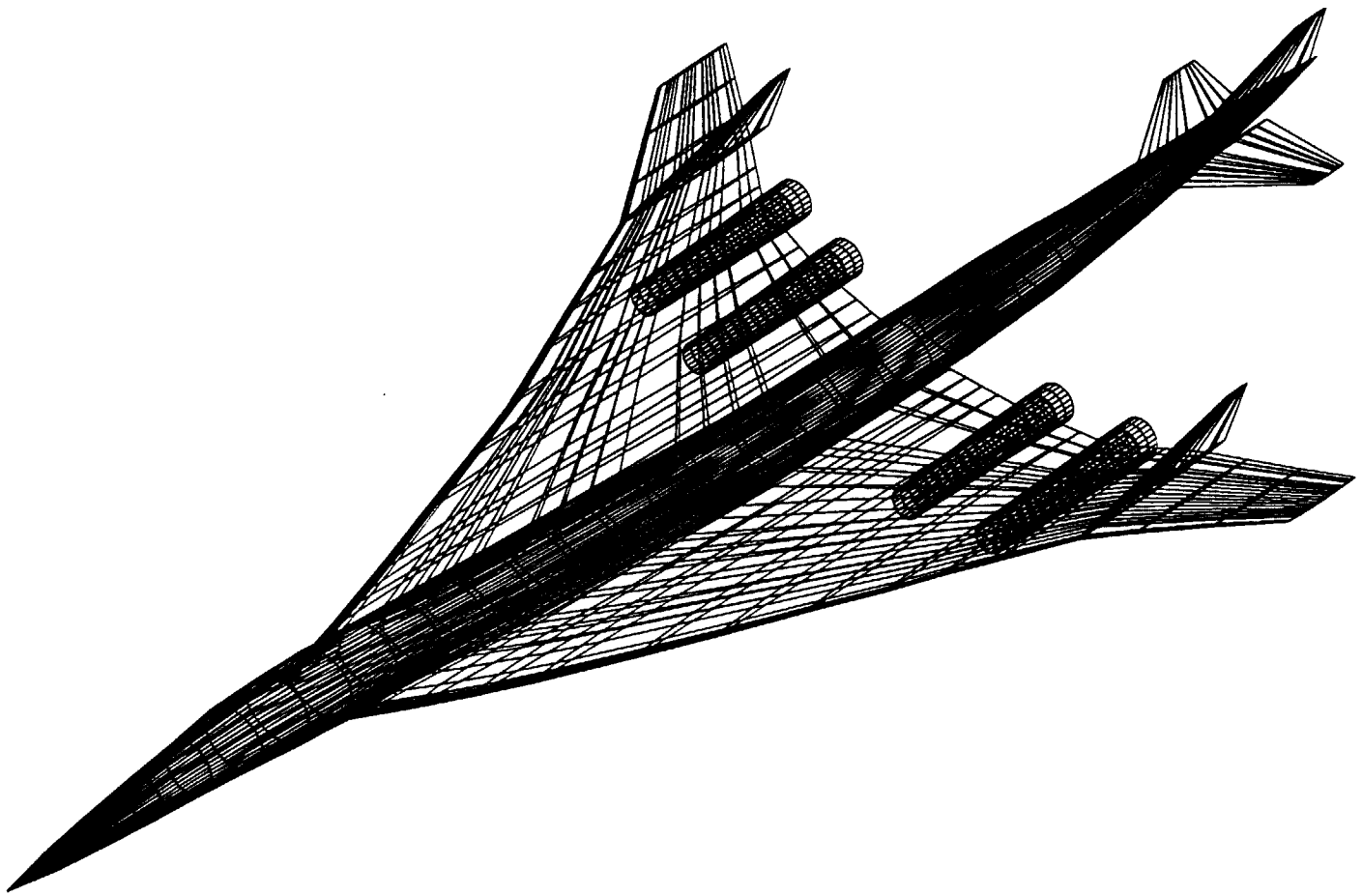

Figure 17. - Numerical model of the complete Mach 2.7 transport configuration.

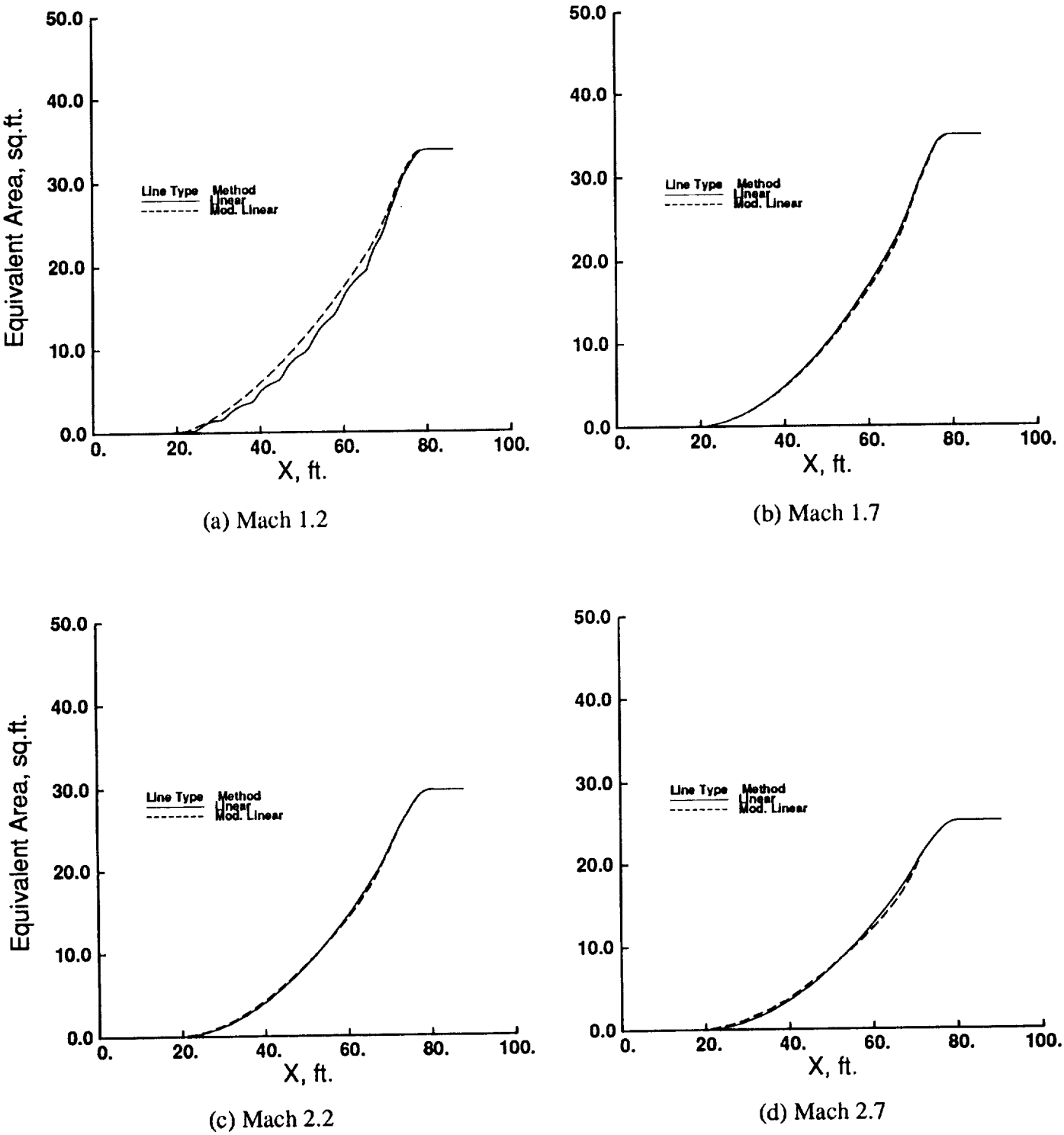

(a) Mach 1.2

(b) Mach 1.7

(c) Mach 2.2

(d) Mach 2.7

Figure 18.- Comparison of lift equivalent area distributions at several Mach numbers Reference arrow wing geometry, h = 50,000 ft., L = 25,000 lbs.

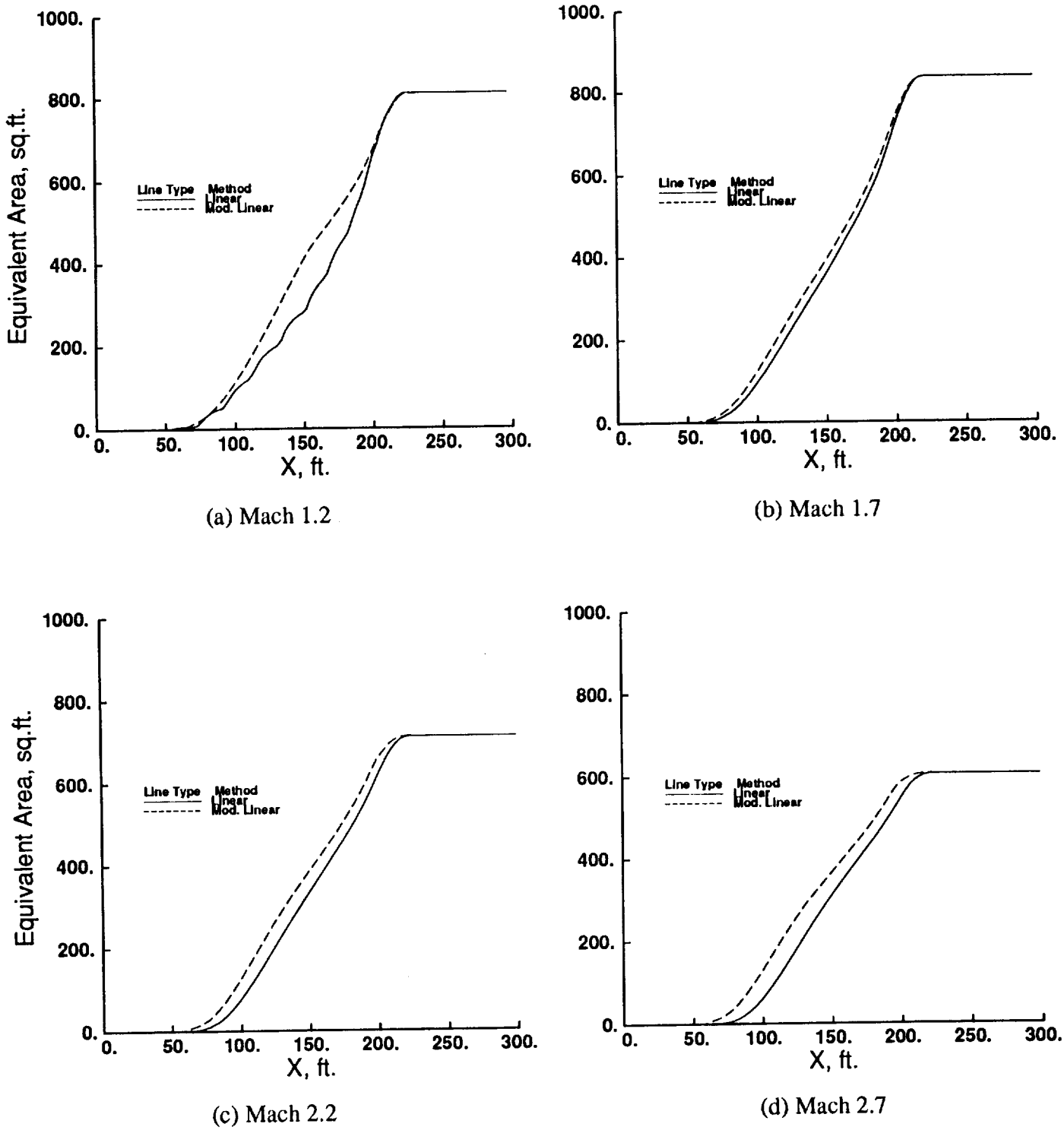

(a) Mach 1.2

(b) Mach 1.7

(c) Mach 2.2

(d) Mach 2.7

Figure 19. - Comparison of lift equivalent area distributions at several Mach numbers. Mach 2.7 configuration wing geometry, h =50,000 ft., L = 600,000 lbs.

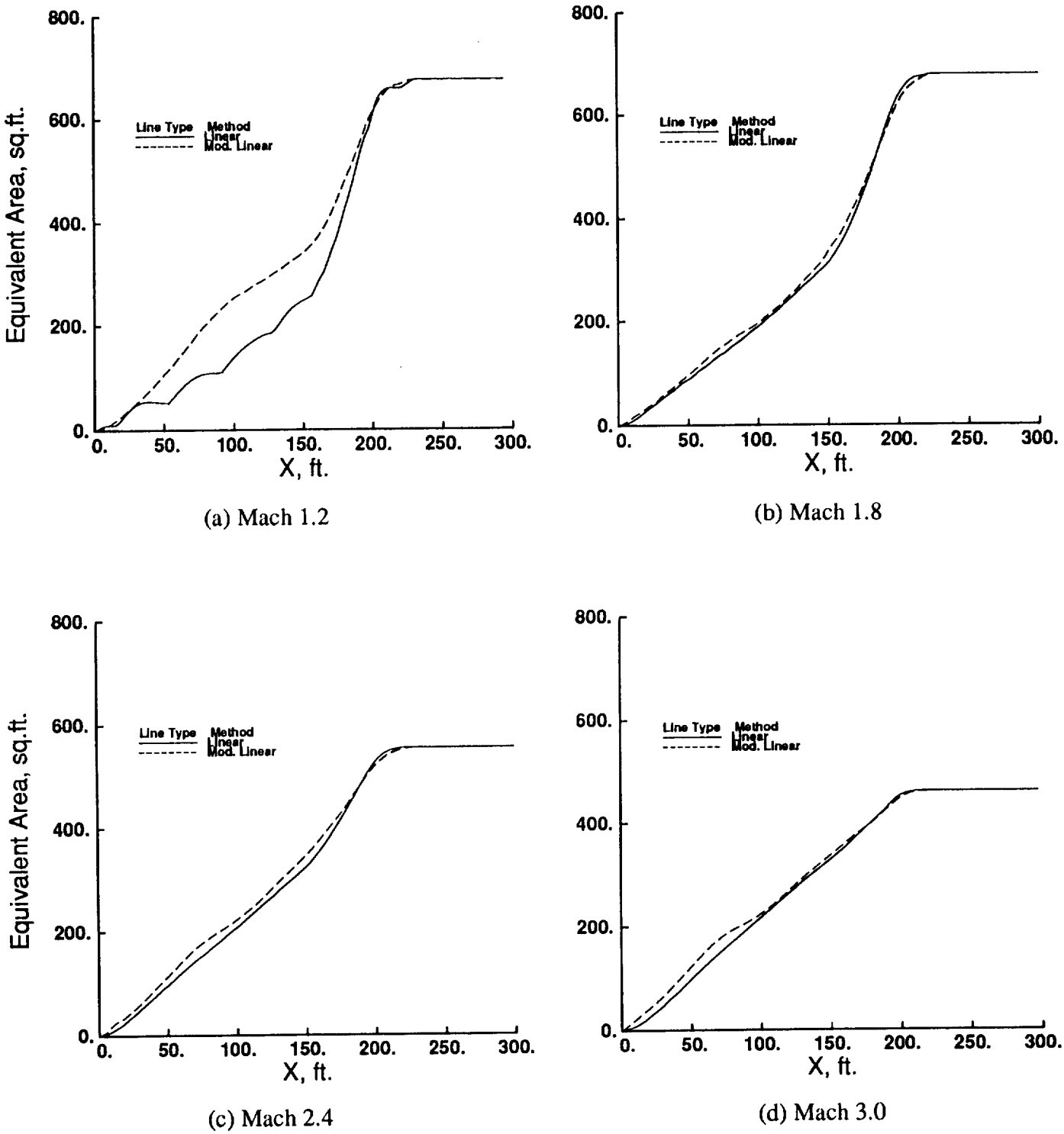

Figure 20. - Comparison of lift equivalent area distributions at several Mach numbers. Mach 3.0 configuration wing geometry, h = 50,000 ft., L = 500,000 lbs.

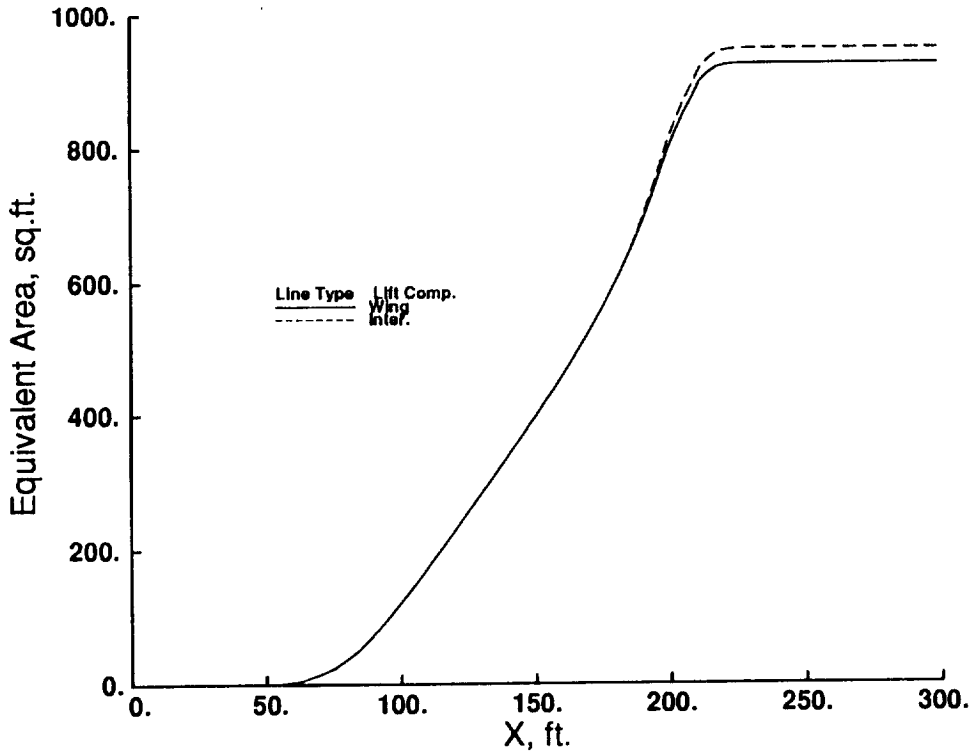

(a) Mach 2.7 Configuration @ Mach = 1.4, L = 400,000 lbs., h = 60,000 ft.

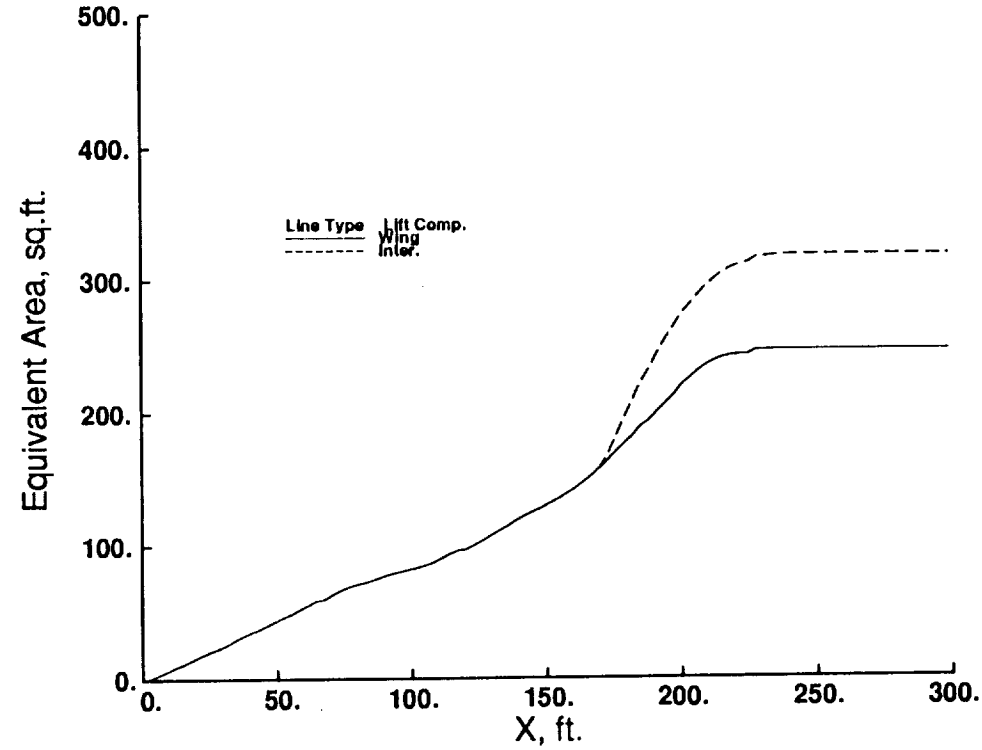

(b) Mach 3.0 Configuration @ Mach = 1.4, L = 350,000 lbs., h = 40,000 ft.

Figure 21. - Examples of the comparative contributions of wing and interference lift to the total lift equivalent area distribution.

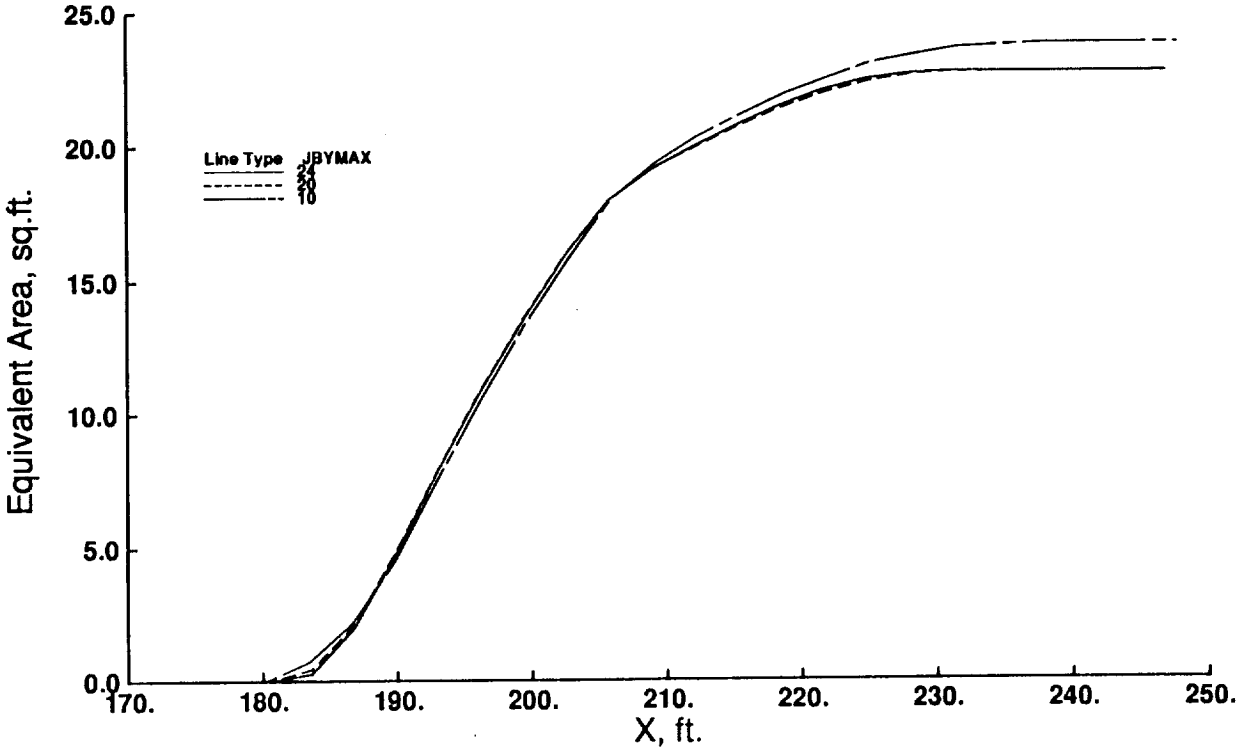

(a) Mach 1.4

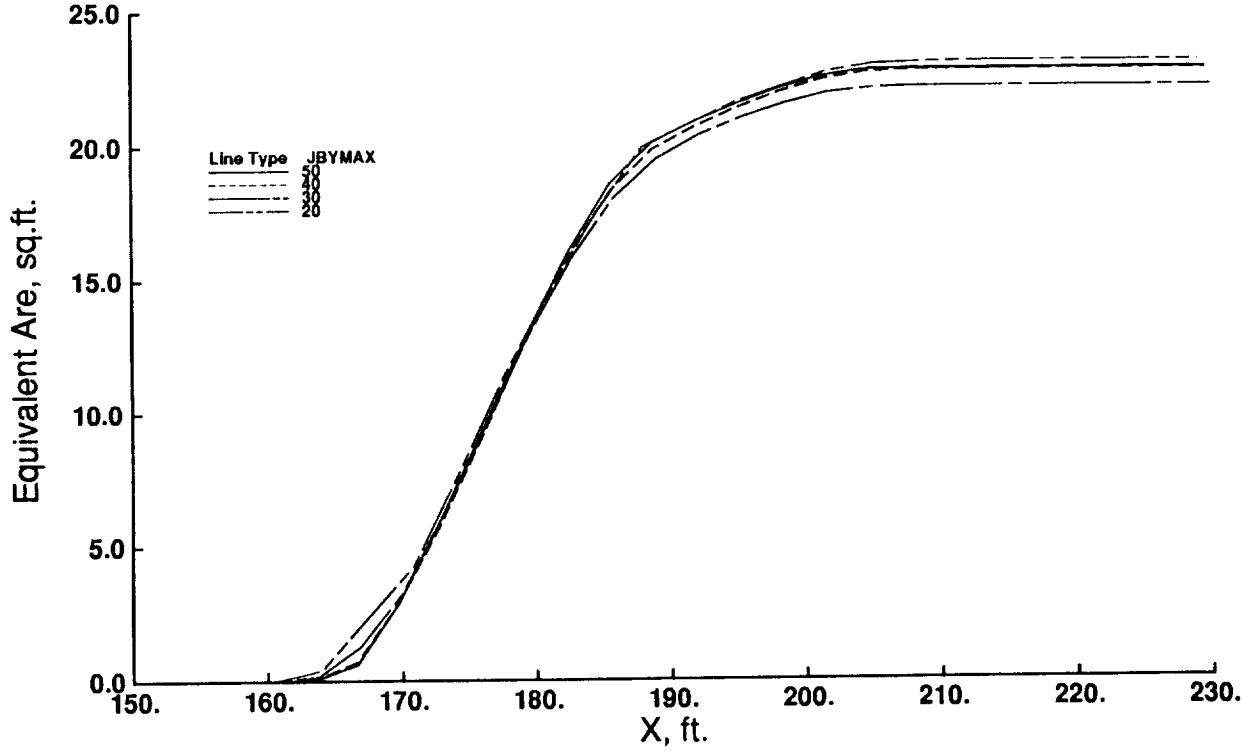

(b) Mach 2.7

Figure 22. - Sensitivity to JBYMAX for the Mach 2.7 configuration geometry Interference lift results.

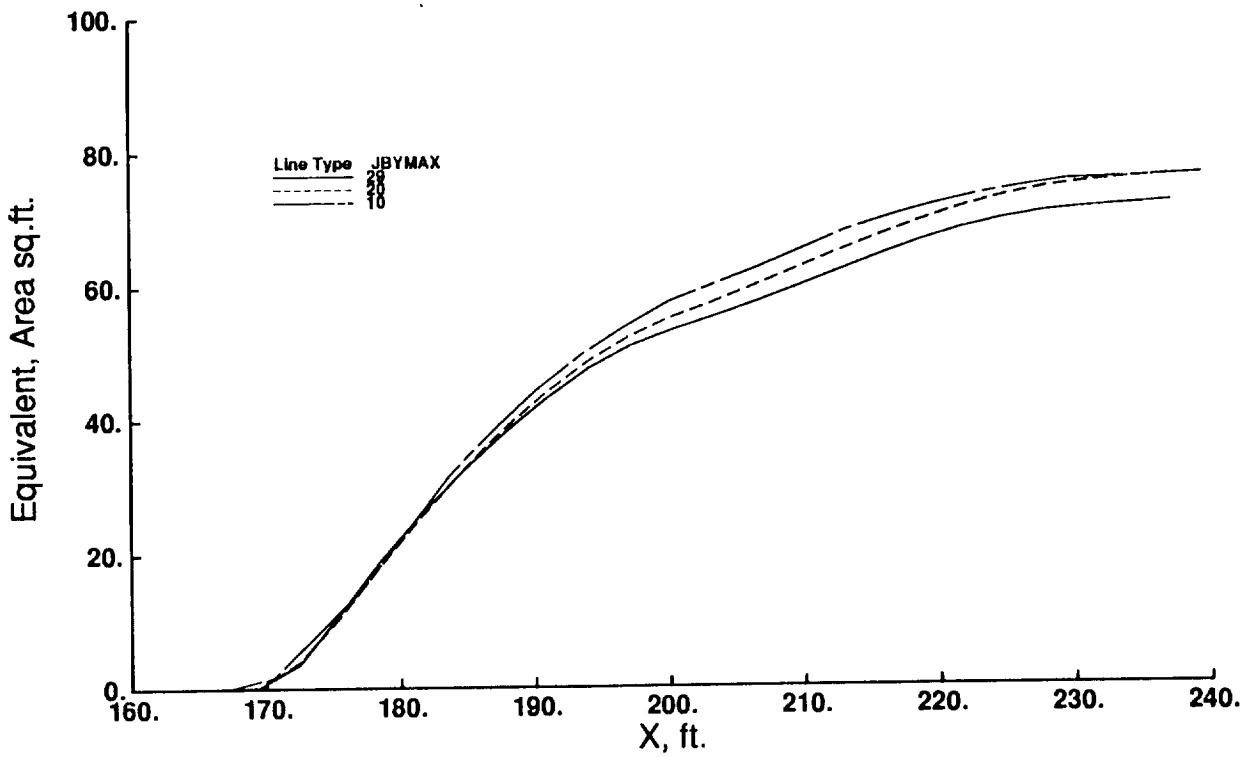

(a) Mach 1.4

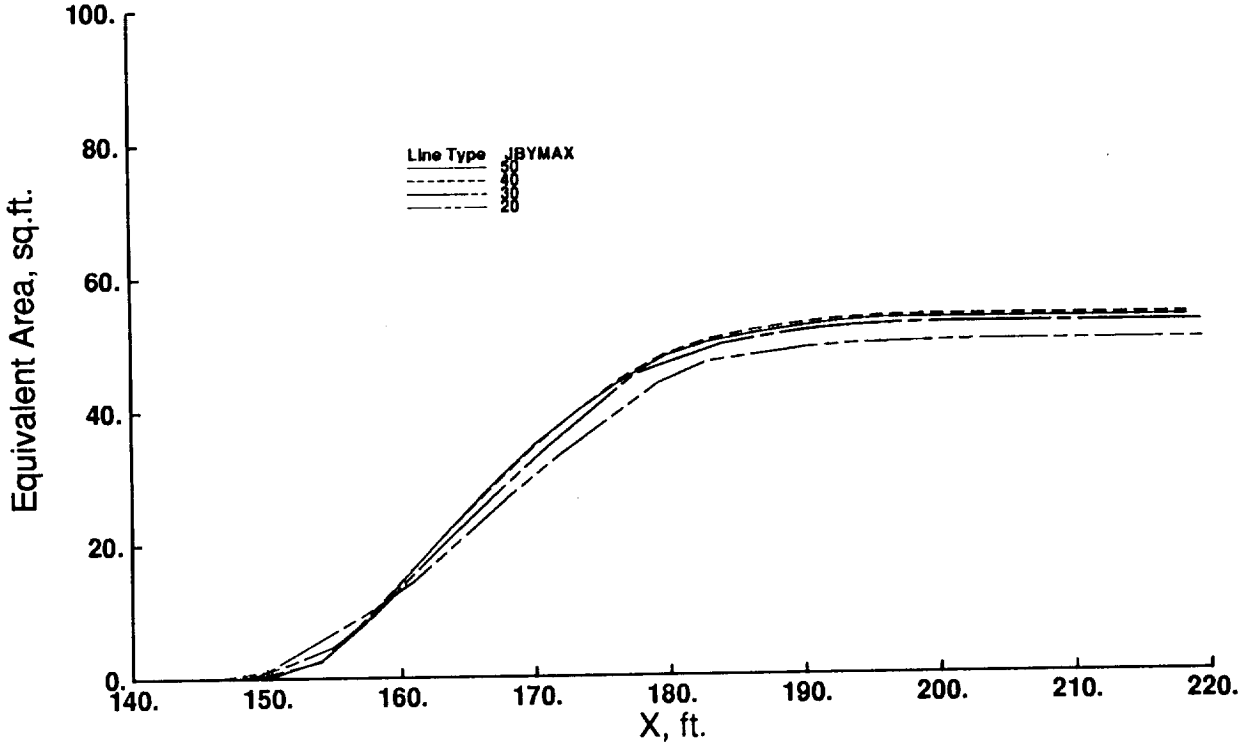

(b) Mach 3.0

Figure 23. - Sensitivity to JBYMAX for the Mach 3.0 configuration geometry. Interference lift results.

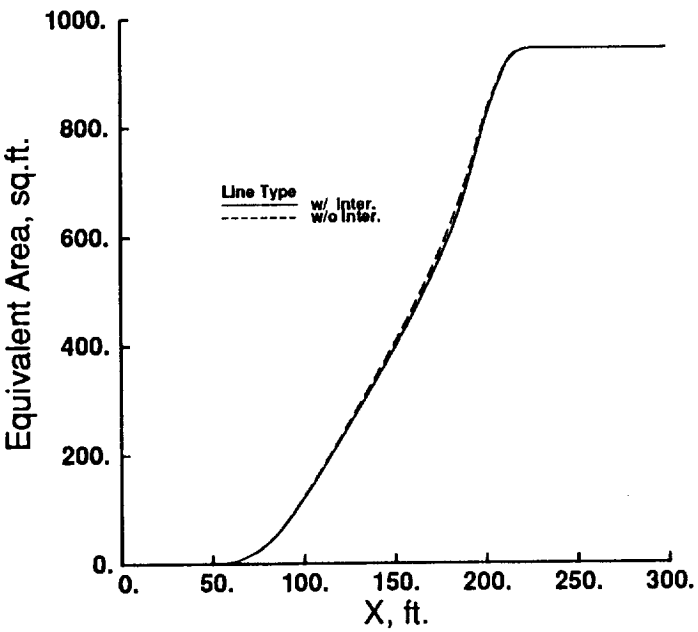

(a) Mach = 1.4, L = 400,000 lbs., h = 60000 ft.

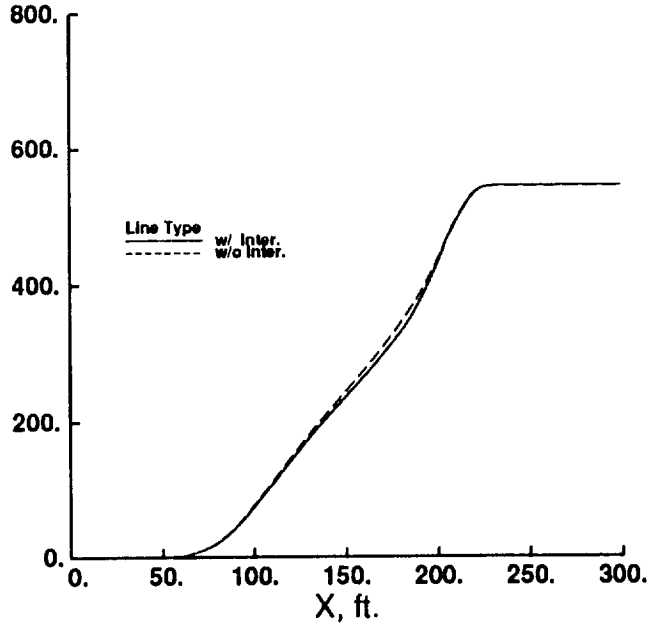

(b) Mach =1.4, L = 600,000 lbs h = 60,000 ft.

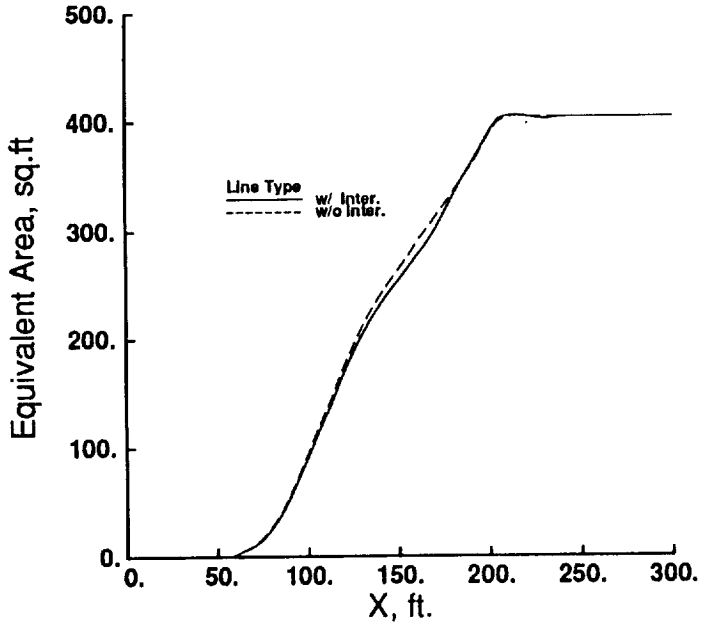

(c) Mach = 2.7 L = 400,000 lbs., h = 50,000 ft.

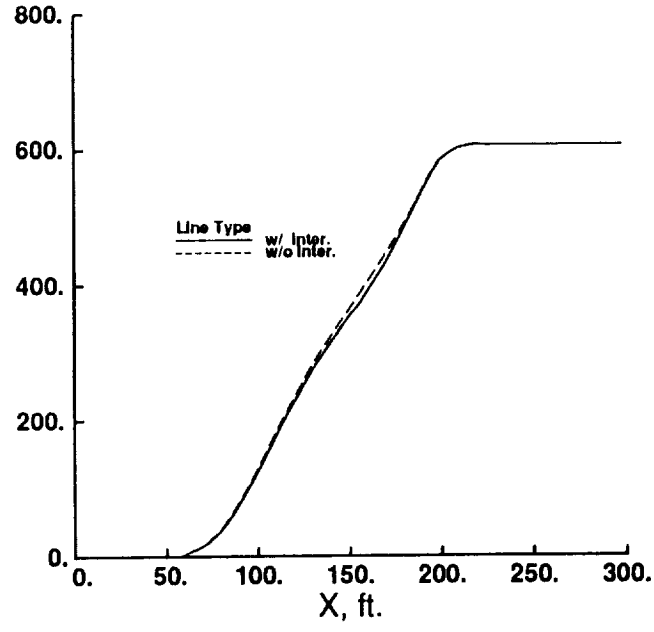

(d) Mach = 2.7, L = 600,000 lbs., h = 50,000 ft.

Figure 24. - Comparison of lift equivalent area distributions computed with and without interference lift component. Mach 2.7 configuration wing geometry.

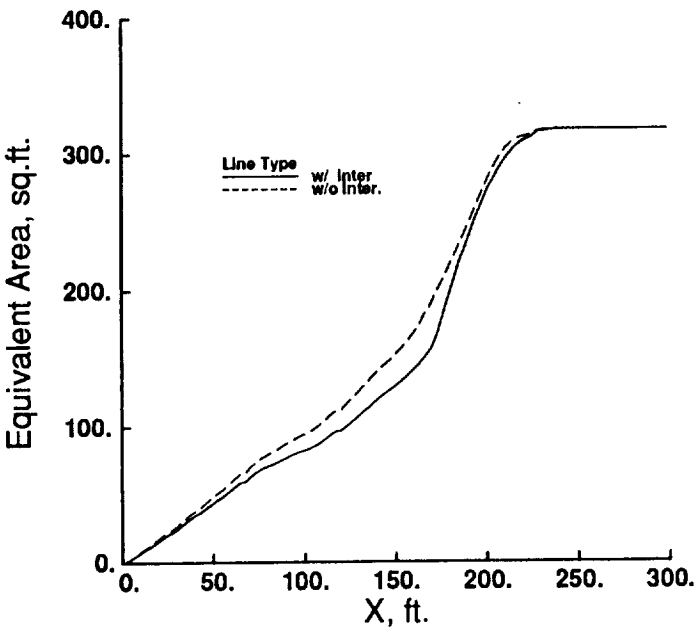

(a) Mach = 1.4, L = 350,000 lbs., h = 40000 ft.

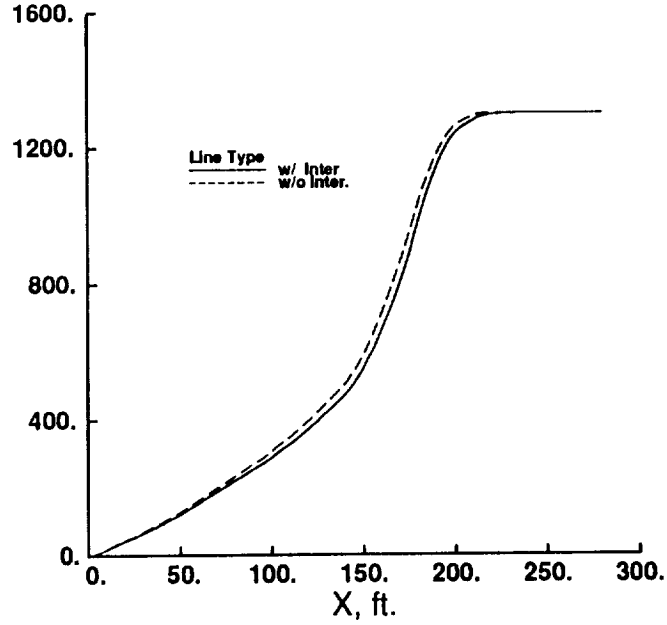

(b) Mach = 1.4, L = 550,000 lbs., h = 60,000 ft.

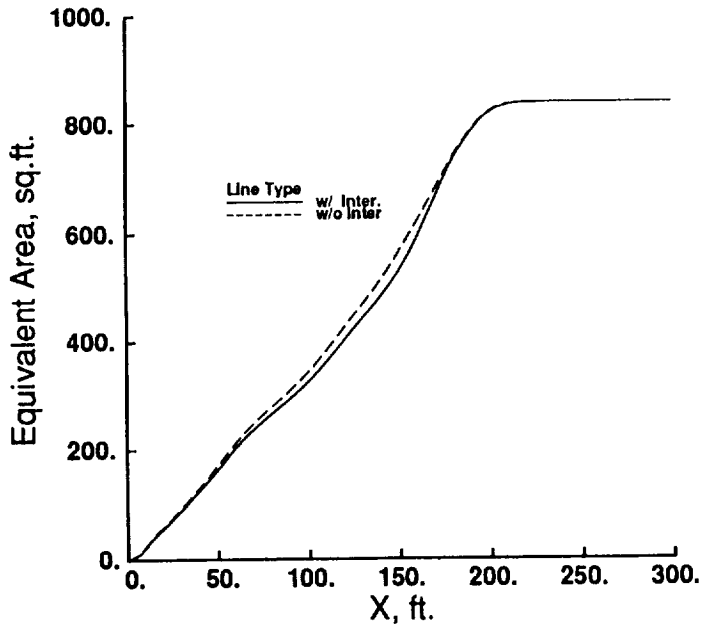

(c) Mach = 3.0, L = 350,000 lbs., h = 70,000 ft.

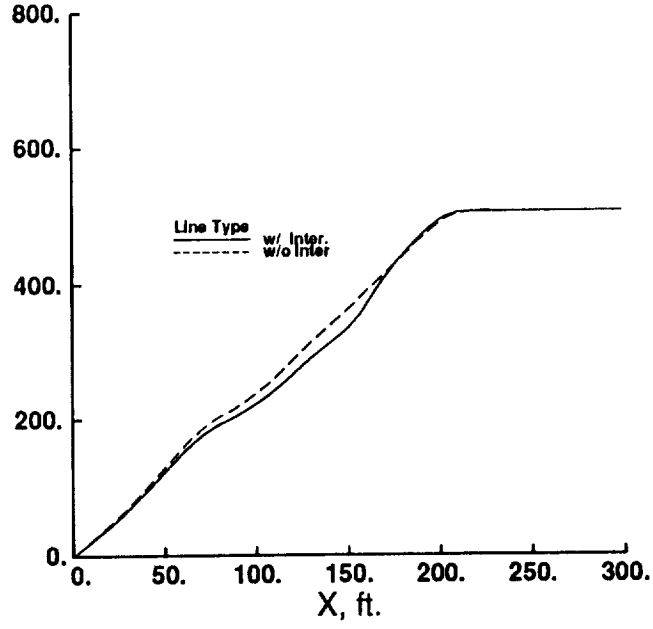

(d) Mach = 3.0, L = 550,000 lbs., h = 50,000 ft.

Figure 25. - Comparison of lift equivalent area distributions computed with and without interference lift component. Mach 3.0 configuration wing geometry.

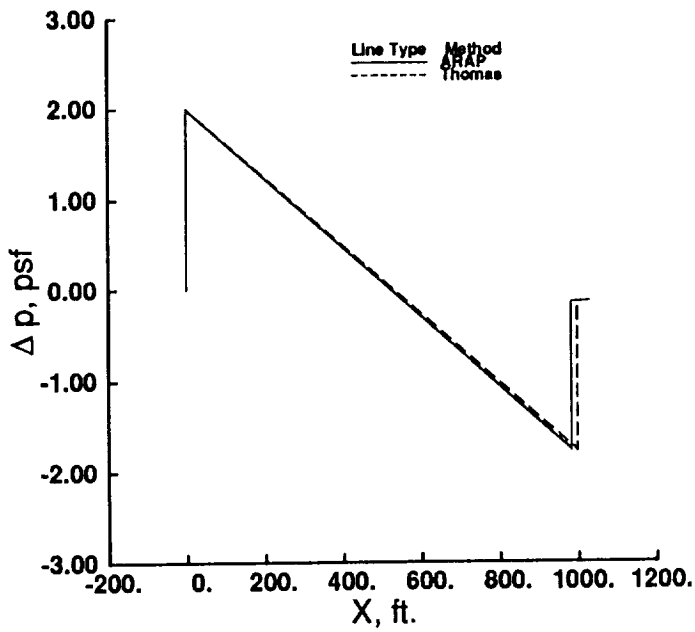

(a) h = 65000 ft.

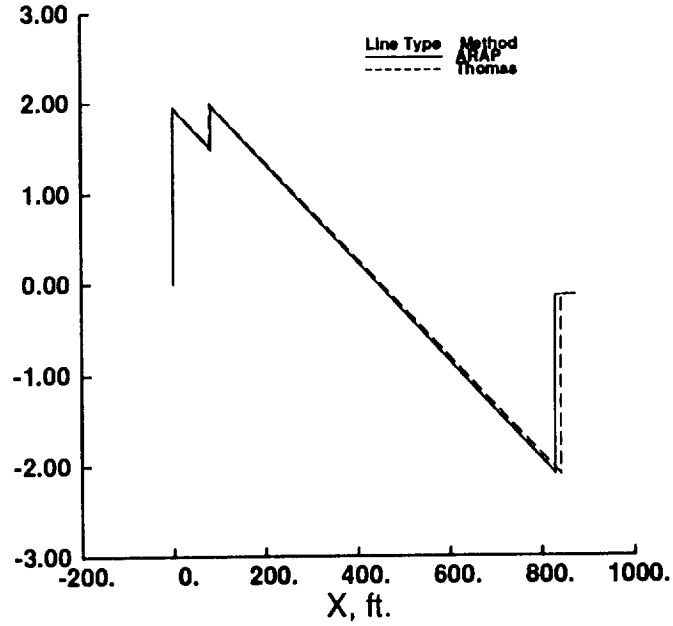

(b) h = 55,000 ft.

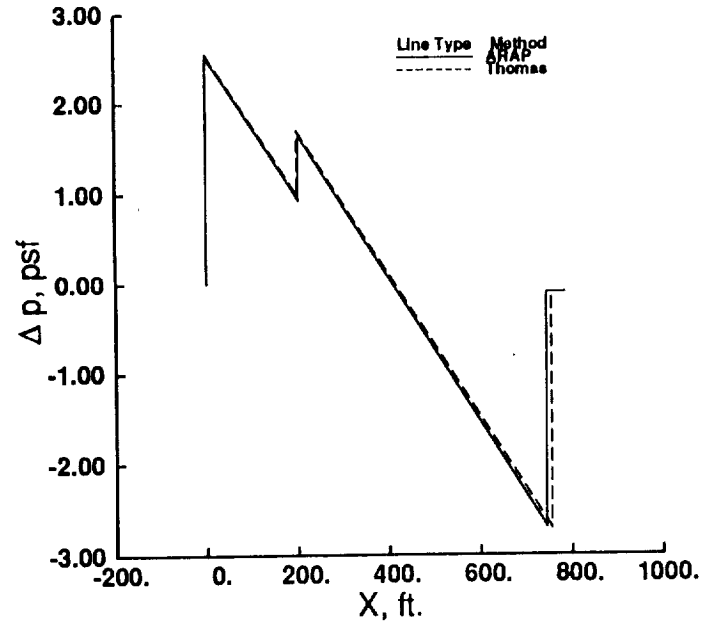

(c) h = 45,000 ft.

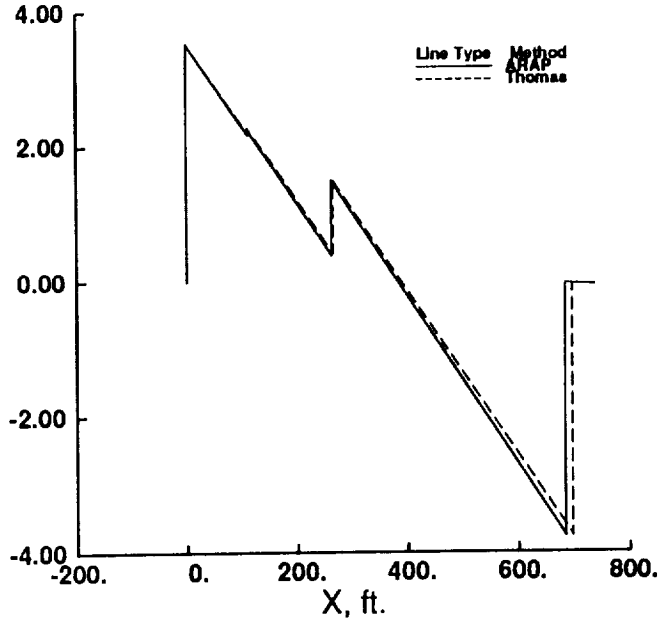

(d) h = 35,000 ft.

Figure 26. - Comparison of signature extrapolation results for steady flight.
Mach 3.0 configuration geometry,
Mach = 3.0, L = 550,000 lbs.

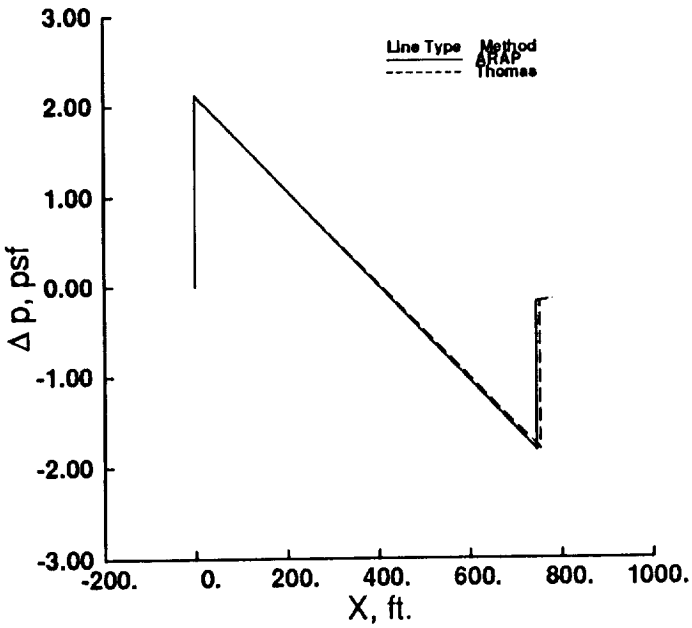

(a) h = 65,000 ft.

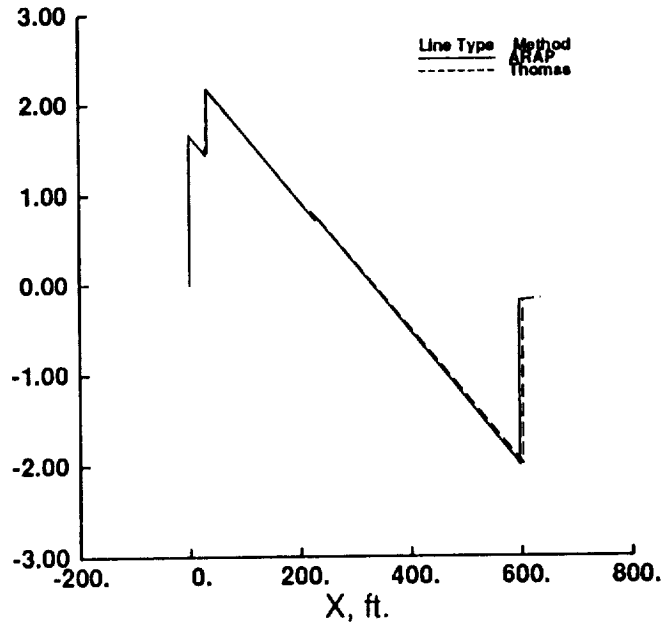

(b) h = 55,000 ft.

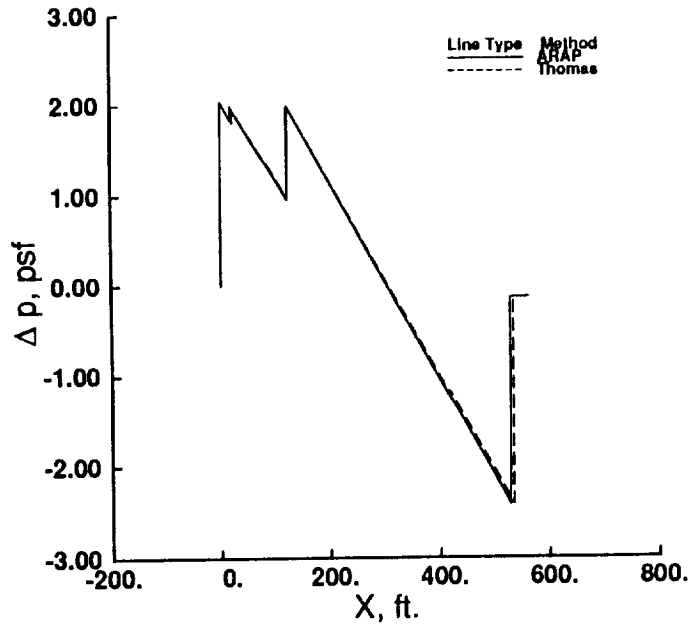

(c) h = 45,000 ft.

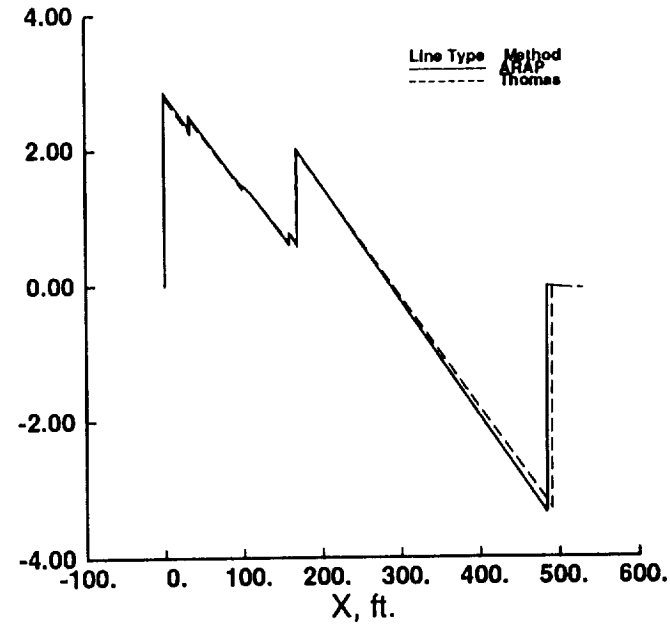

(d) h = 35,000 ft.

Figure 27. - Comparison of signature extrapolation results for steady flight.
Mach 3.0 configuration geometry,
Mach = 2.0, L = 550,000 lbs.

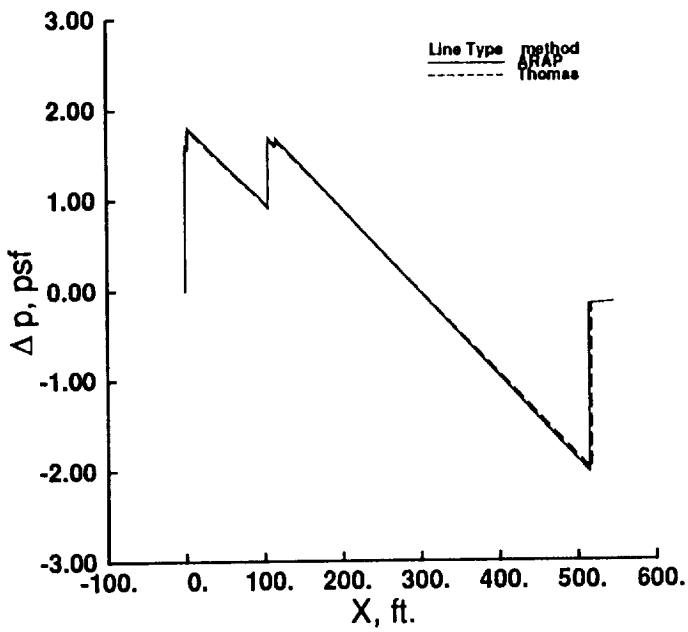

(a) h = 55, 000 ft.

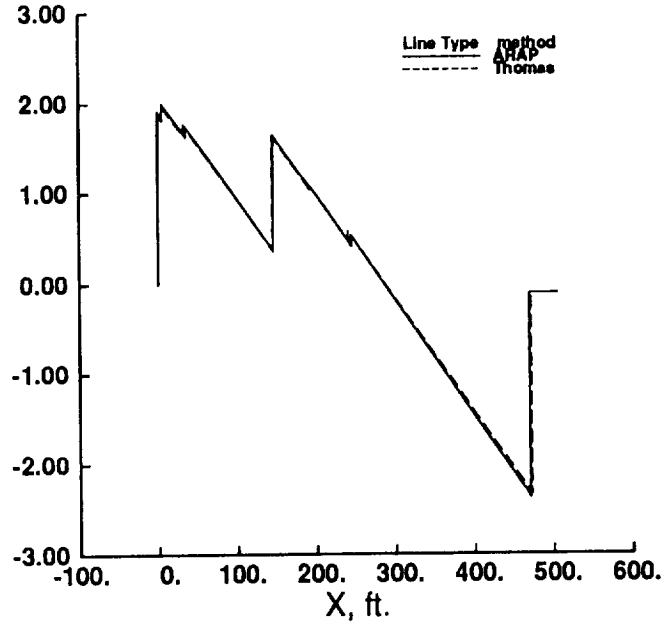

(b) h =4 5,000 ft.

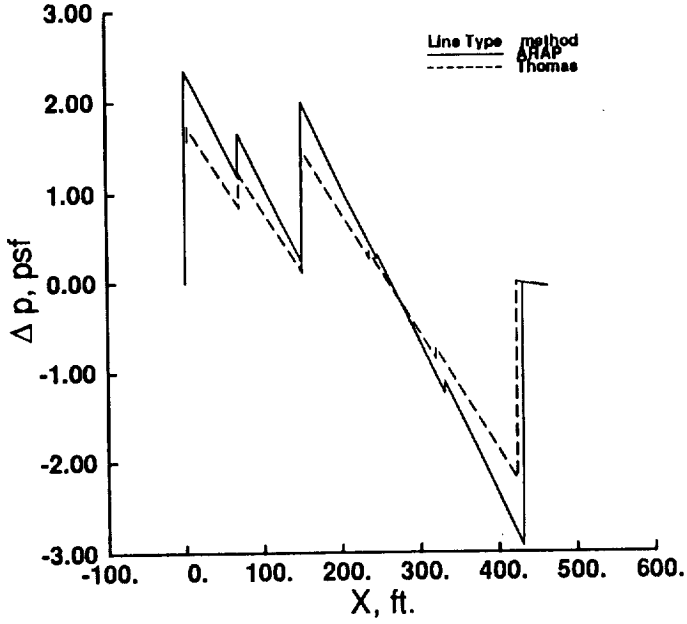

(c) h = 35,000 ft.

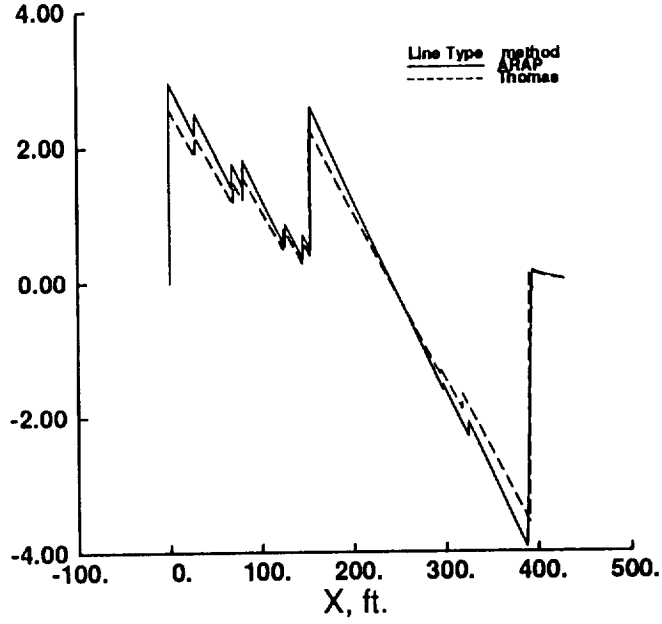

(d) h = 25,000 ft.

Figure 28. - Comparison of signature extrapolation results for steady flight.
Mach 3.0 Configuration geometry,
Mach = 1.2, L = 550,000 lbs.

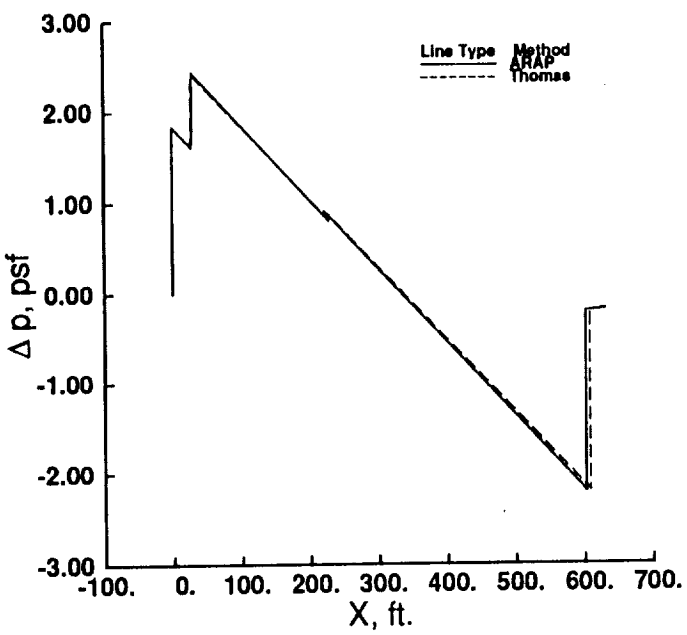

(a) a/g = .5

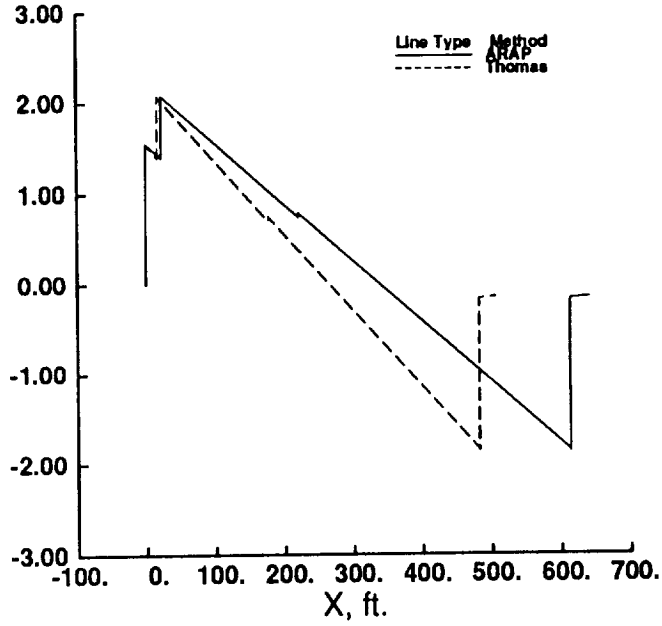

(b) γ = 10 deg.

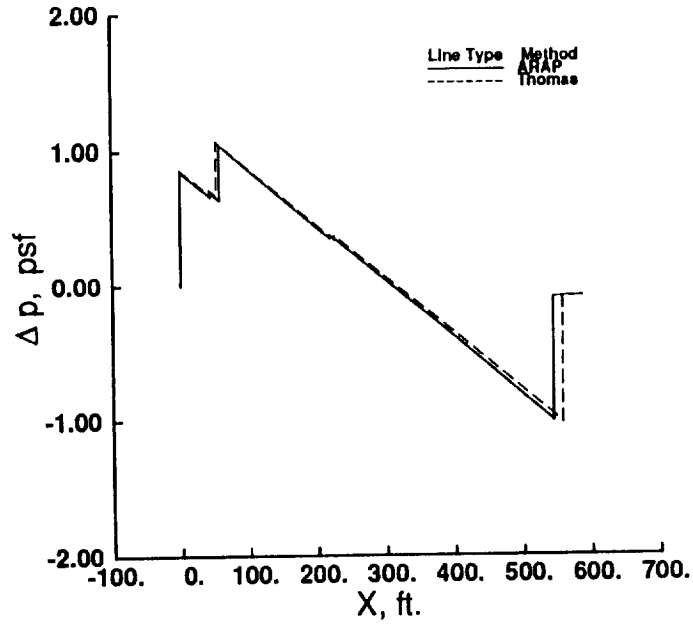

(c) $\dot{\gamma}$ = 5 deg./sec

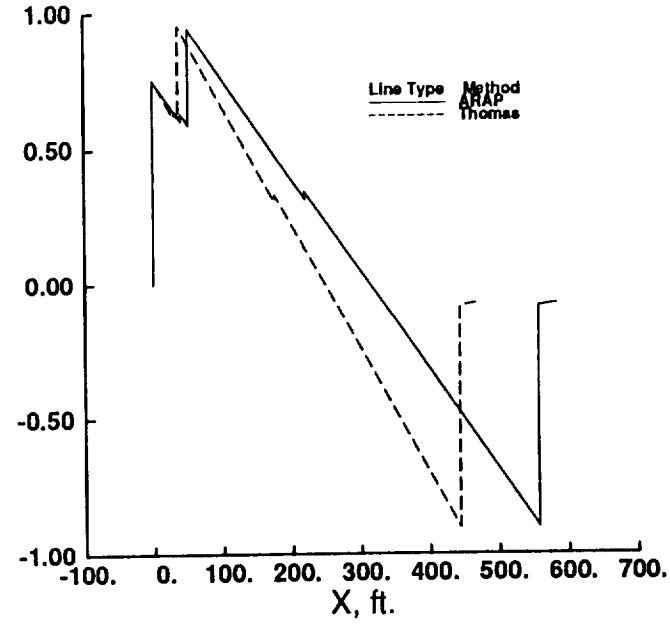

(d) a/g = .5g, γ = 10 deg., $\dot{\gamma}$ = 5

Figure 29. - Comparison of signature extrapolation results for maneuvering flight.
Mach 3.0 configuration geometry,
Mach = 2.0, L = 550,000 lbs., h = 55,000 ft.

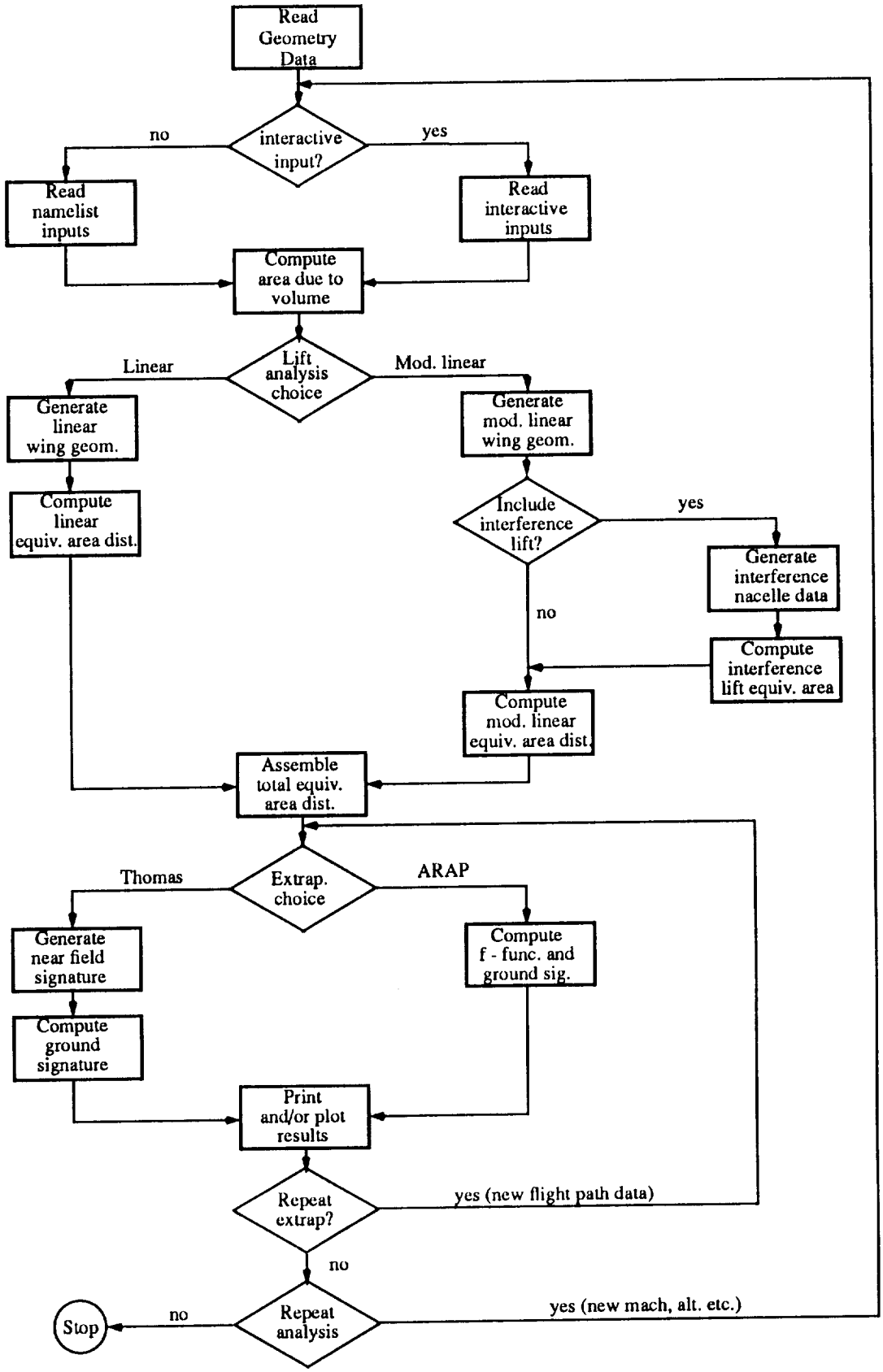

Figure 30. - Flowchart for the stand-alone integrated sonic boom analysis program.

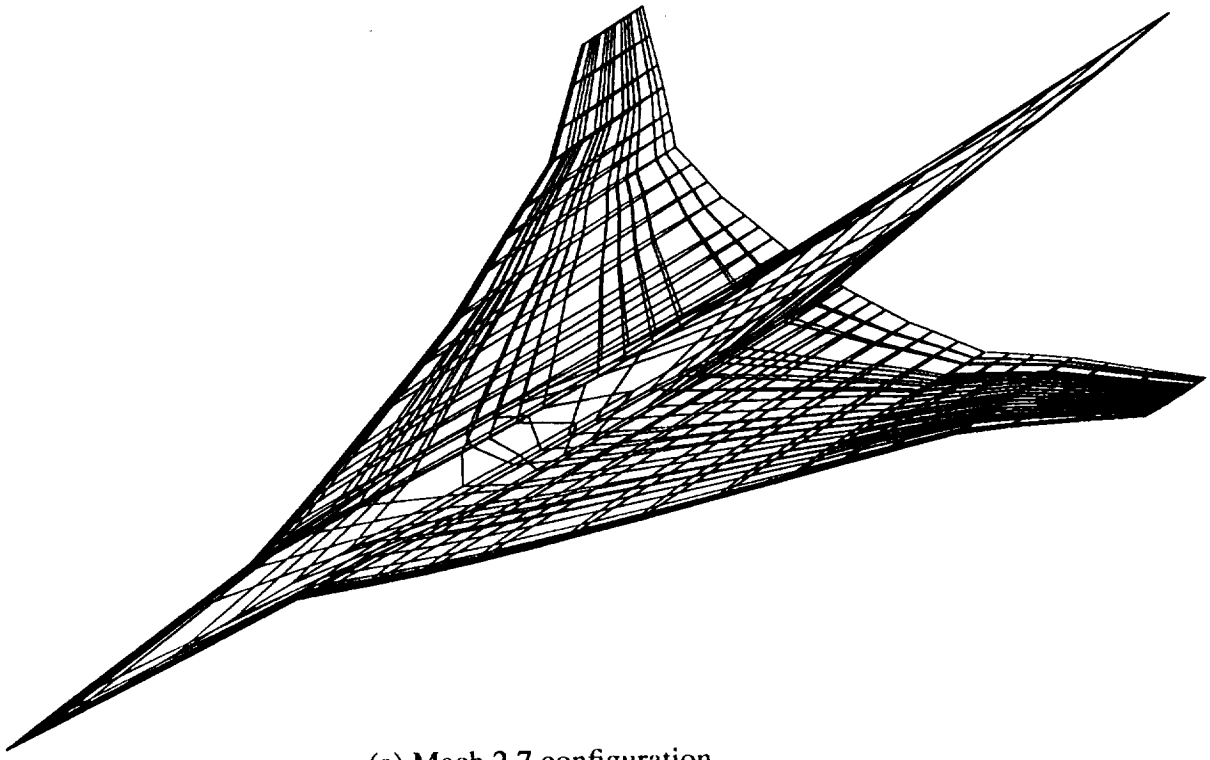

(a) Mach 2.7 configuration

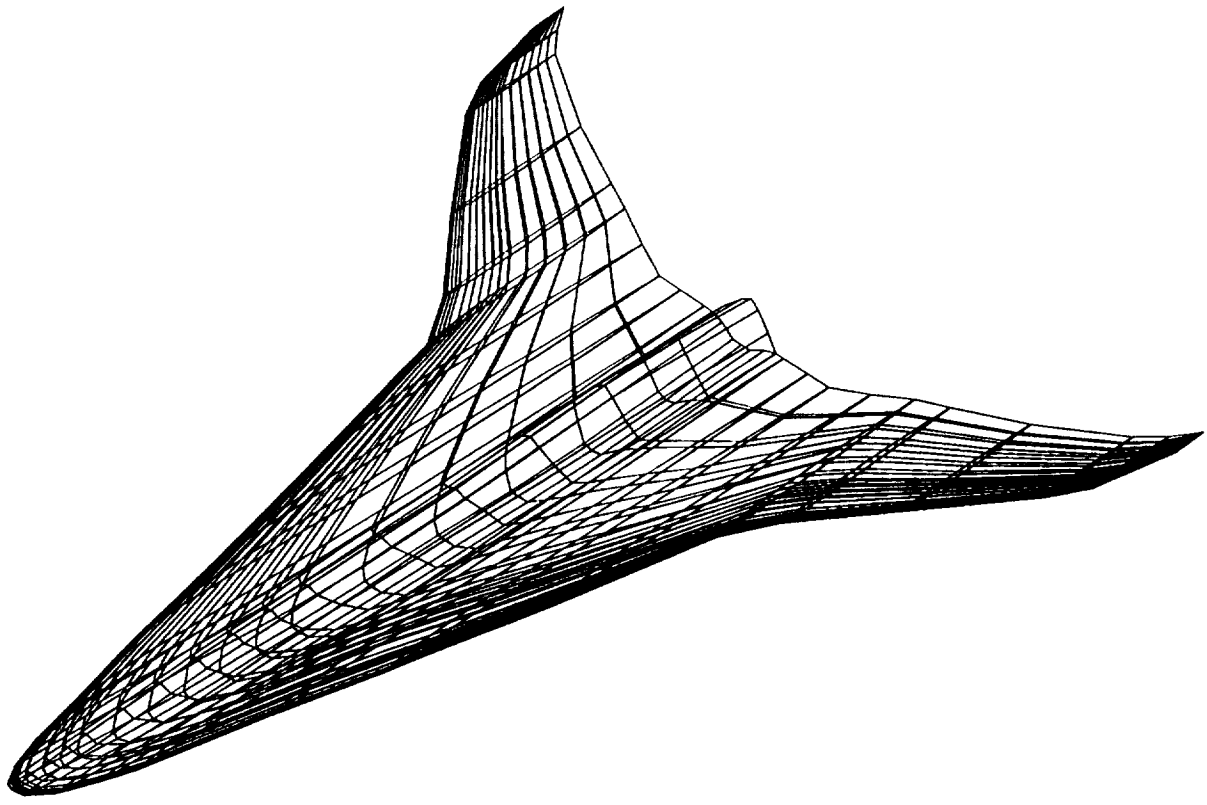

(b) Mach 3.0 configuration

Figure 31. - Examples of numerical models used in configuration lift analysis.

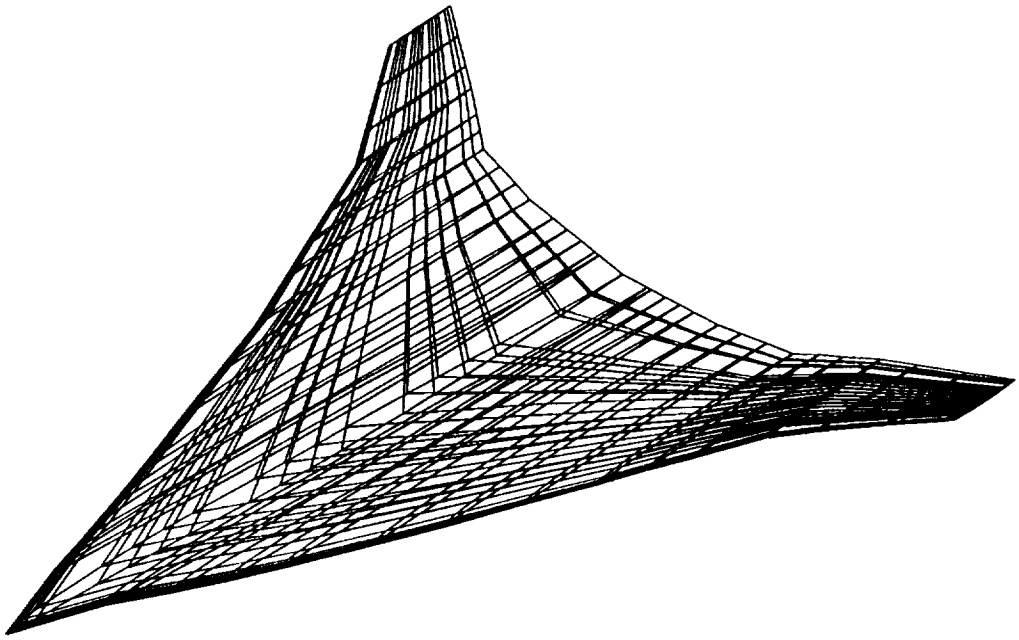

(a) Wing only model

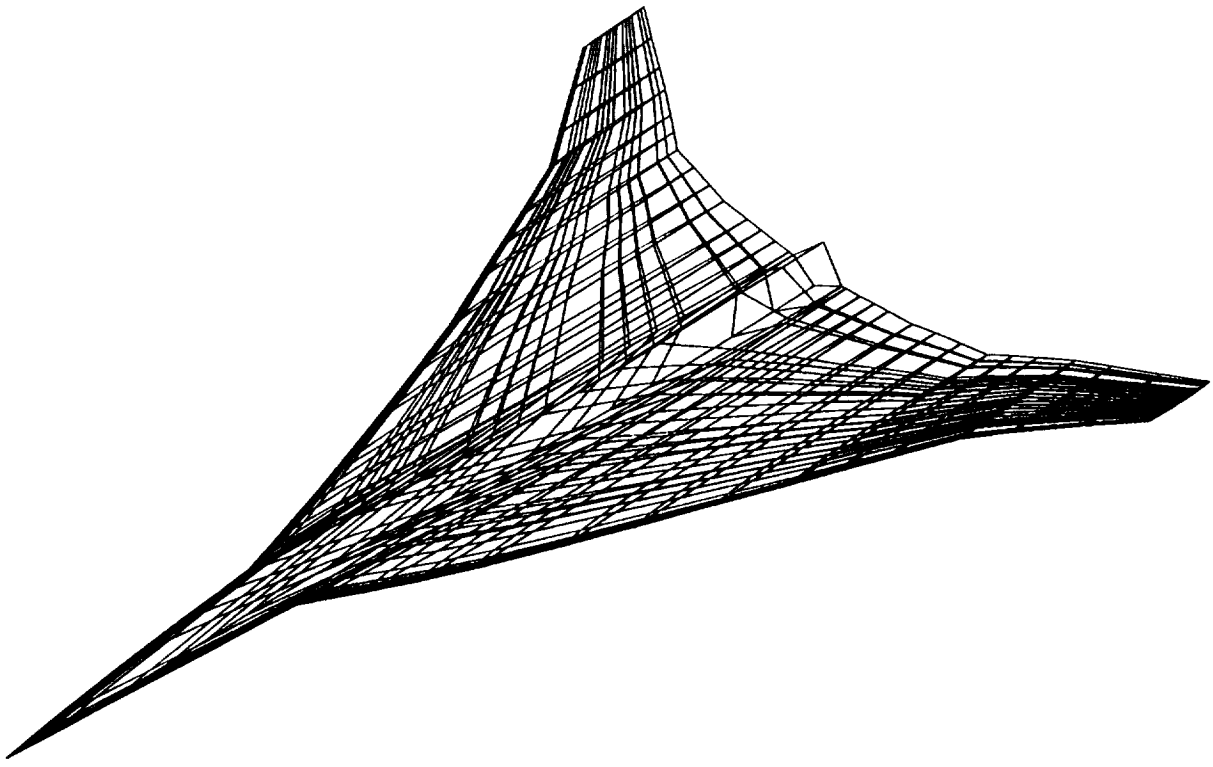

(b) Wing and fuselage model

Figure 32. - Wing lift analysis numerical models generated from the Mach 2.7 configuration geometry description.

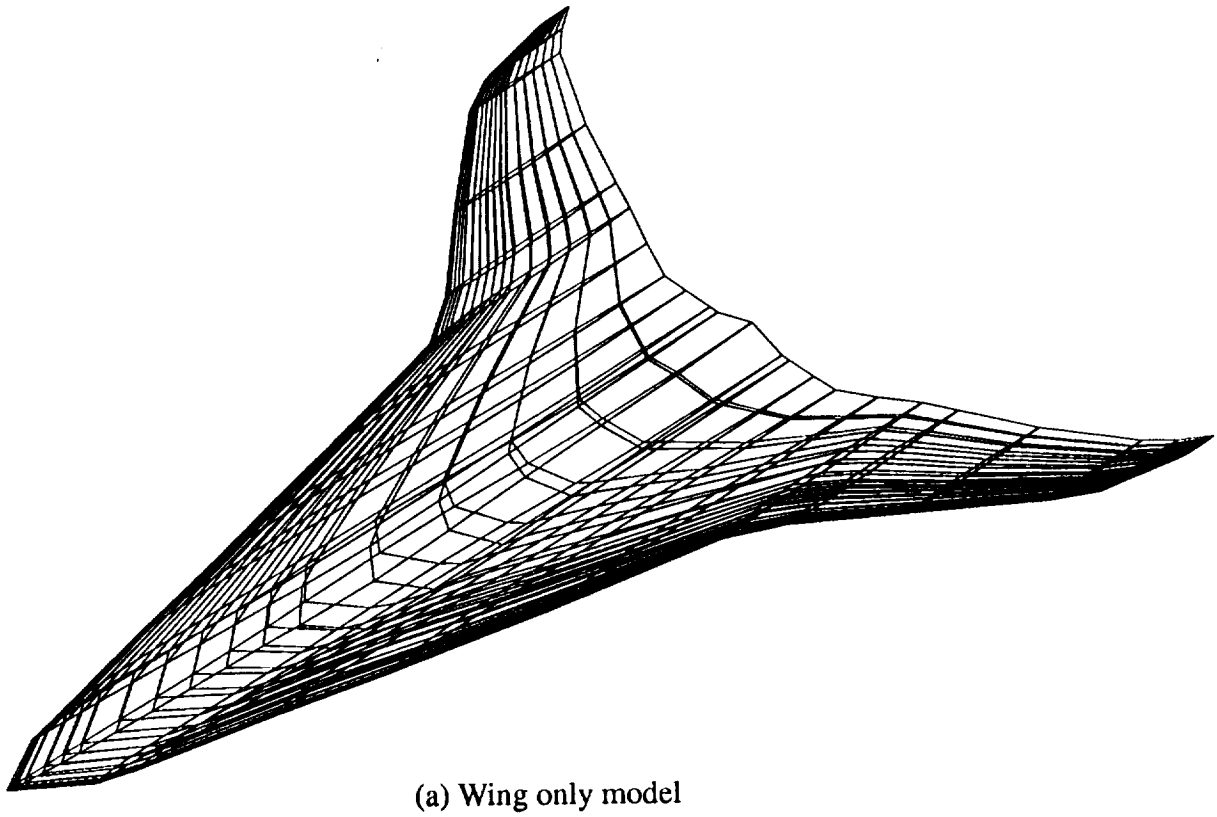

(a) Wing only model

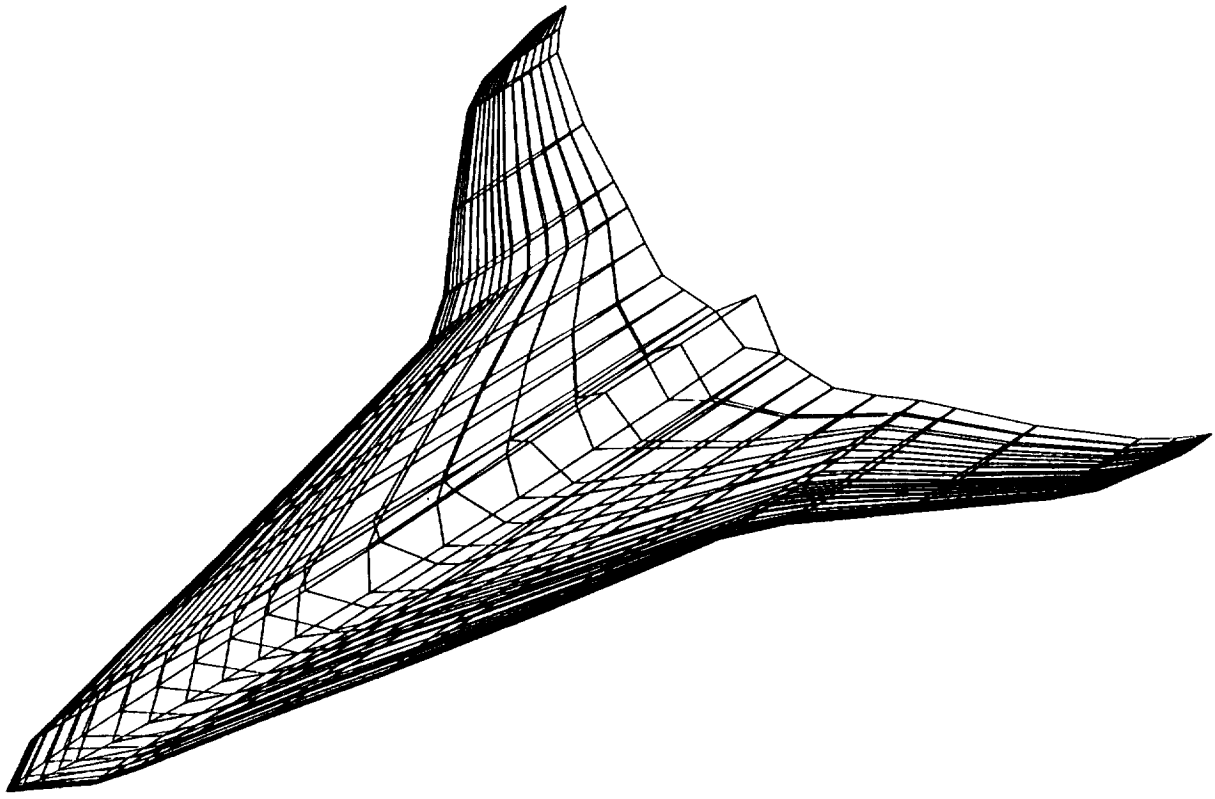

(b) Wing and fuselage model

Figure 33. - Wing lift analysis numerical models generated from the Mach 3.0 configuration geometry description.

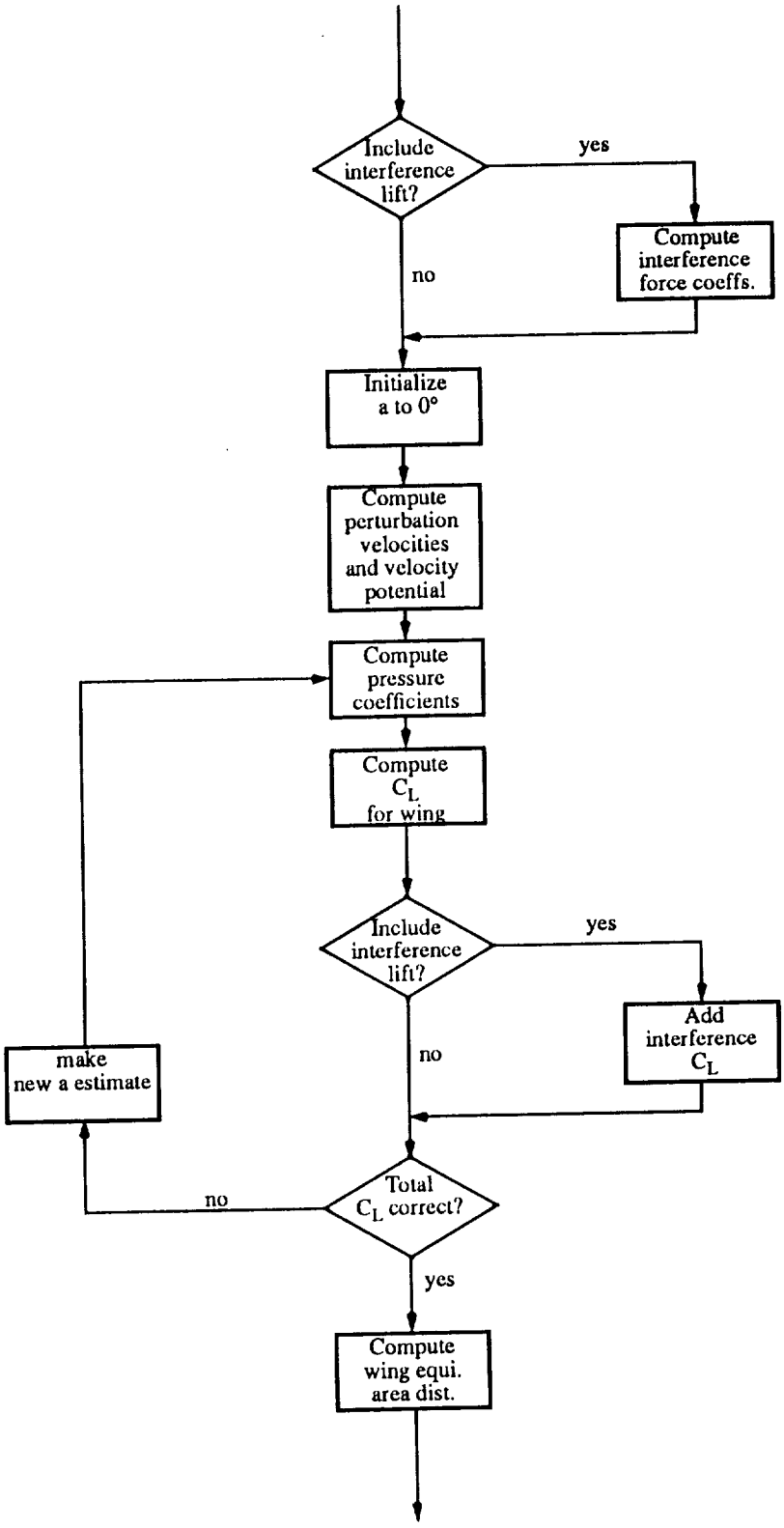

Figure 34 - Flowchart illustrating the procedure used to determine α required for a given total lift in the modified linear lift analysis.

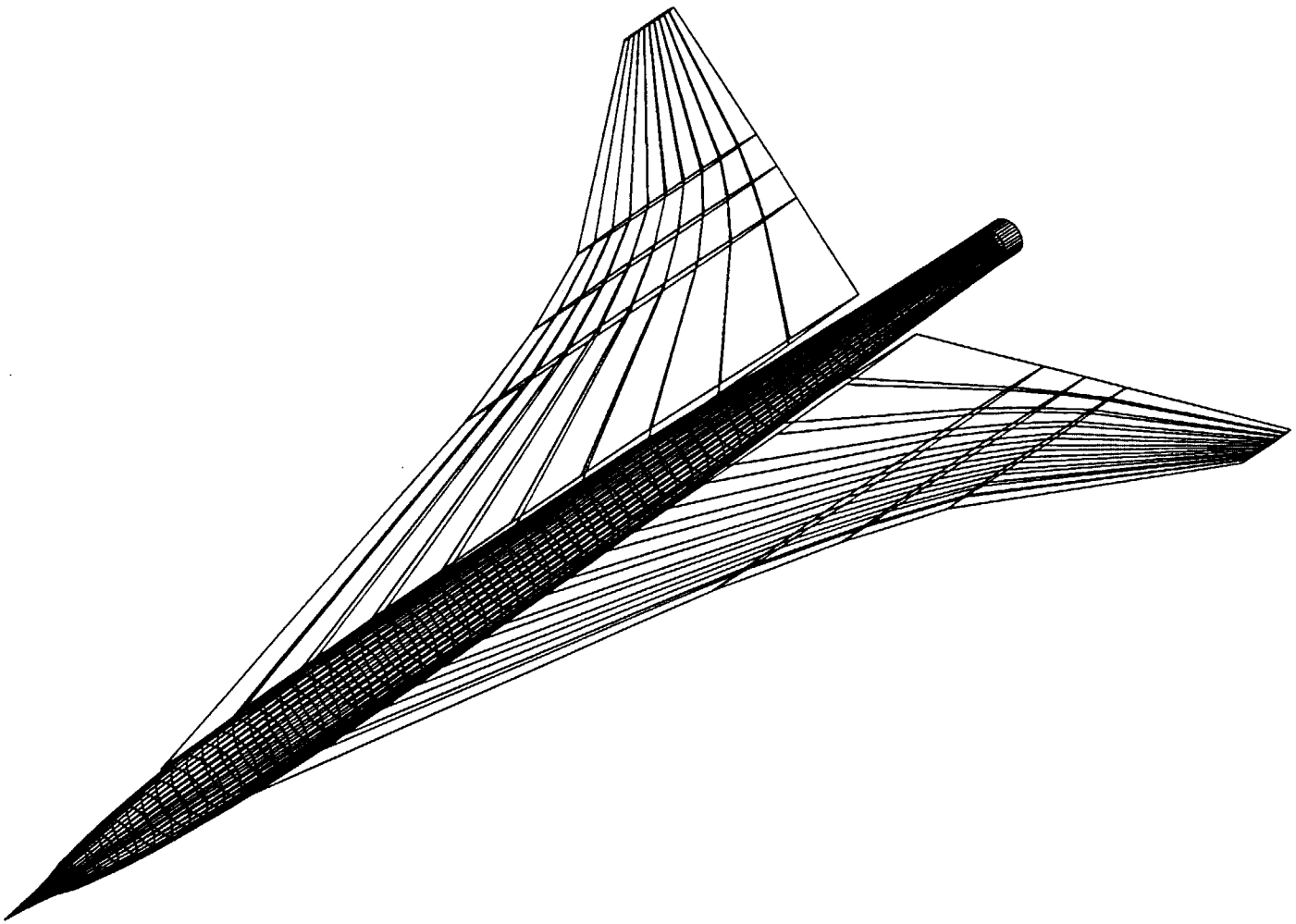

Figure 35. - Numerical model for the Mach 2.7 low boom arrow wing configuration from reference 14.

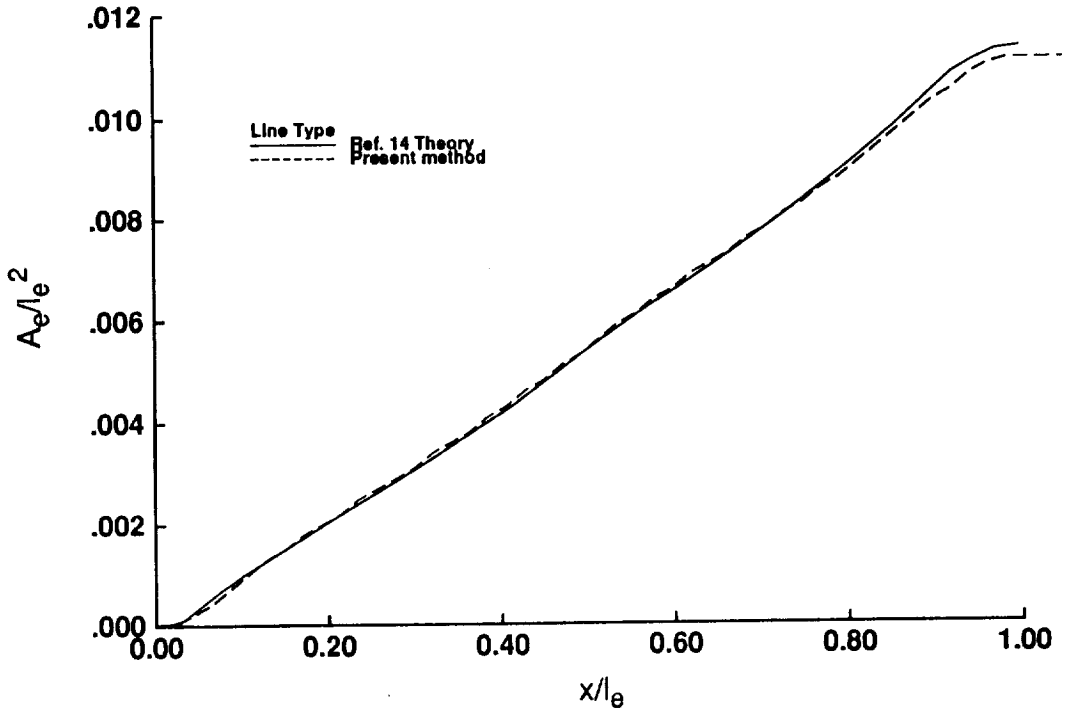

(a) Equivalent area distribution.

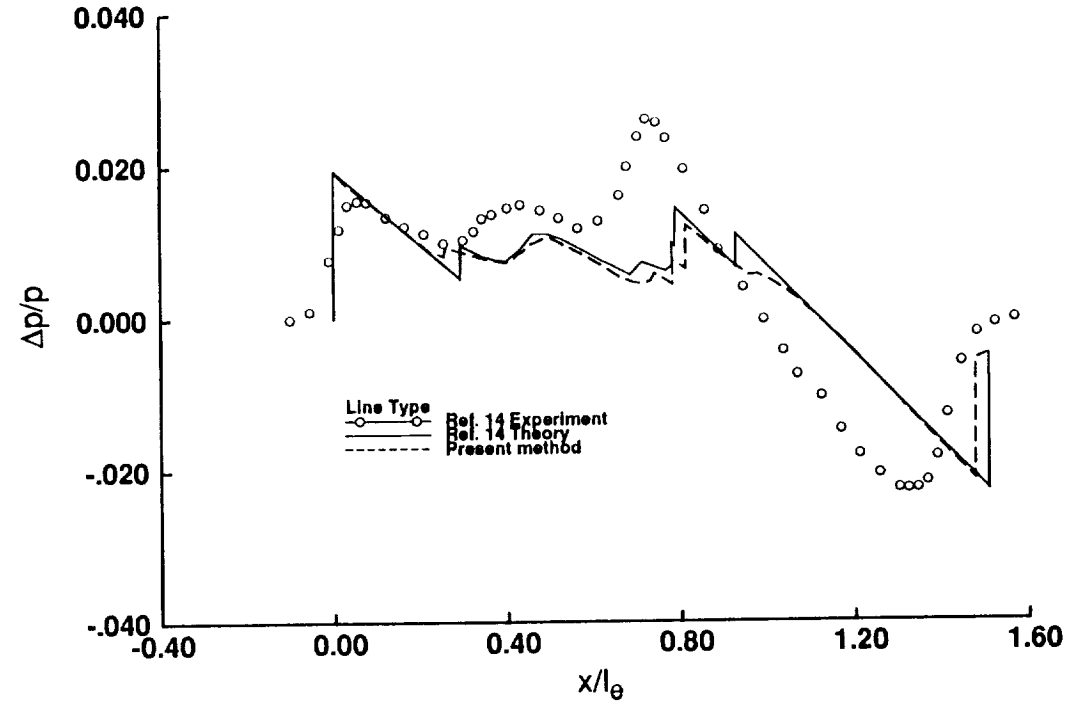

(b) Pressure signature

Figure 36. - Comparison of overpressure module results with experimental and theoretical data from reference 14.
Low Boom Arrow Wing, Mach 2.7, α = 2.033 deg.

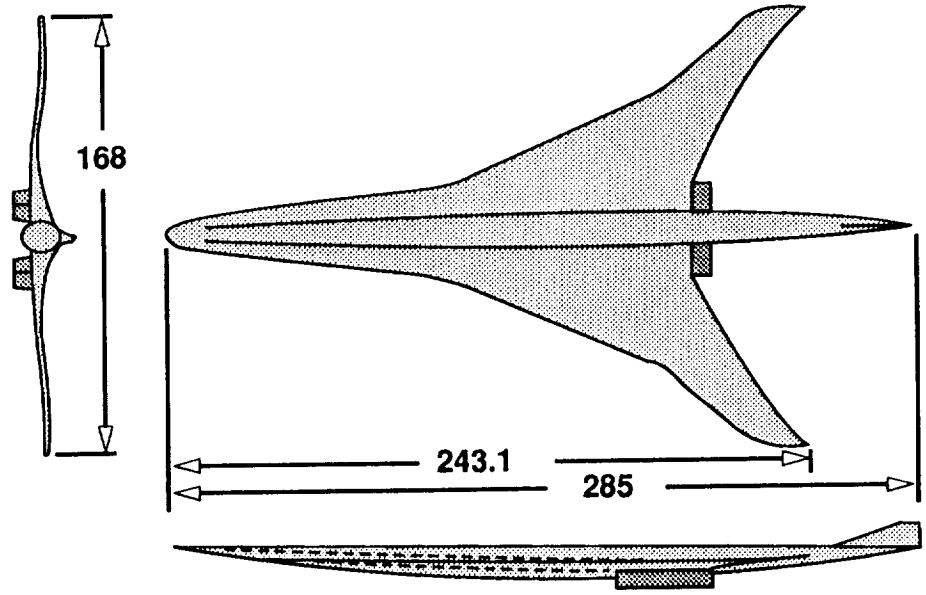

Figure 37. - Mach 2.0 configuration I from reference 26.

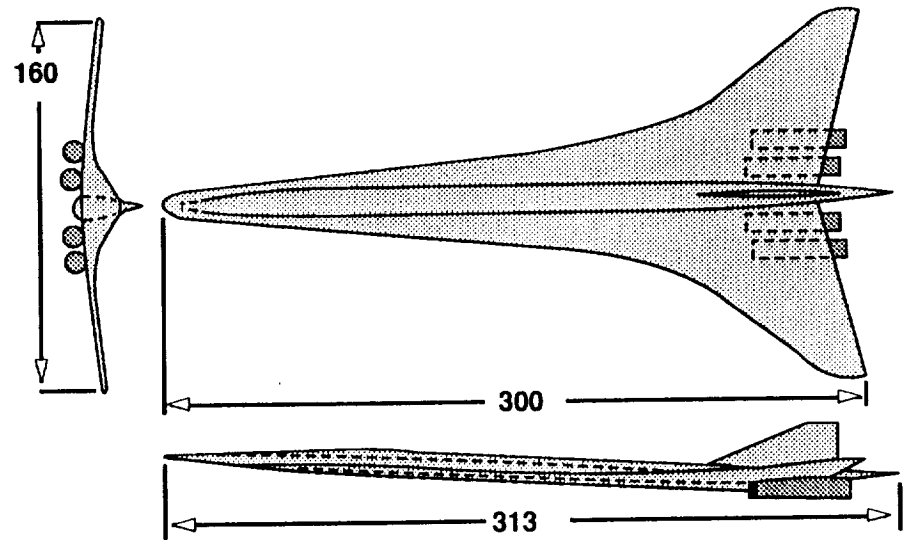

Figure 38. - Mach 2.0 configuration II from reference 26.

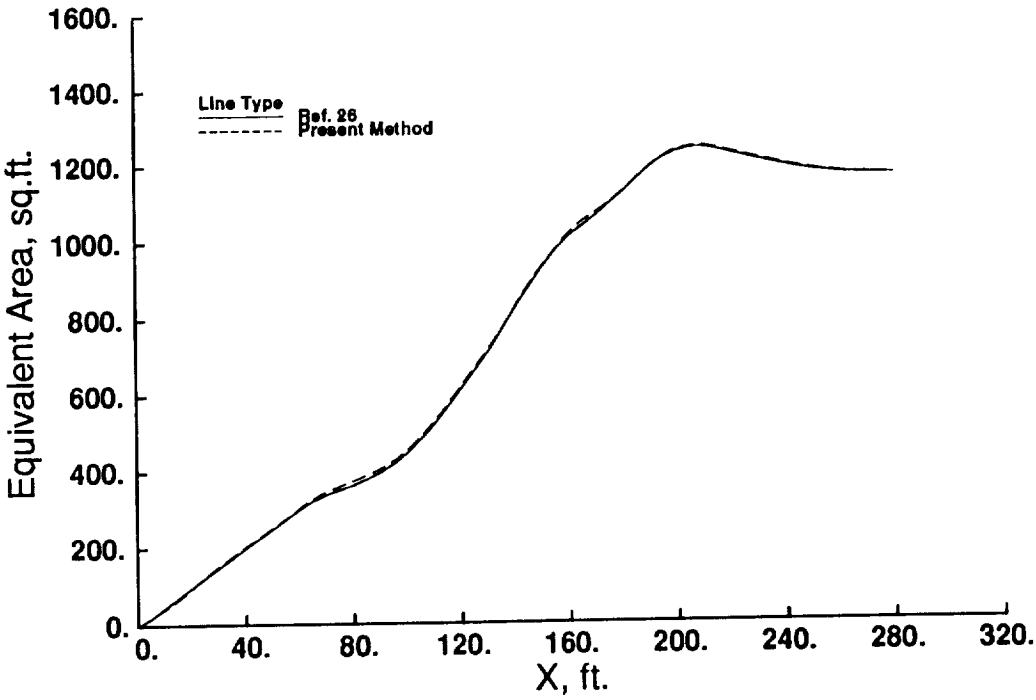

(a) Equivalent area distribution.

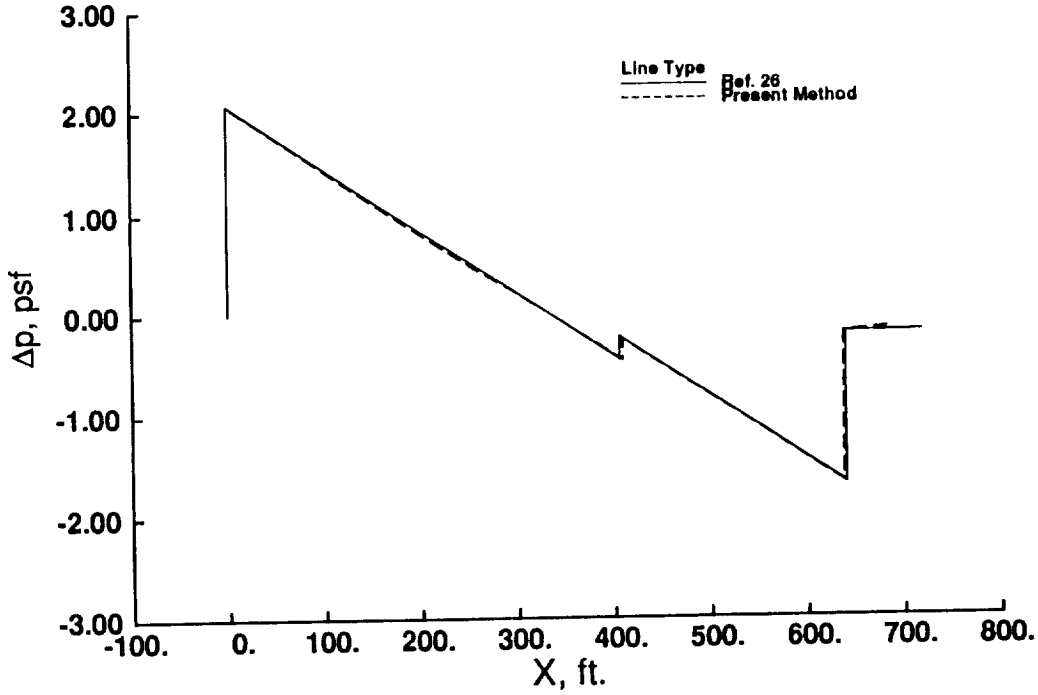

(b) Ground pressure signature

Figure 39. - Comparison of overpressure module results with calculated data from reference 26.
Mach 2.0 configuration I,
Mach = 2.0, L = 550,000 lbs. h = 60,000 ft.

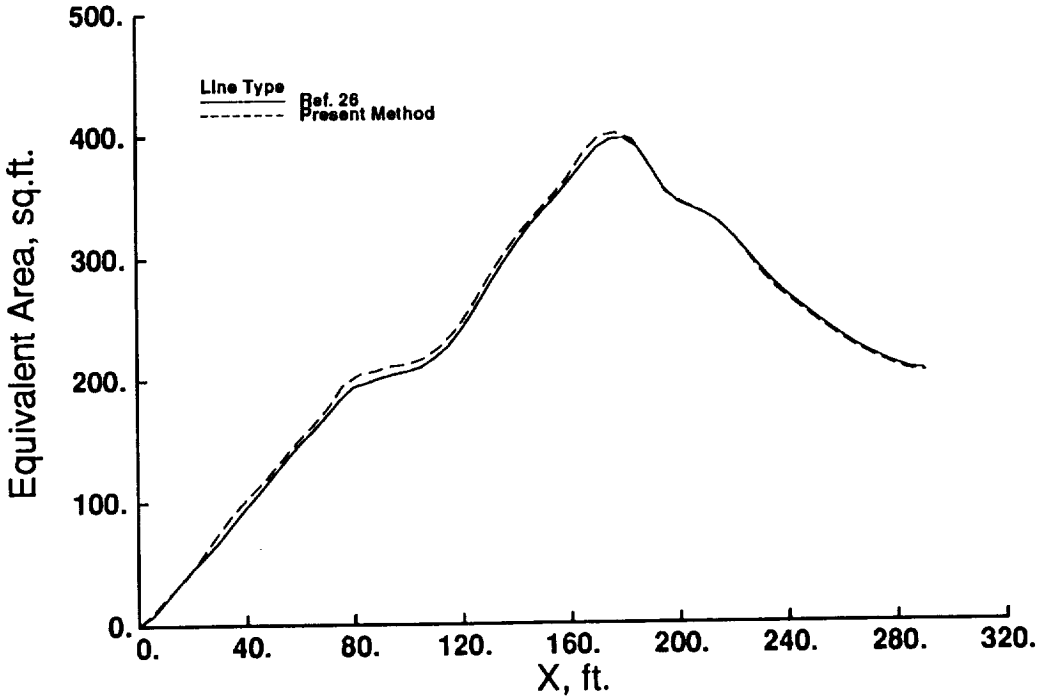

(a) Equivalent area distribution.

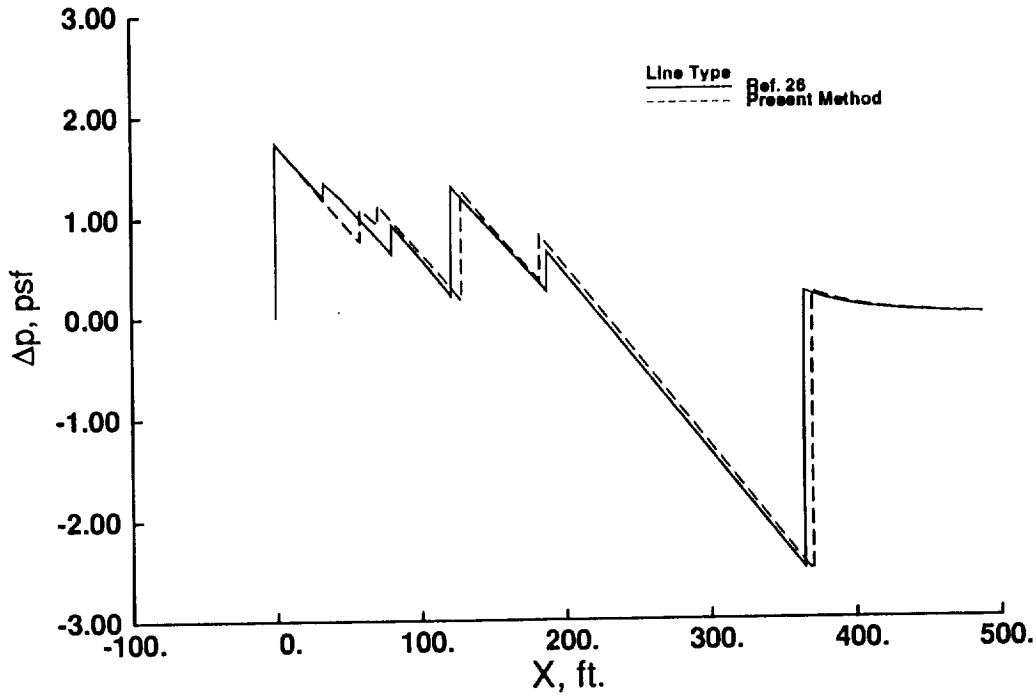

(b) Ground pressure signature

Figure 40. - Comparison of overpressure module results with calculated data from reference 26.
Mach 2.0 configuration I,
Mach = 1.2, L = 250,000 lbs., h = 35,000 ft.

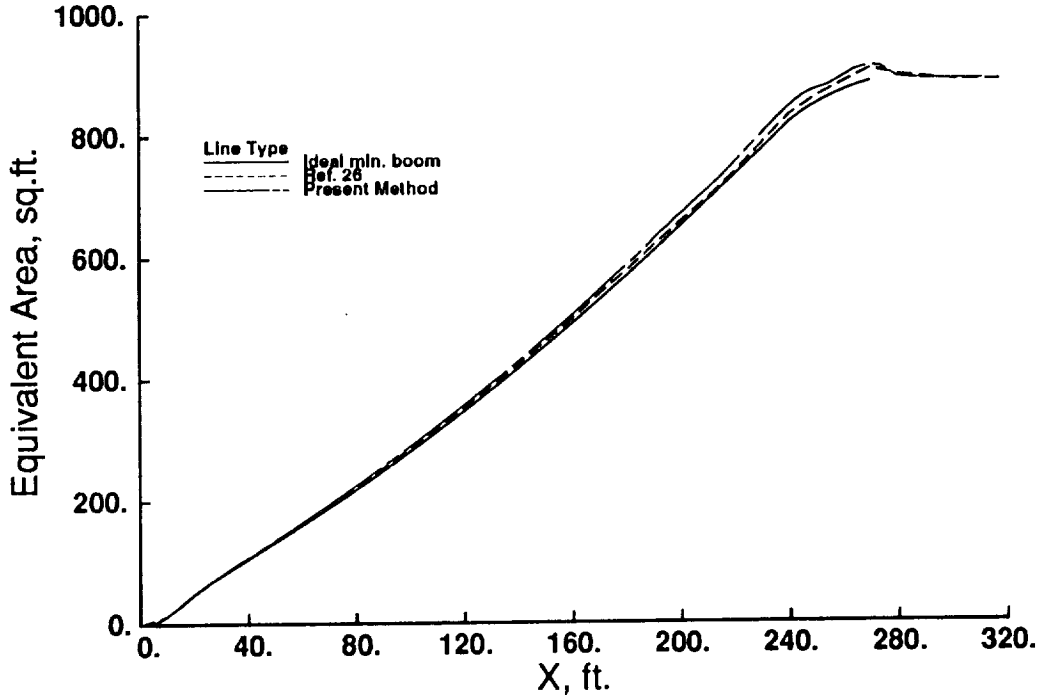

(a) Equivalent area distribution.

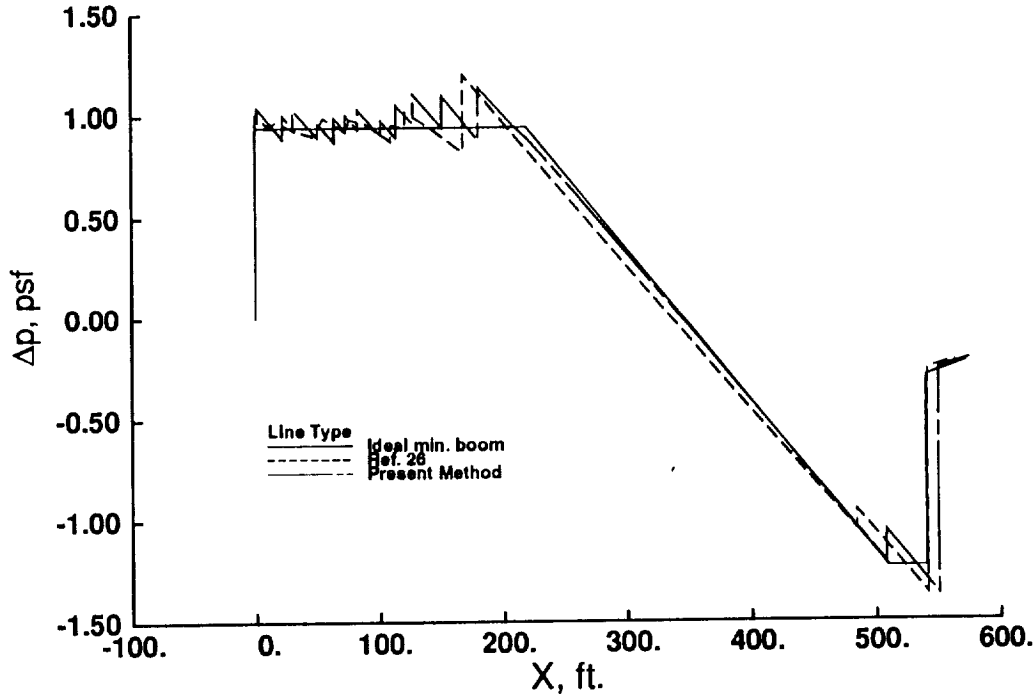

(b) Ground pressure signature

Figure 41. - Comparison of overpressure module results with calculated data from reference 26.
Mach 2.0 configuration II,
Mach = 2.0, L = 550,000 lbs., h = 55,000 ft.

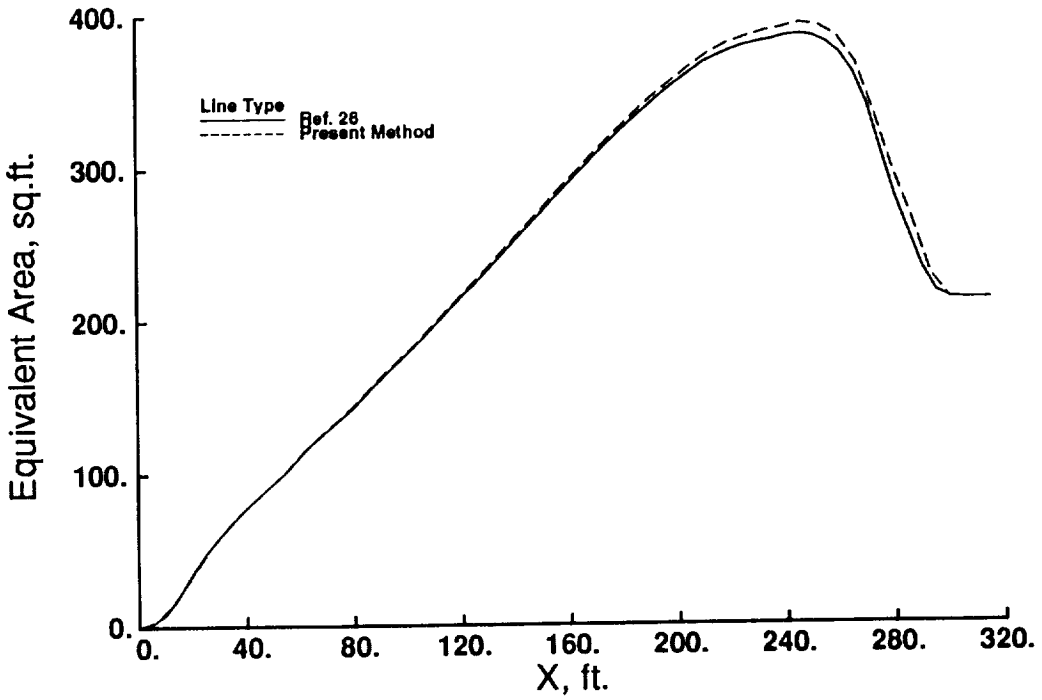

(a) Equivalent area distribution.

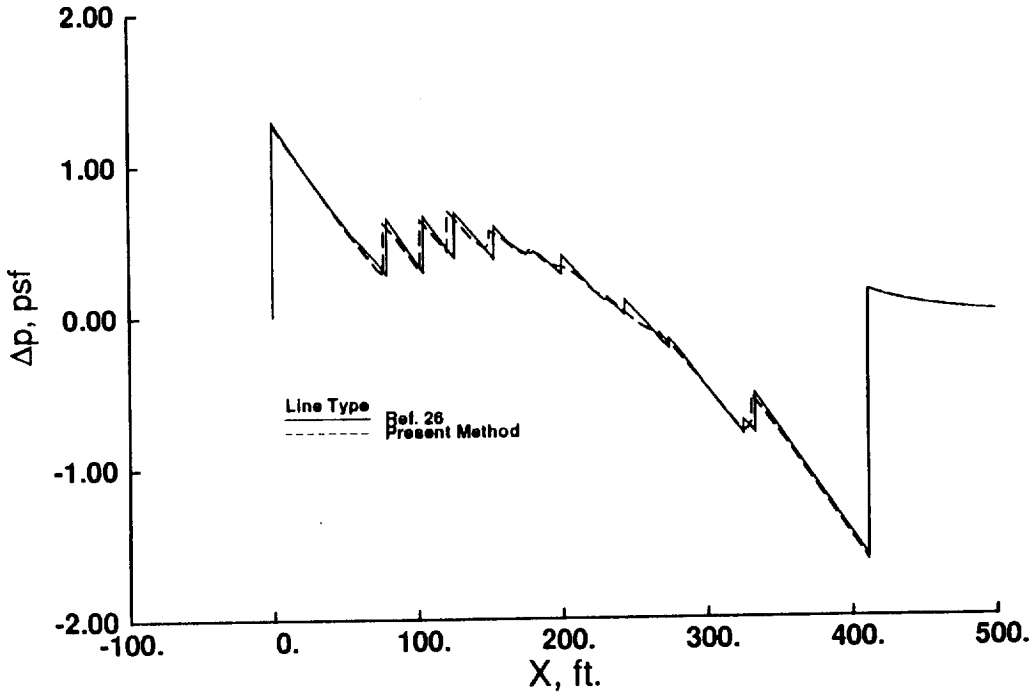

(b) Ground pressure signature

Figure 42. - Comparison of overpressure module results with calculated data from reference 26.
Mach 2.0 configuration II,
Mach = 1.2, L = 250,000 lbs., h = 40,000 ft.

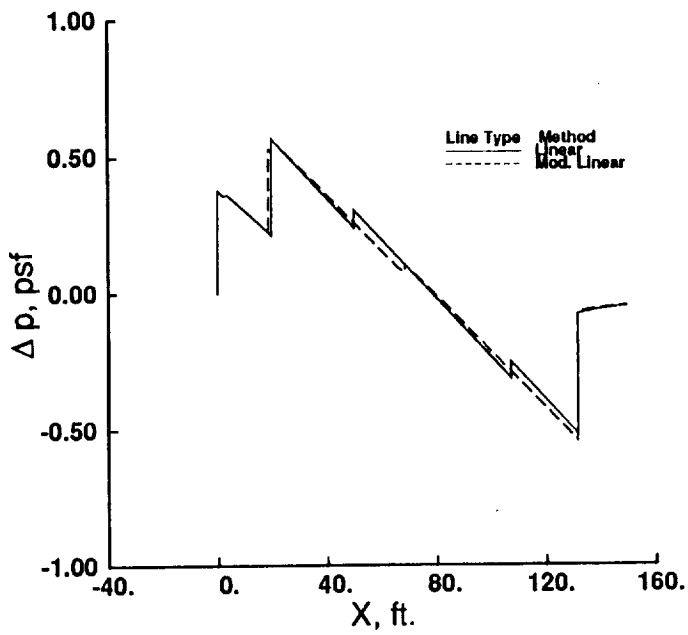

(a) Mach 1.2

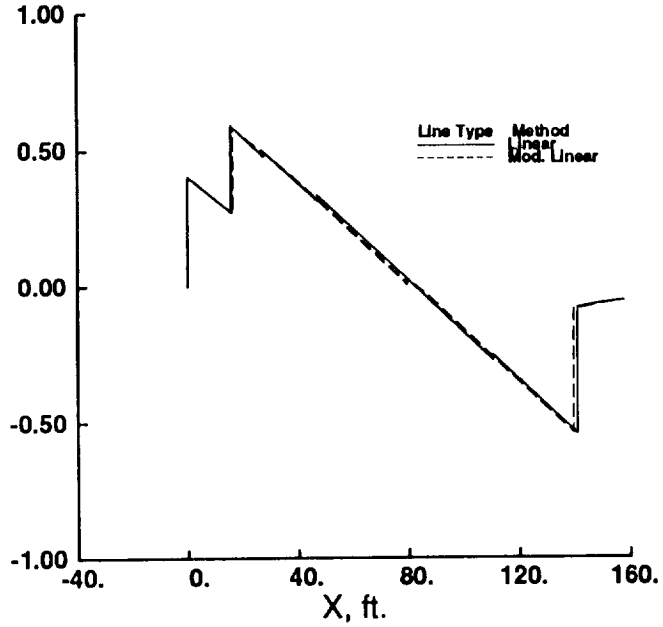

(b) Mach 1.7

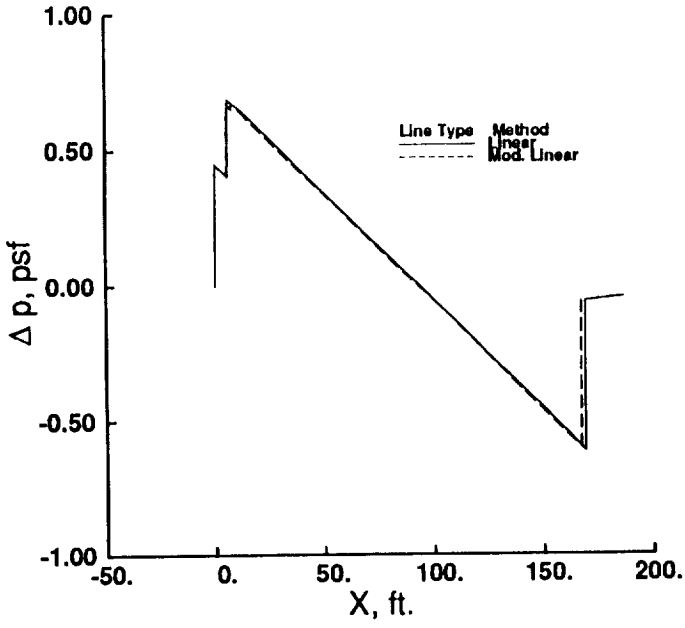

(c) Mach 2.2

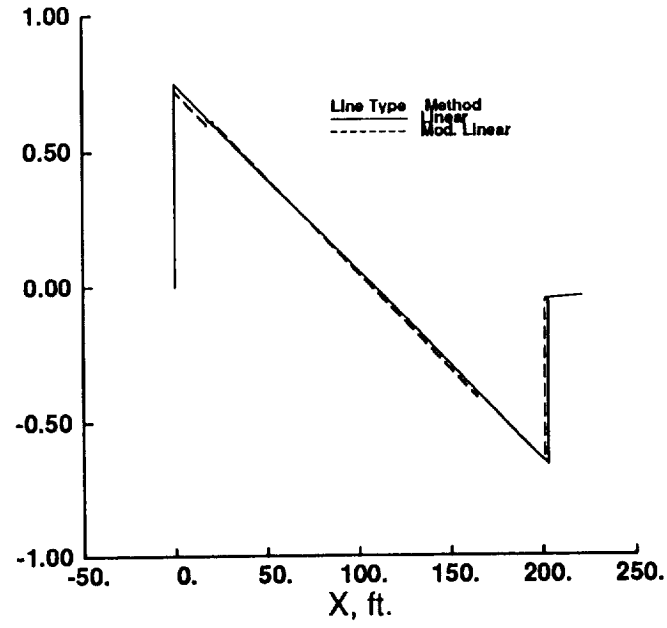

(d) Mach 2.7

Figure 43. - Comparison of complete ground pressure signature results computed with linear and modified linear lift methods.
Reference arrow wing geometry,
L = 25,000 lbs., h = 50,000 ft.

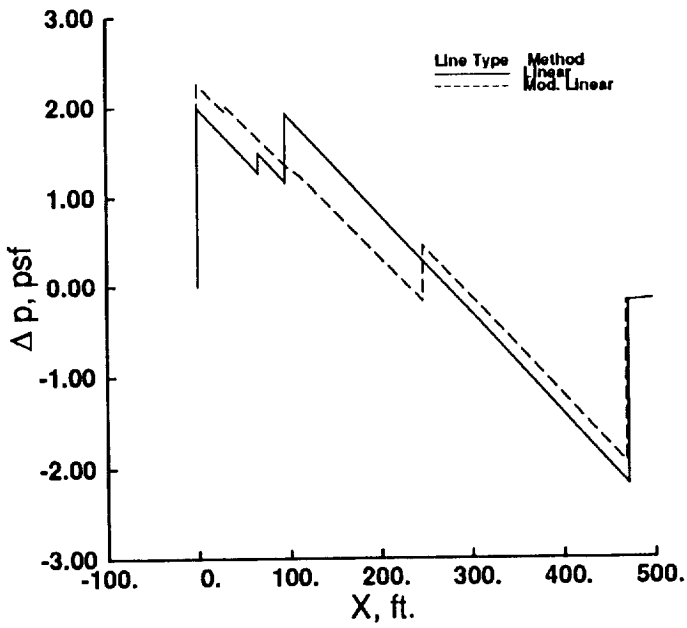

(a) Mach 1.2

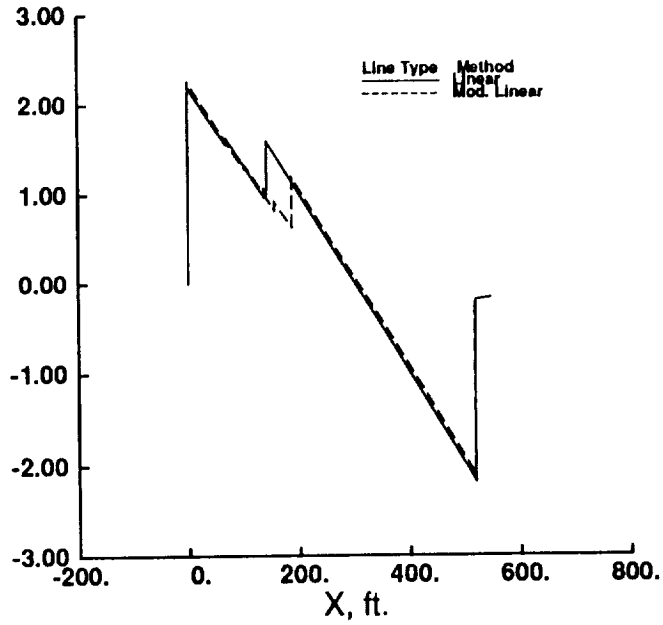

(b) Mach 1.7

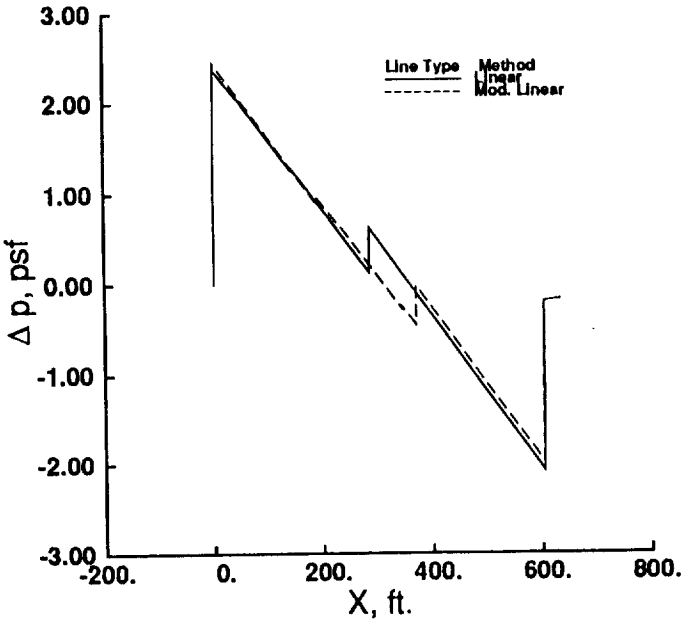

(c) Mach 2.2

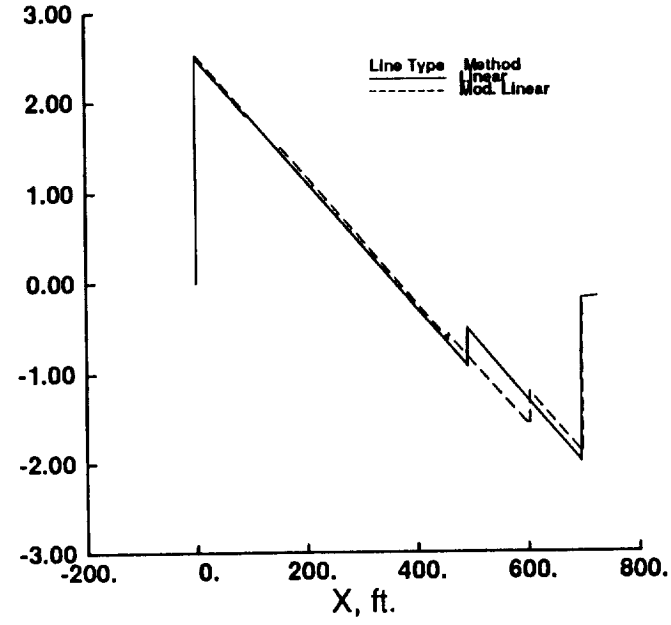

(d) Mach 2.7

Figure 44. - Comparison of complete ground pressure signature results computed with linear and modified linear lift methods.
Mach 2.7 configuration geometry,
L = 600,000 lbs., h = 50,000 ft.

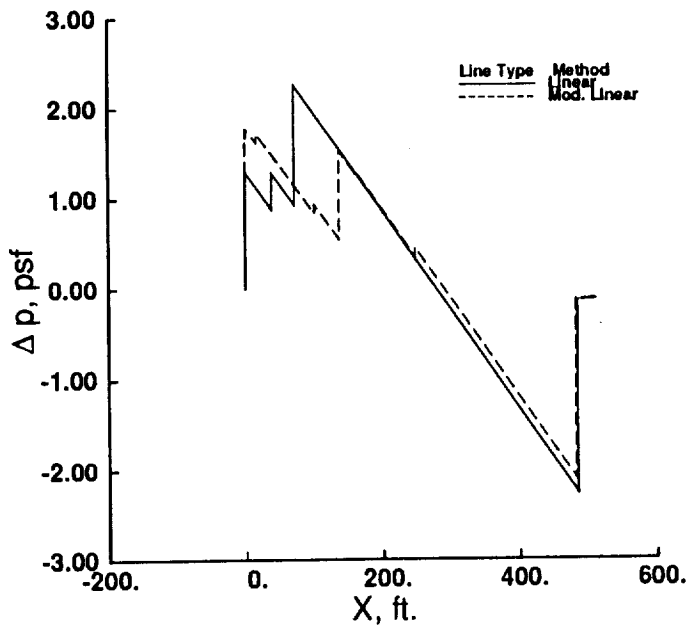

(a) Mach 1.2

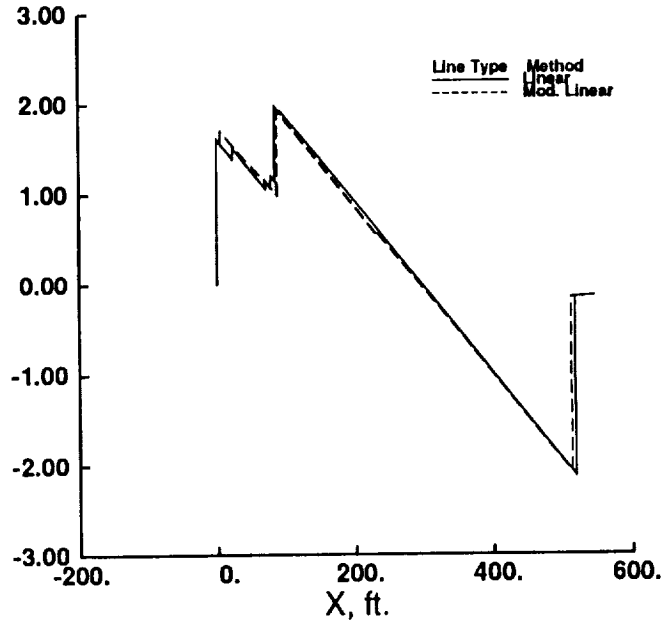

(b) Mach 1.8

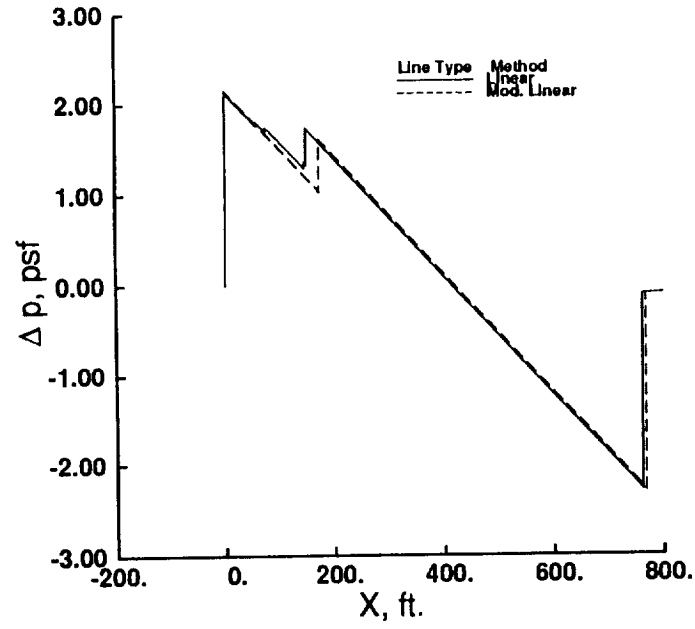

(c) Mach 2.4

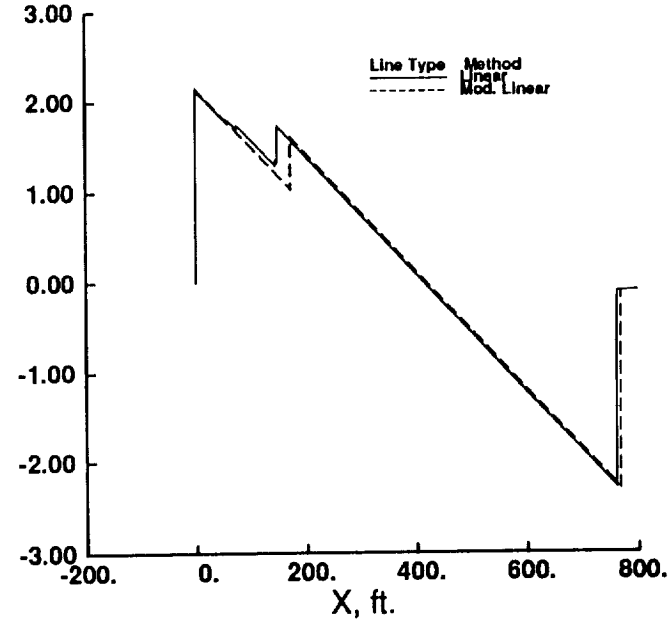

(d) Mach 3.0

Figure 45. - Comparison of complete ground pressure signature results computed with linear and modified linear lift methods,
Mach 3.0 configuration geometry.
L = 500,000 lbs., h = 50,000 ft.

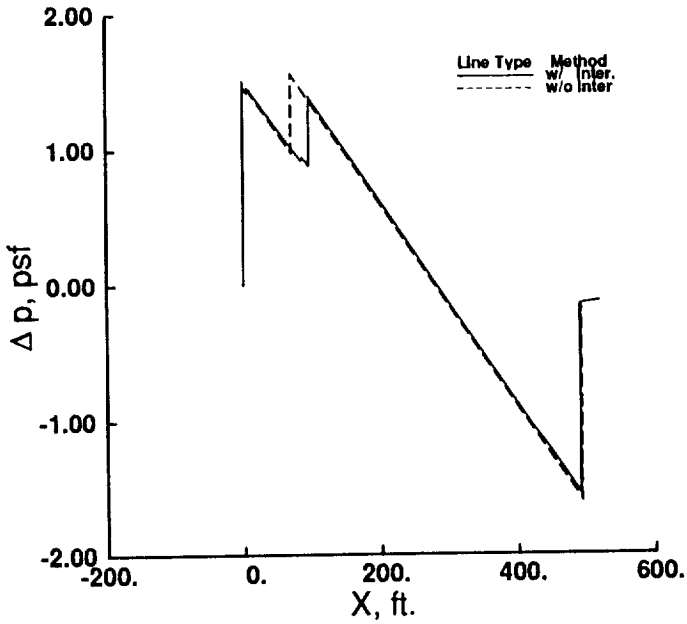

(a) Mach = 1.4, L = 400,000 lbs., h = 60,000 ft.

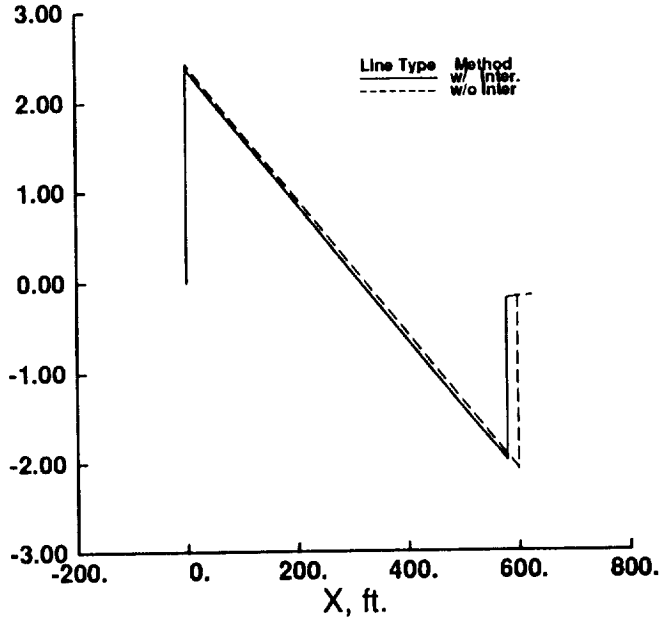

(b) Mach = 1.4, L = 600,000 lbs., h = 0,000 ft.

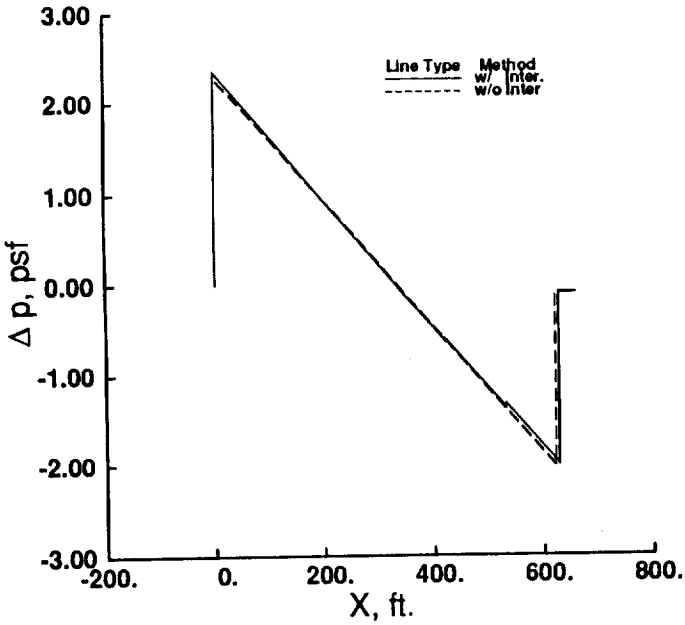

(c) Mach = 2.7 L = 400,000 lbs., h =5 0,000 ft.

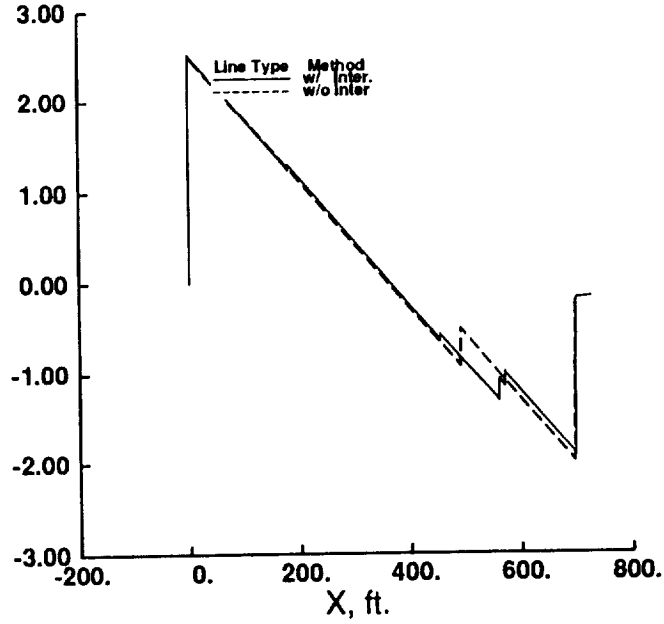

(d) Mach = 2.7 L = 600,000 lbs., h = 50,000 ft.

Figure 46. - Comparison of complete ground pressure signature results computed with and without interference lift.
Mach 2.7 configuration geometry.

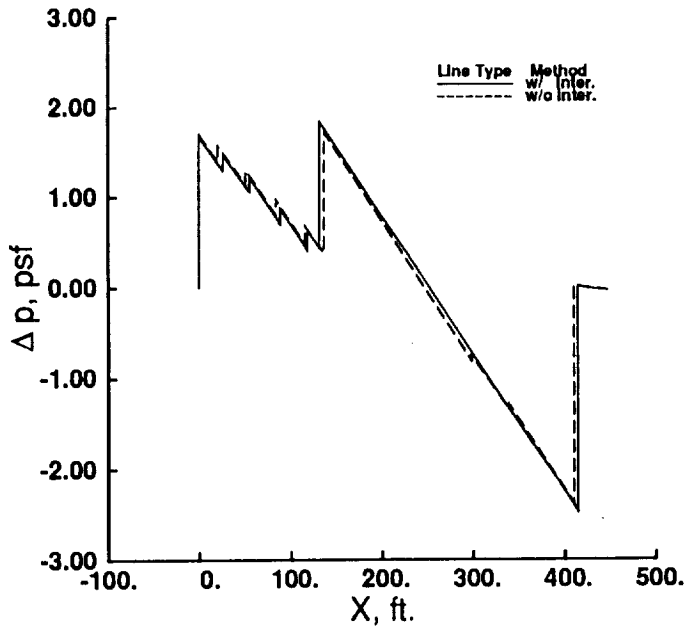

(a) Mach = 1.4, L = 350,000 lbs., h = 40,000 ft.

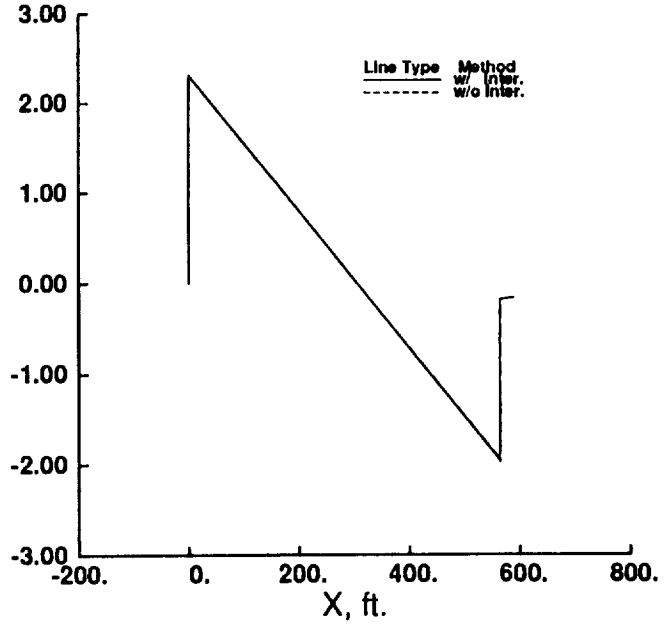

(b) Mach = 1.4, L = 550,000 lbs., h =60,000 ft.

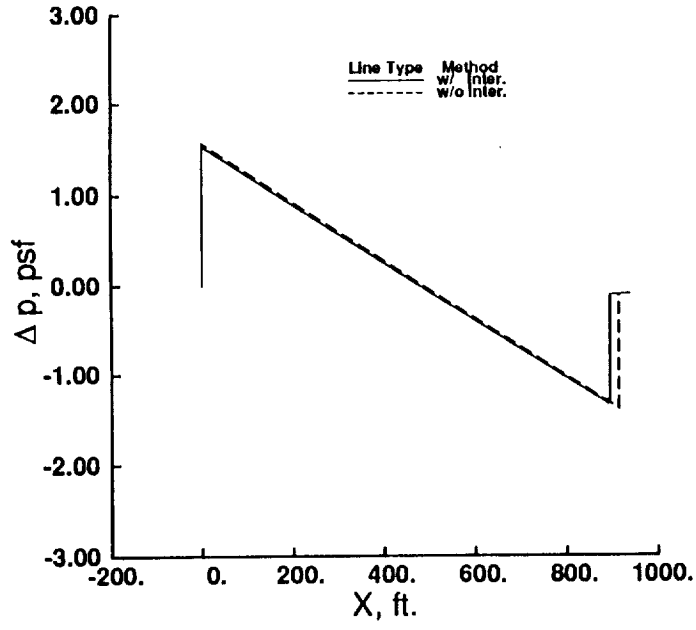

(c) Mach = 3.0, L = 350,000 lbs., h = 70,000 ft.

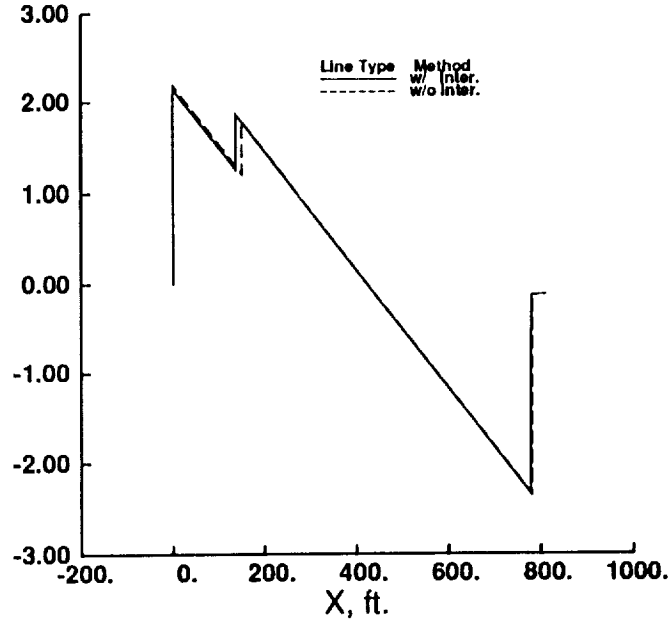

(d) Mach = 3.0, L = 550,000 lbs., h = 50,000 ft.

Figure 47. - Comparison of complete ground pressure signature results computed with and without interference lift. Mach 3.0 configuration geometry.

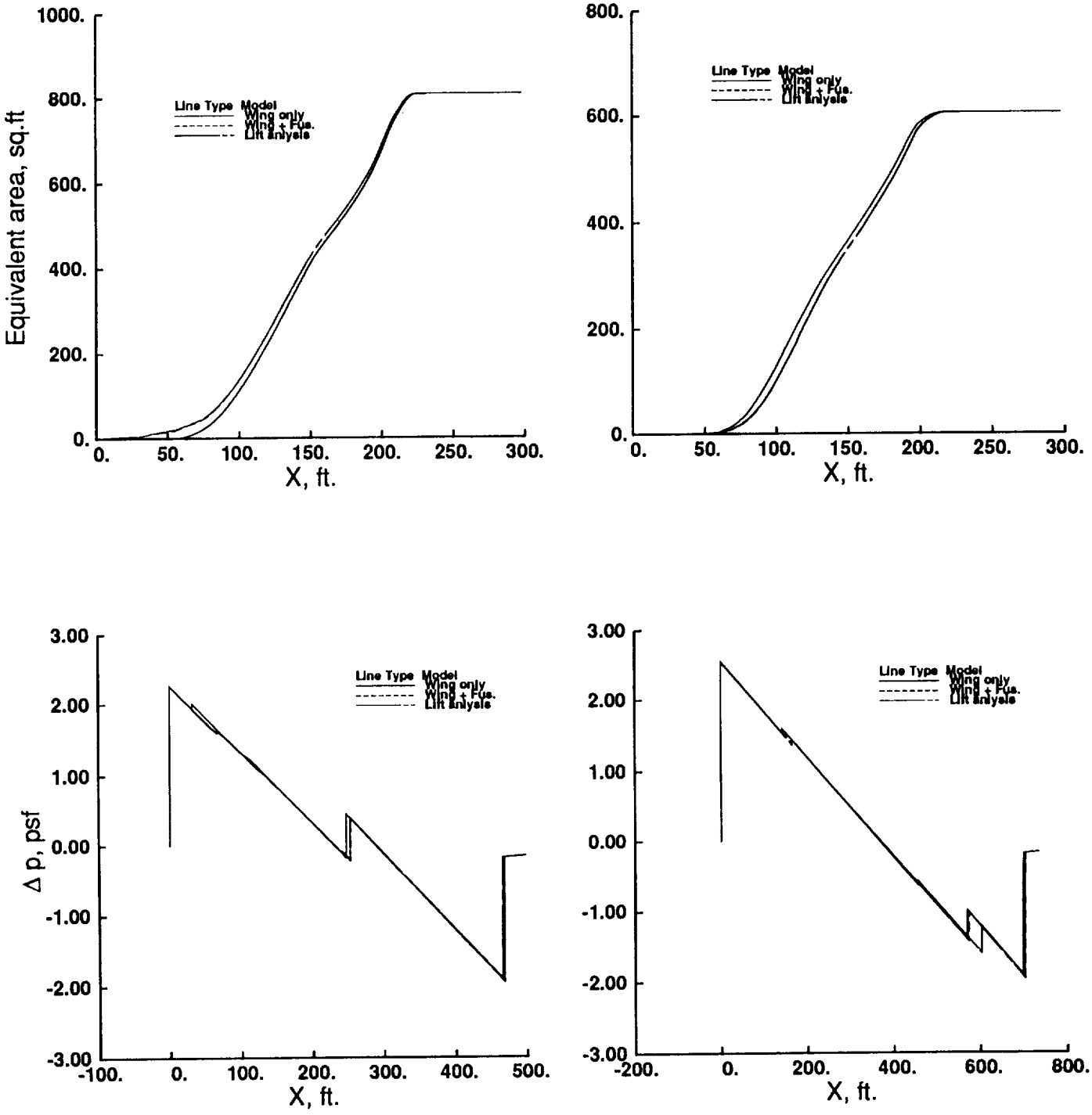

(a) Mach 1.2

(b) Mach 2.7

Figure 48. - Comparison of lift equivalent area distributions and complete ground pressure signature results computed with different wing modeling methods. Mach 2.7 configuration, L = 600,000 lbs., h = 50,000 ft.

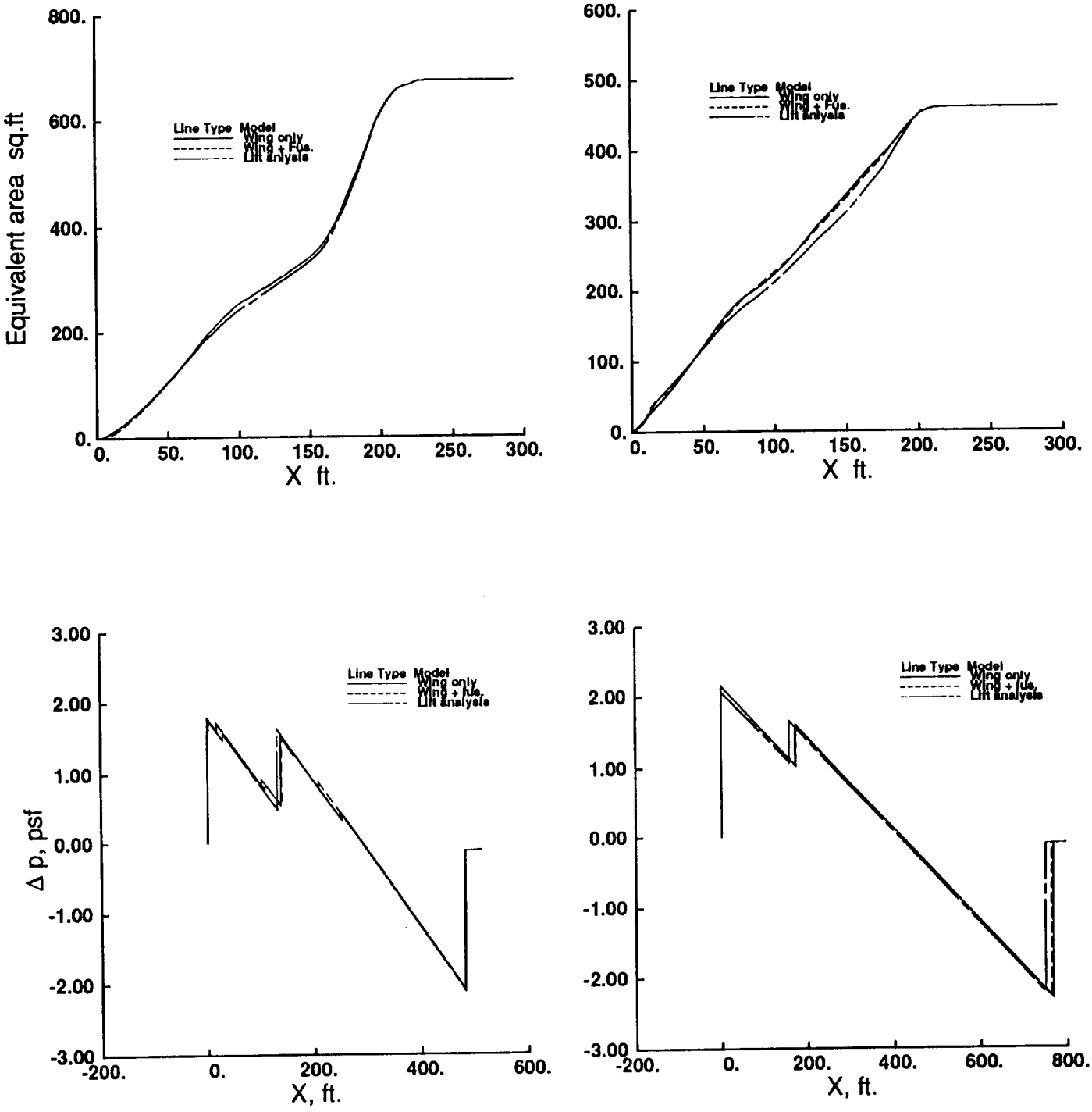

(a) Mach 1.2

(b) Mach 3.0

Figure 49. - Comparison of lift equivalent area distributions and complete ground pressure signature results computed using different wing modeling methods. Mach 3.0 configuration, L = 500,000 lbs., h = 50,000 ft.

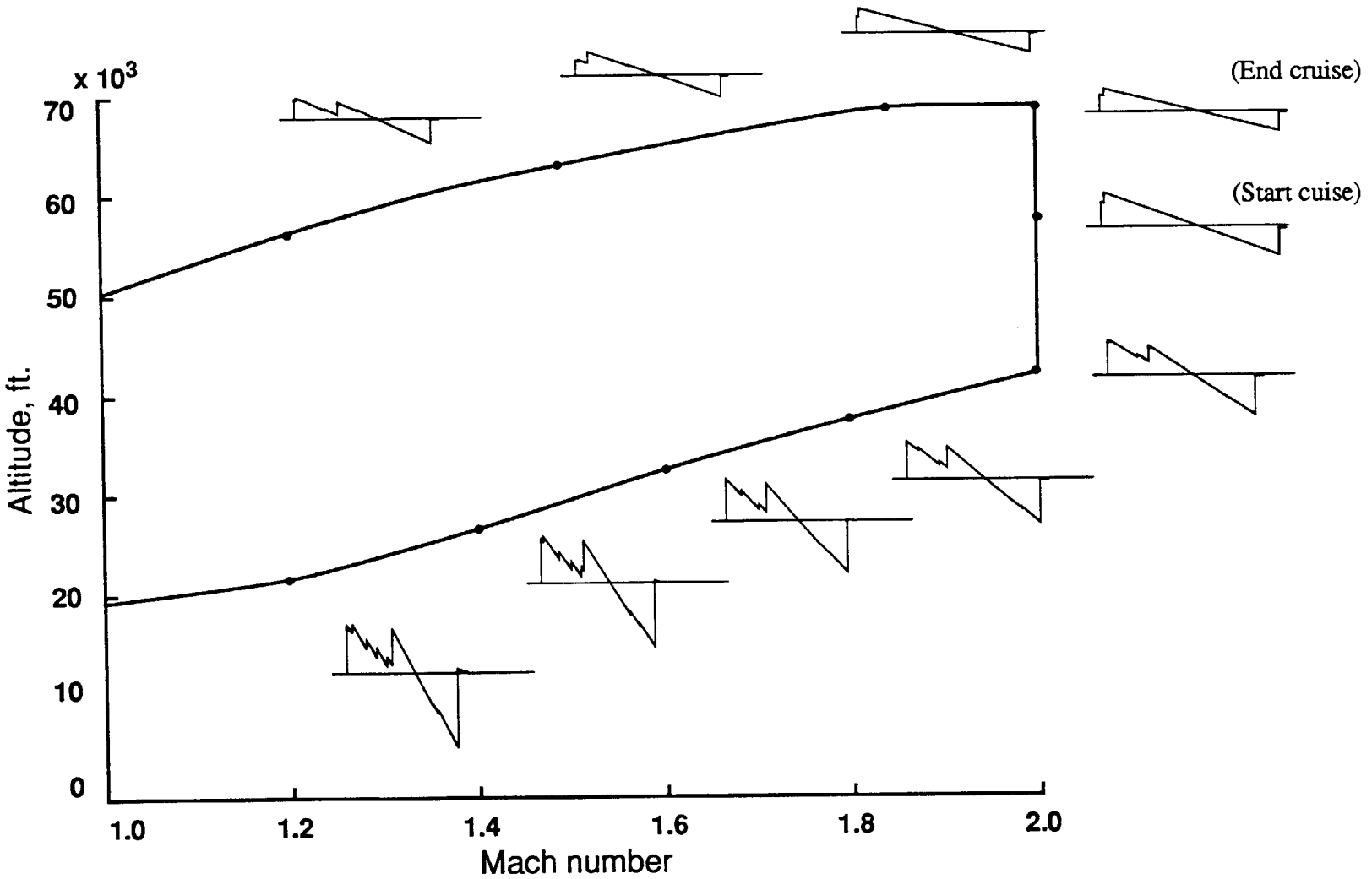

Figure 50. - Ground overpressure signature shapes corresponding to selected flight profile points.
Mach 2.0 configuration I, TOGW = 585,000 lbs.

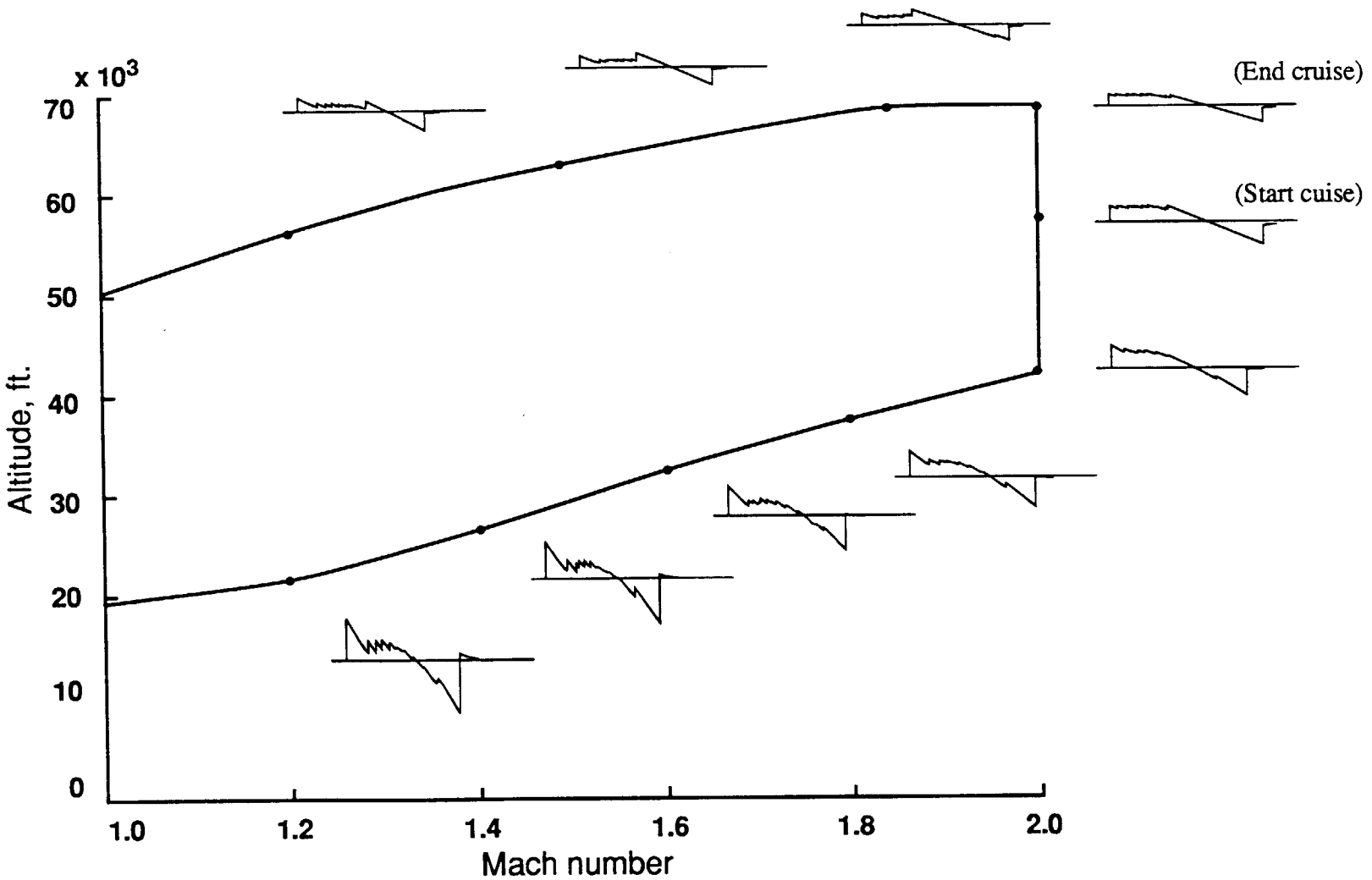

Figure 51. - Ground overpressure signature shapes corresponding to selected flight profile points.
Mach 2.0 configuration II, TOGW = 590,000 lbs.

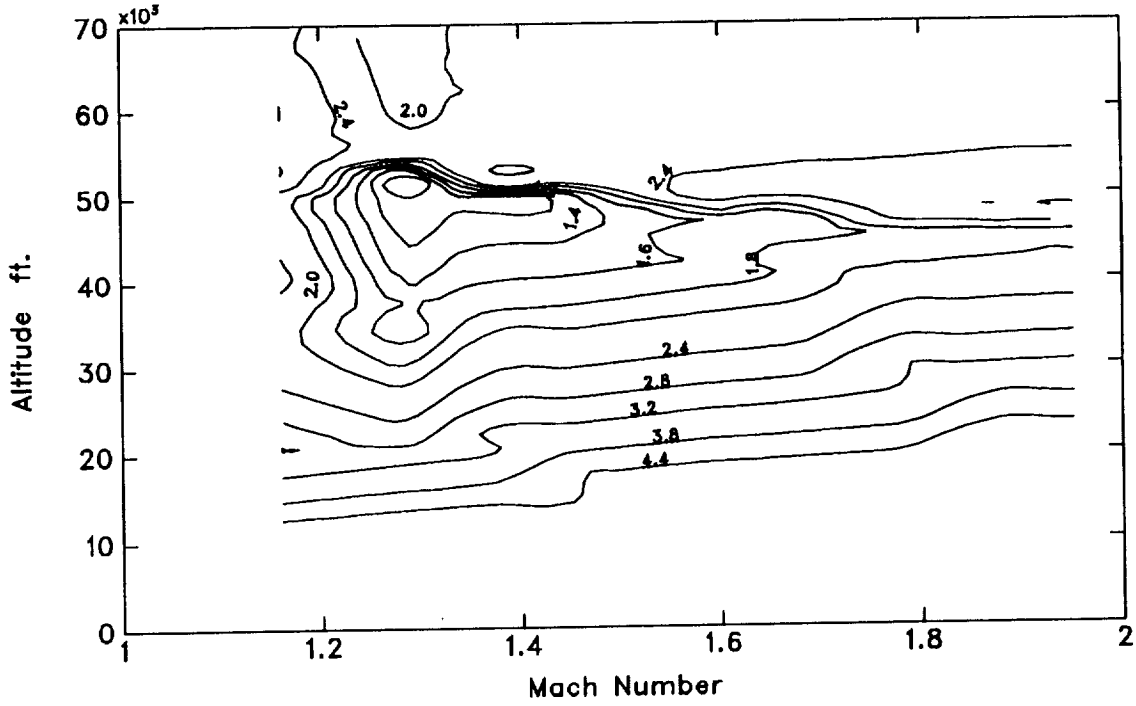

(a) L= 550,000 lbs.

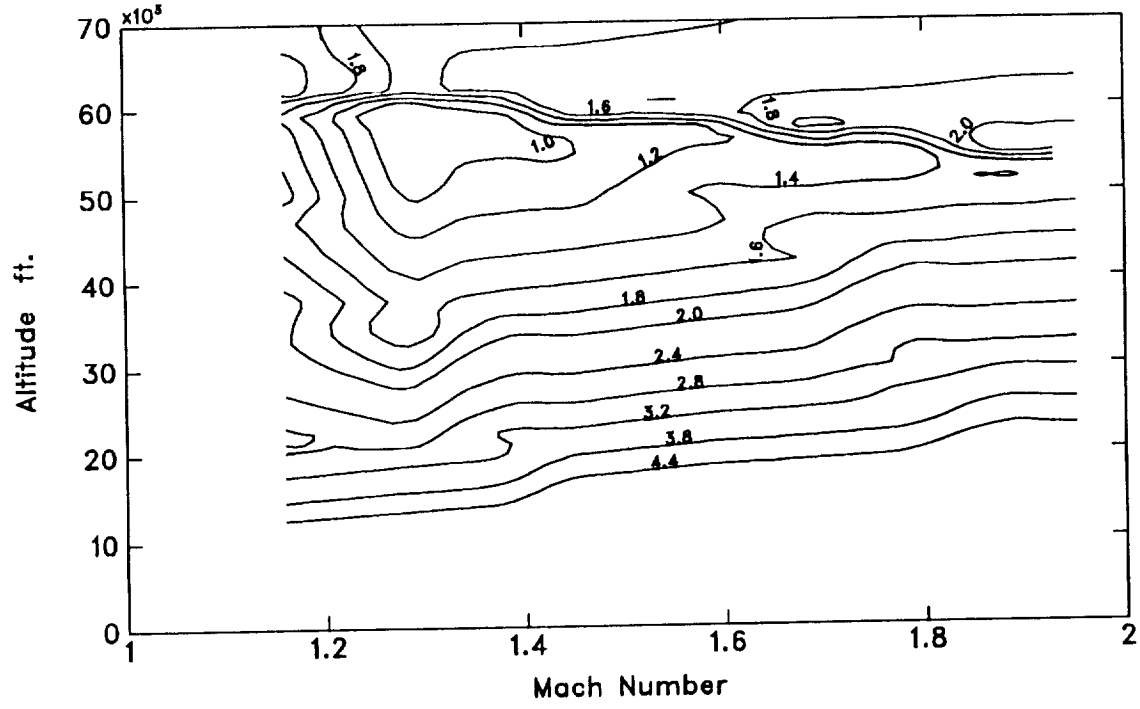

(b) L= 350,000 lbs.

Figure 52. - Contours of constant nose shock Δp for steady flight.
Mach 2.0 configuration I.

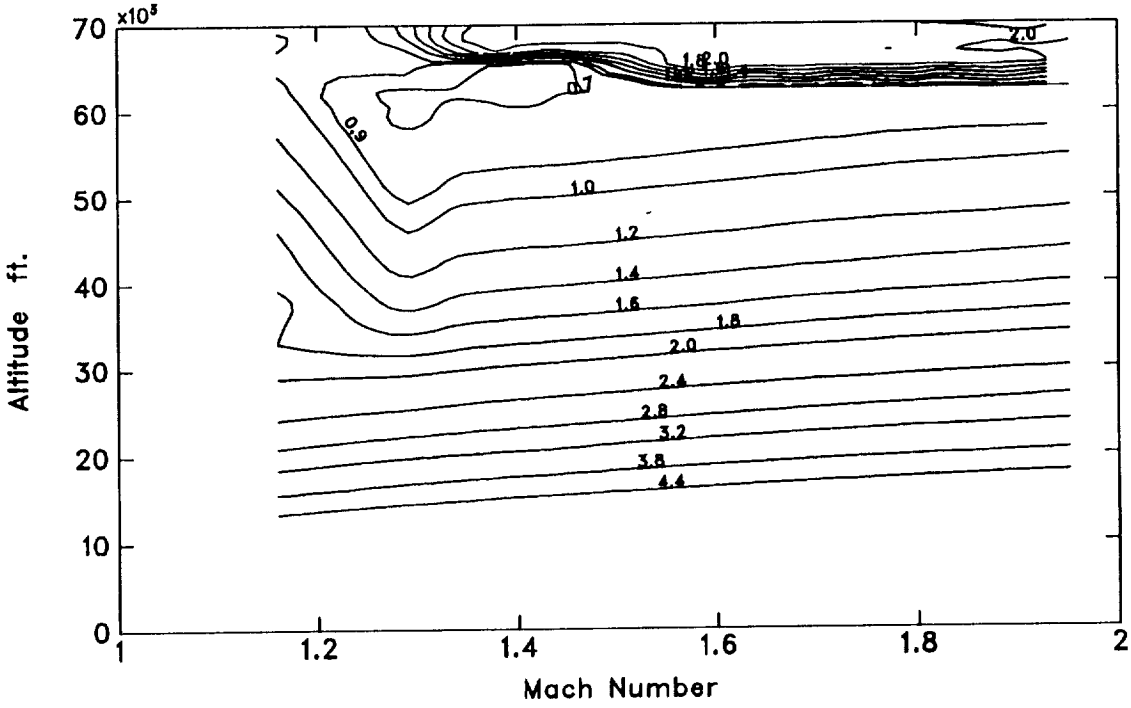

(a) L= 550,000 lbs.

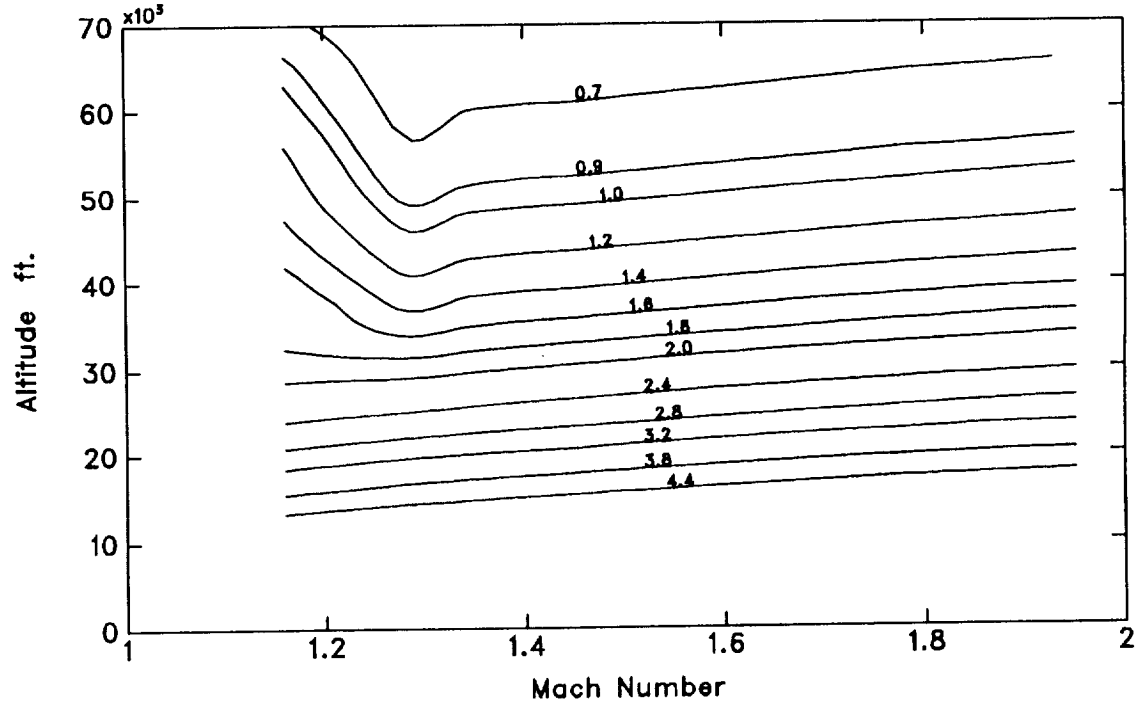

(b) L= 350,000 lbs.

Figure 53. - Contours of constant nose shock Δp for steady flight Mach 2.0 configuration II.

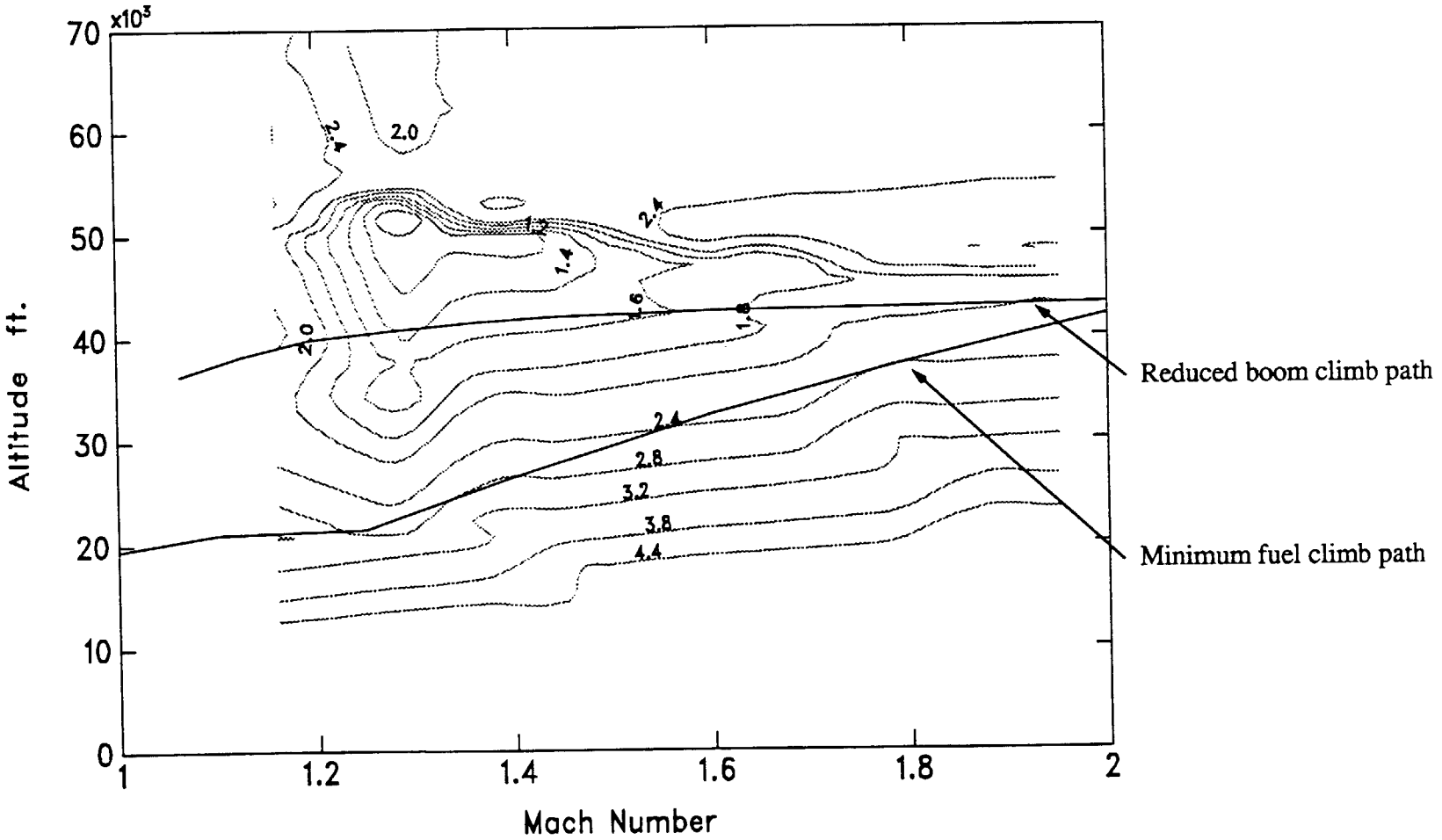

Figure 54. - Contours of constant nose shock Δp. Illustrating selected climb profiles for minimum fuel burn and reduced Δp at the ground.
Mach 2.0 configuration I, TOGW= 585,000 lbs.

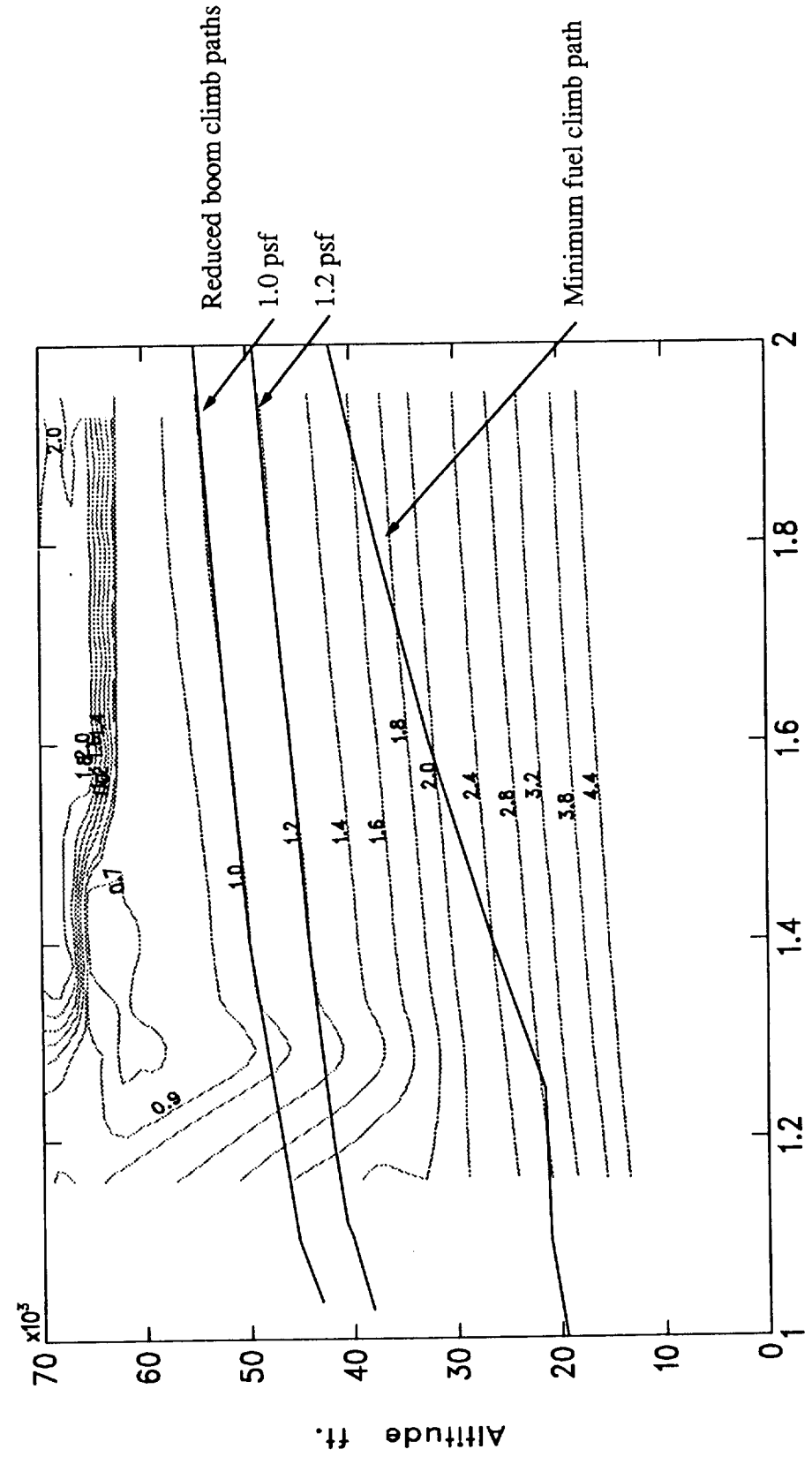

Figure 55. - Contours of constant nose shock Δp. Illustrating selected climb profiles for minimum fuel burn and reduced Δp at the ground.
Mach 2.0 configuration II, TOGW= 590,000 lbs.

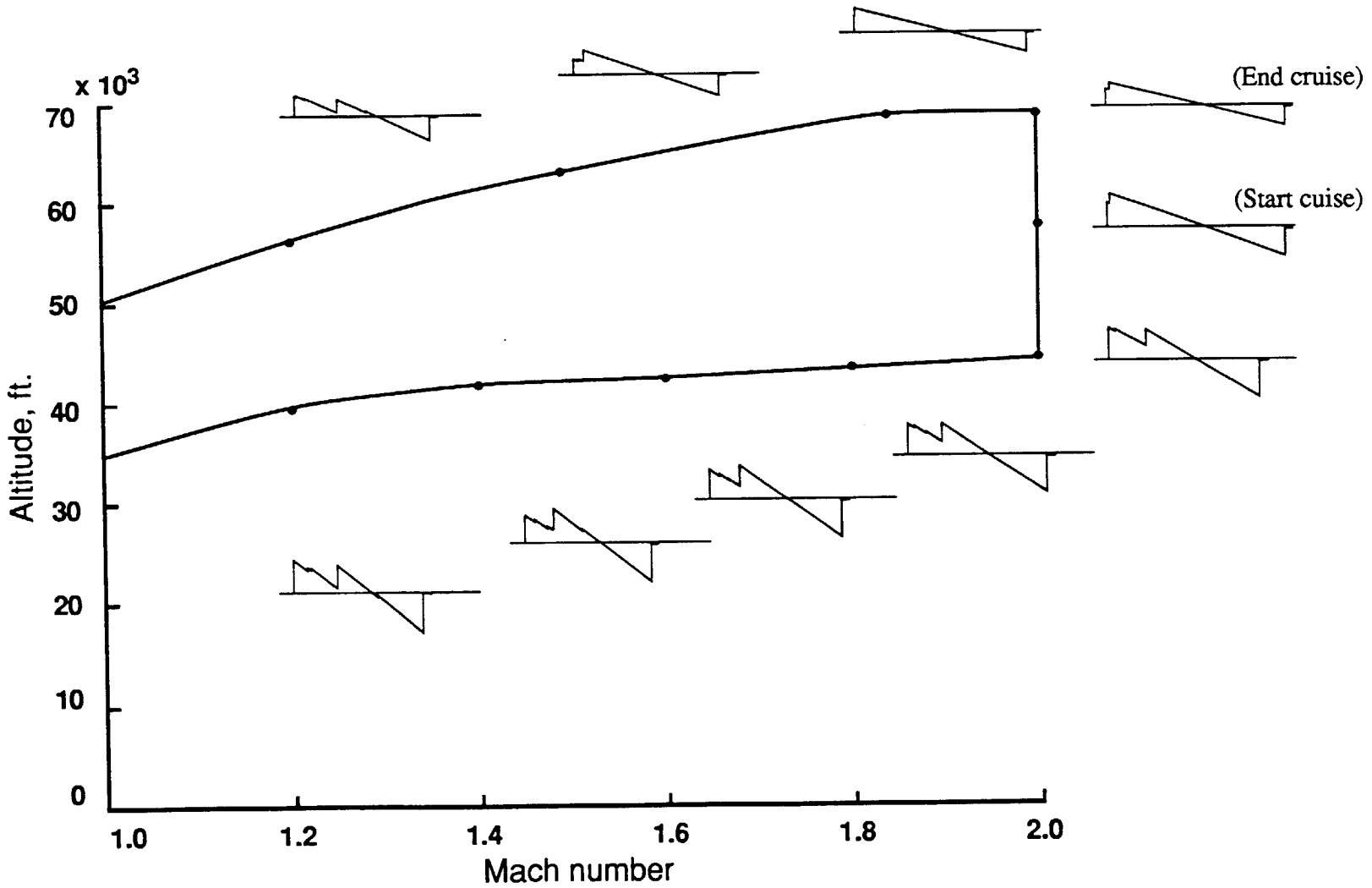

Figure 56. - Ground overpressure signature shapes corresponding to selected reduced boom flight profile points.
Mach 2.0 configuration I, TOGW = 590,000 lbs.

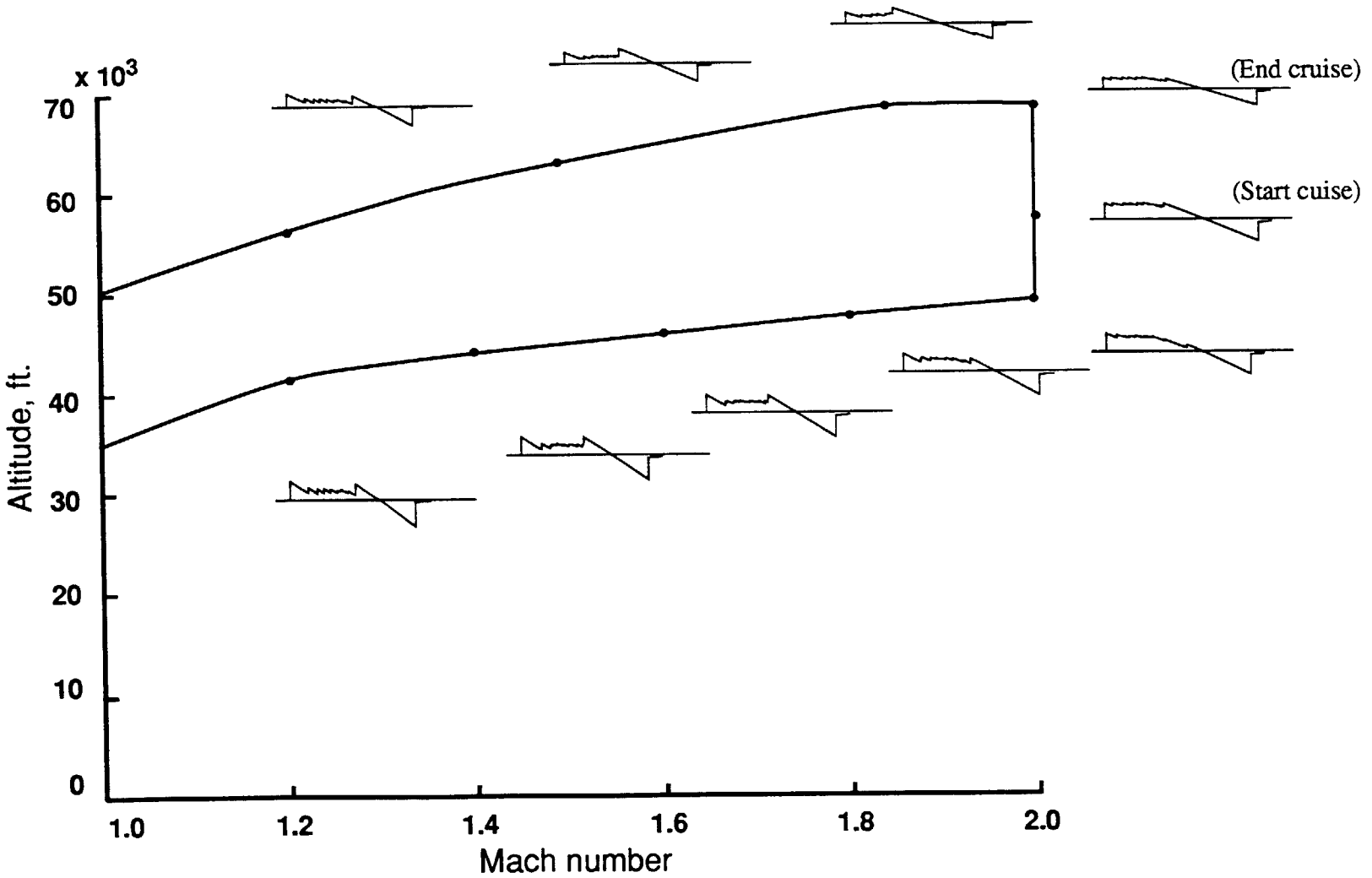

Figure 57. - Ground overpressure signature shapes corresponding to selected reduced boom flight profile points.
Mach 2.0 configuration II, TOGW = 590,000 lbs., Δp_{max} = 1.2 psf.

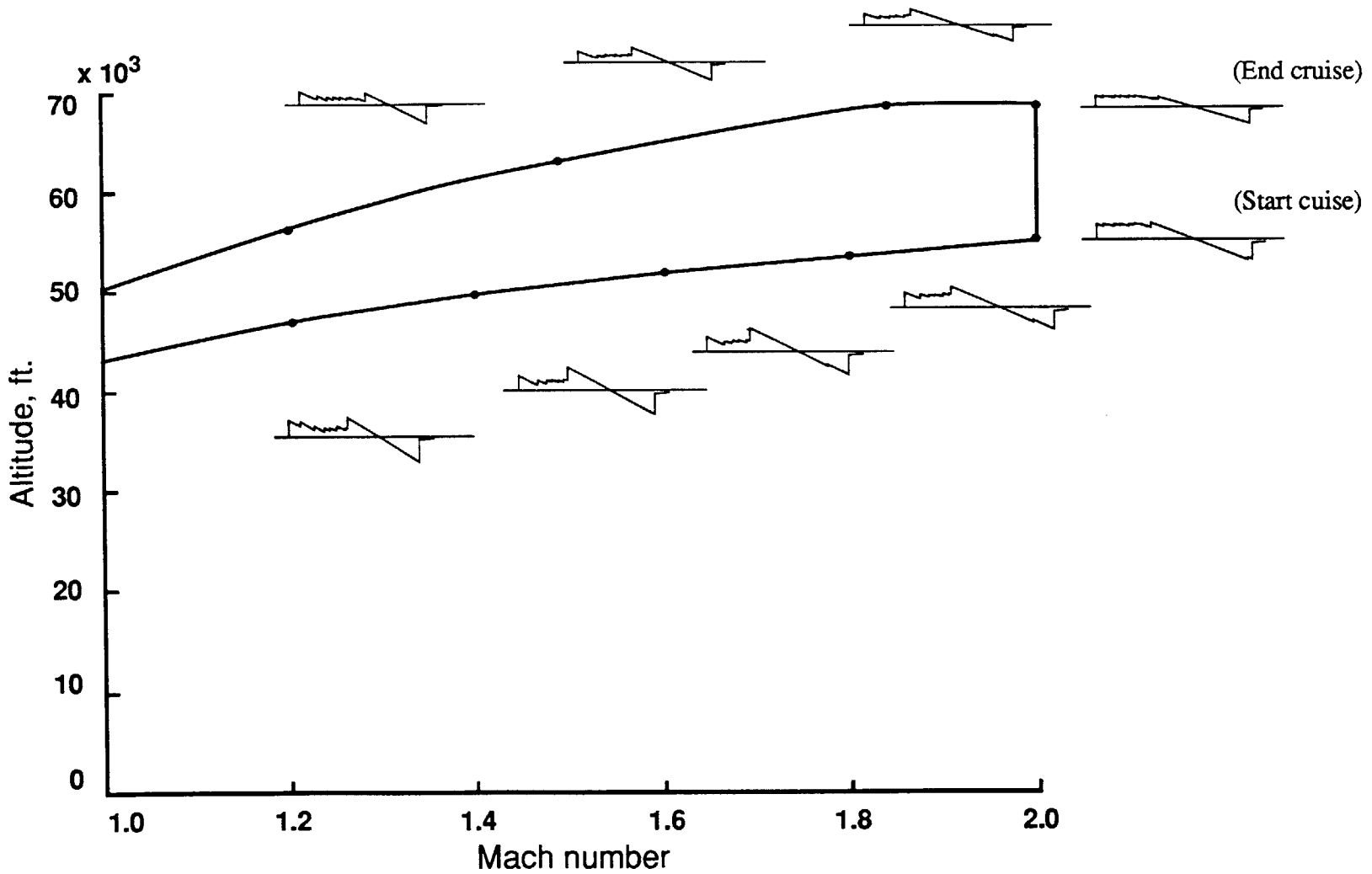

Figure 58. - Ground overpressure signature shapes corresponding to selected reduced boom flight profile points.
Mach 2.0 configuration II, TOGW = 590,000 lbs., Δp_{max}= 1.0 psf.